AV-95 *SUN DEVIL*

High-Speed Military Rotorcraft

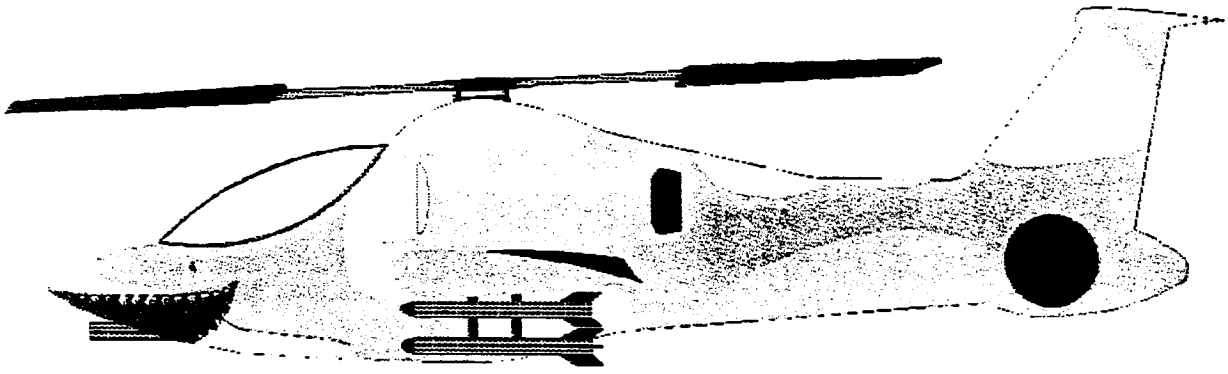

Arizona State University

Design Team: Terry Ivener
Todd Ivener
Jay Moore
Brian Hermesmeyer

Professors: Dr. Valana Wells
Dr. David H. Laananen
Dr. Jack Rutherford

EXECUTIVE SUMMARY

The AV-95 *Sun Devil* must combine helicopter capabilities, such as vertical takeoff and landings (VTOL) and rotor-powered flight, along with long-duration cruise and high-speed dash capabilities unobtainable by conventional helicopters. To be able to perform both tasks, and perform them well, the AV-95 *Sun Devil* design incorporates several unconventional devices; the AV-95 uses two convertible turbofan engines, able to provide both shaft power for the main rotor and tail fan as well as jet thrust either separately or simultaneously. Other devices used for the AV-95 include a variable diameter main rotor and a blown flap.

In helicopter mode, the AV-95 *Sun Devil* performs like a winged helicopter. The addition of wings to an attack helicopter results in two significant advantages. First, the addition of wings makes a helicopter more maneuverable than a wingless, but otherwise similar helicopter. Second, since the wings produce lift, rotor stall and compressibility effects can be significantly delayed at high tip velocities. In fixed-wing mode, the main rotor is completely off-loaded but slightly powered, and the rotor diameter has been minimized.

Conversion is very simple. In fact, conversion begins when the AV-95 starts forward flight from hover in helicopter mode. When forward flight occurs, the wings produce lift; therefore, the rotor lift must be reduced to compensate. The faster the *Sun Devil* flies, the greater the wing lift, and the further the rotor gets off-loaded. However, the wing was sized for cruise at 228 knots, and the rotor would not be completely off-loaded until this speed is reached.

To solve this problem, a blown flap was incorporated into the design (see Chapter 15). This device can operate as a conventional flap without blowing, or it can use engine bleed air to create much higher lift at relatively low velocities at any flap deflection.

Also, the flap can rotate 180 degrees and fold under the wing to reveal a Coanda trailing edge.

The AV-95 *Sun Devil* has many advantages over other VTOL aircraft. The conversion process is simple and fast; conversion does not make the AV-95 vulnerable to enemy attack during conversion such as a tilt-wing or a tilt-rotor. Stop-rotor aircraft and a stowed rotor aircraft require heavy breaking of the rotor for conversion; this adds time for conversion and weight to the aircraft. Because the AV-95 never stops the rotor in flight, much weight is spared, and conversion is much simpler and faster.

Another significant edge for the *Sun Devil* is illustrated in the survivability of the aircraft. Because the method of propulsion, either rotor thrust and jet thrust combination or strictly jet thrust, is relatively independent, the *Sun Devil* has the ability to completely lose one propulsion system and still complete the mission. For example, during a ground attack, the aircraft will most often be in the helicopter mode. If the rotors are disabled by the enemy, the *Sun Devil* has the ability to switch its propulsion dependence from the rotor-turbofan combination (helicopter mode) to just the turbofan (fixed-wing mode). By doing this, the AV-95 can not only return home, but it can also complete its mission.

AV-95 Sun Devil

High Speed Military Rotorcraft

Total Empty Weight . . . . 21836 lb

Take-off Gross Weight . . 27350 lb

Engine Thrust . . . . . 6811.20 lb

Wing Loading . . . . . 73.45 psf

Disk Loading . . . . . 20.00 psf

Rotor Tip Speed . . . . . 700 fps

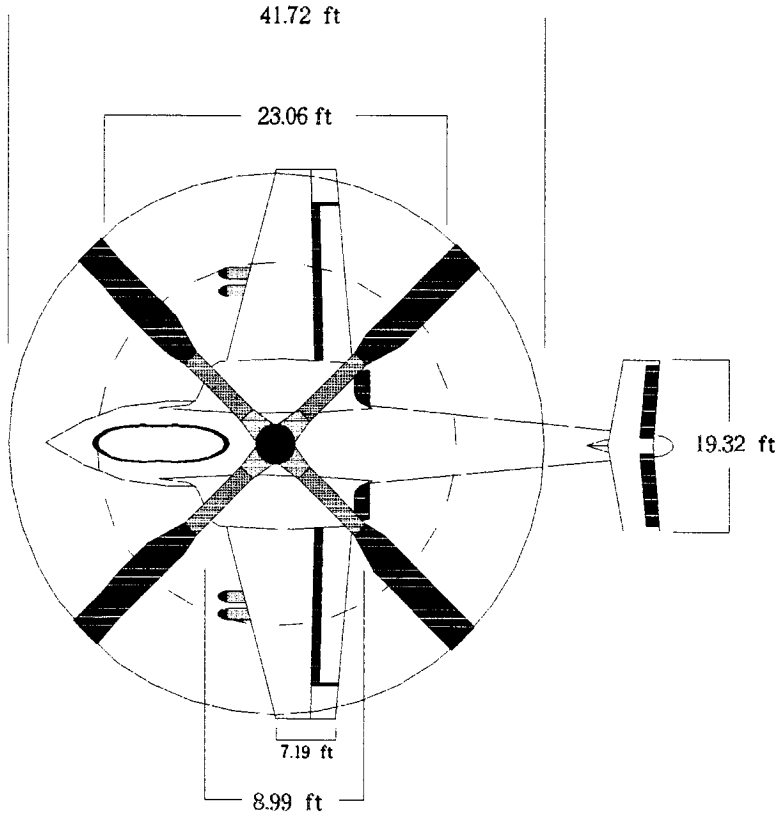

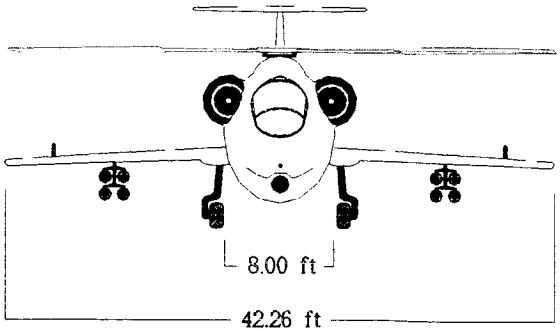

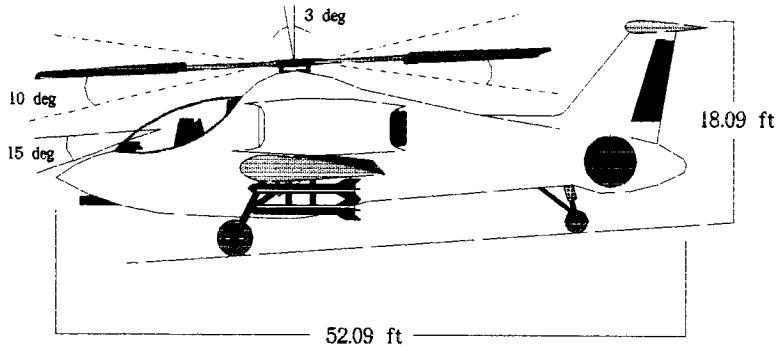

Side View

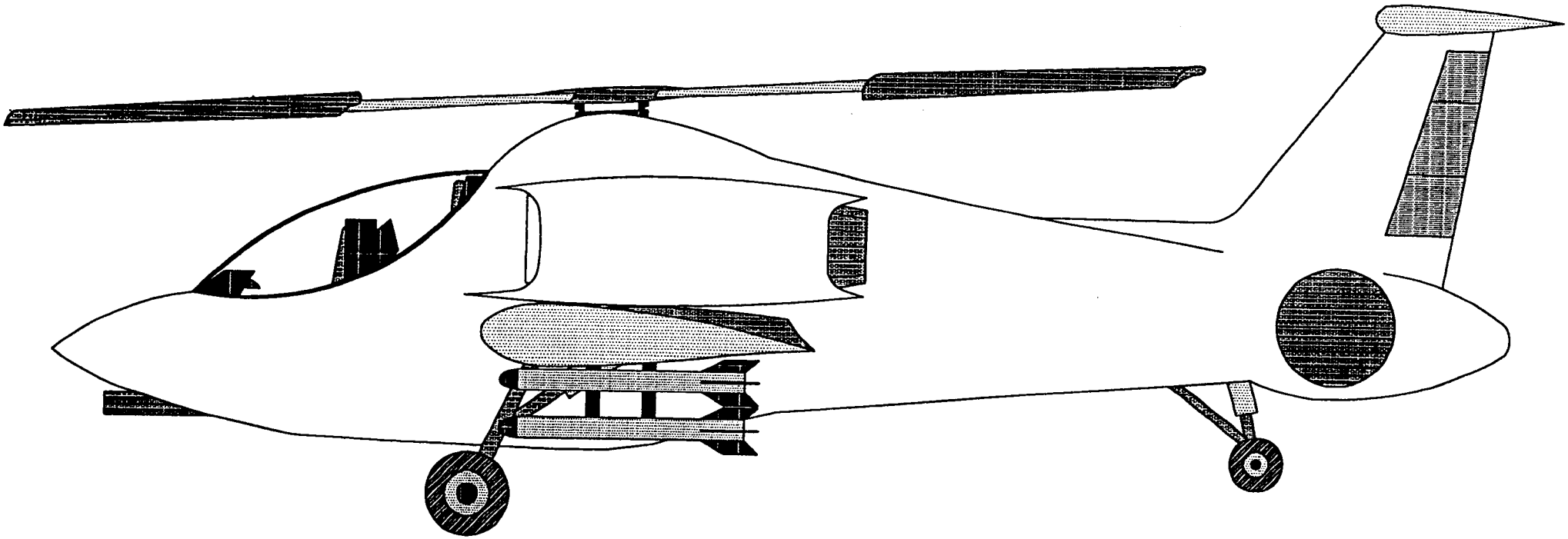

Top View

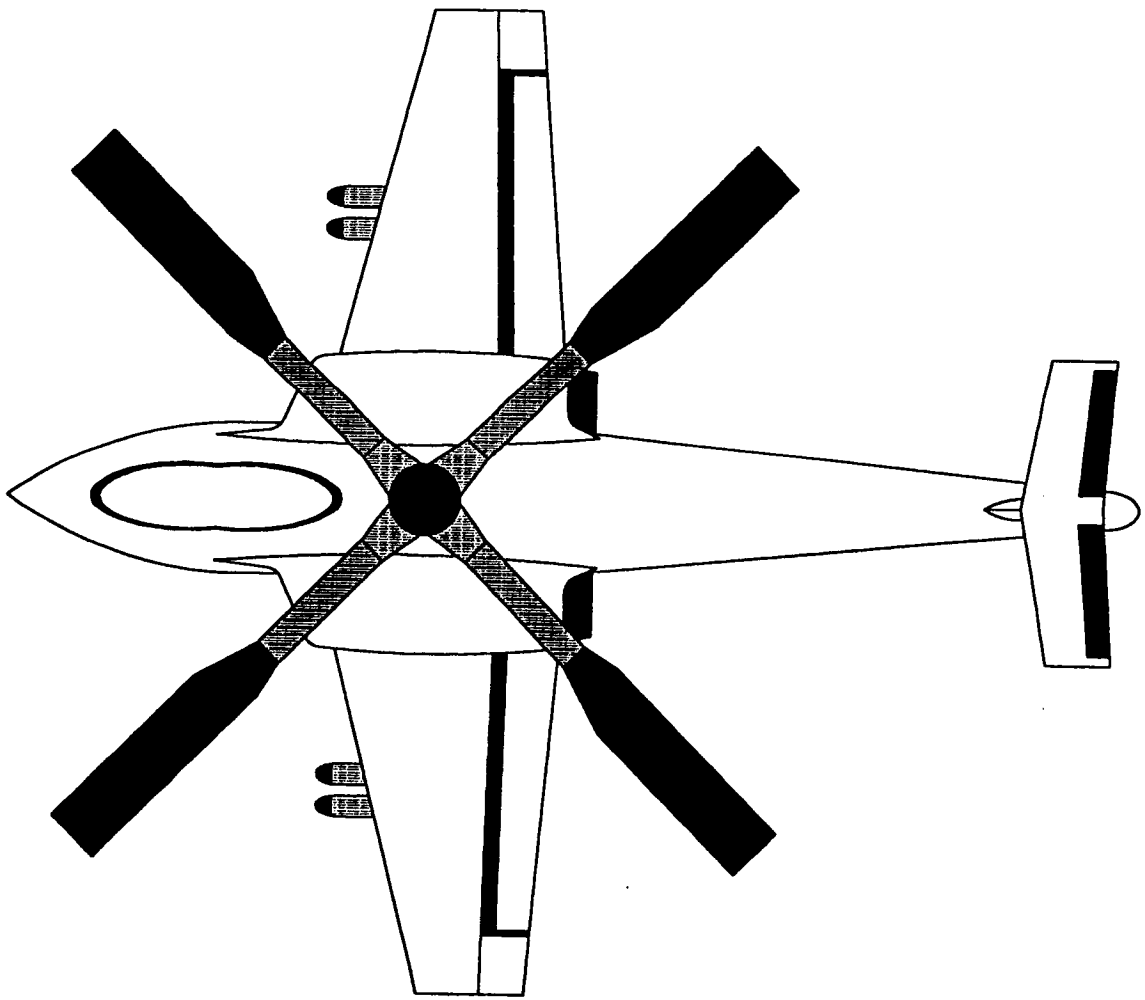

Front View

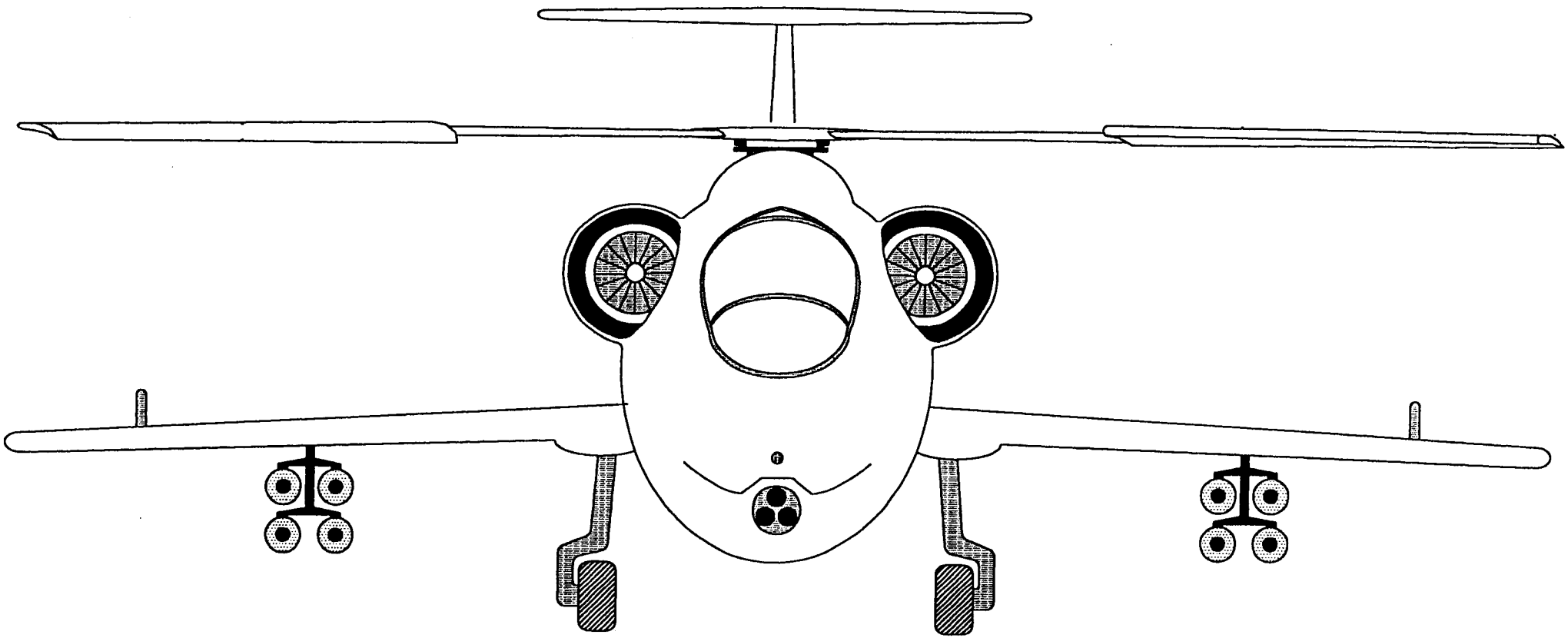

Internal Layout

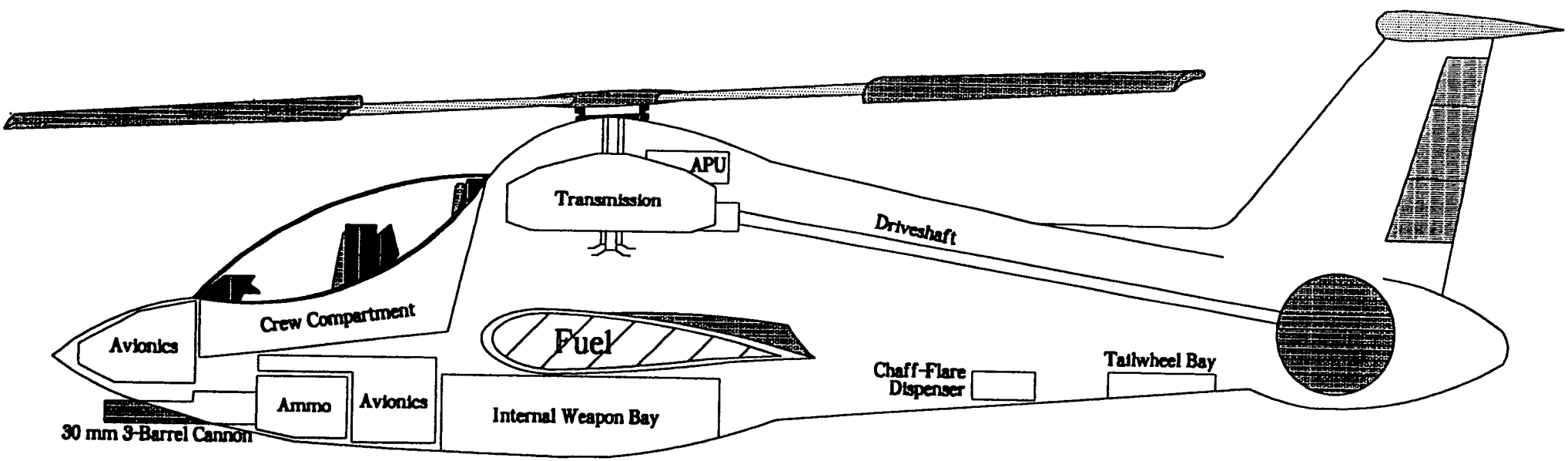

TABLE OF CONTENTS

LIST OF FIGURES

LIST OF FIGURES
(Cont)

LIST OF TABLES

1. INTRODUCTION

A current problem in the United States military aviation is the absence of a high speed rotorcraft. Helicopters provide unmatched maneuverability and precision in ground attack and ground support while also having the versatility to takeoff and land on almost any land surface. However, helicopters have an inherent problem. Because of retreating blade stall and compressibility effects on the advancing blade, current helicopters are limited to speeds around 200 knots.

The fact that the military is cutting their budgets means that they will be looking for a superior aircraft with unprecedented versatility and performance. The days of single-purpose attack aircraft are over; the military needs aircraft which can provide multiple functions and fly many varieties of missions not just adequately, but exceptionally. Also, the military requires aircraft that can accomplish its mission by dropping its ordinance with unsurpassed precision, not by mere quantity.

The AV-95 *Sun Devil* jumps to the forefront of a new wave of aircraft that may sweep across the military in the very near future. The *Sun Devil* is a unique compound helicopter; in the helicopter mode, the *Sun Devil* is basically a compound helicopter, powered by both rotor thrust and jet thrust. However, in the high-speed portions of the mission, the *Sun Devil* retracts its rotor diameter roughly by half and uses the two turbofan engines for thrust; consequently, with the exception of the rotors, the *Sun Devil* performs very much like a conventional, fixed-wing aircraft. The *Sun Devil* is an outstanding attack vehicle because it can fly and attack like today's attack helicopters. However, this aircraft has been optimized to fly at speeds well over twice the speeds of even the fastest helicopters. Among numerous advantages, the *Sun Devil* can strike targets over 1157 mi (1862 km) away without the need of refueling. With the *Sun Devil*'s unmatched performance and versatility, every branch of the military can utilize the United States' newest and unrivaled attack rotorcraft.

This design report discusses the preliminary design and analysis of the AV-95 *Sun Devil*. A conceptual design process was performed to determine the configuration of the aircraft. Then, this configuration is optimized to fit the mission profile, and a design point is found. This design point is then analyzed to obtain the performance characteristics of the aircraft. A graphic representation of the mission profile, Figure 1-1, follows the complete mission profile, Table 1-1.

MISSION PROFILE for a HIGH SPEED ROTORCRAFT

(MILITARY GROUND ATTACK)

- Entire mission at 4000 ft, 95° F
- Take off and HOGE for 1 minute
- Fly to conversion speed and convert to cruise configuration in 1g flight
- Cruise at $V_{99\%}$ for 150 nautical miles
- Dash at 400 knots TAS for 50 nautical miles at IRP
- Convert to hover mode
- NOE maneuver including 15 min HOGE and 15 min at 40 knots
- Attack target at IRP for 5 min without dropping weapons
- Convert to cruise mode
- Cruise at $V_{99\%}$ for 200 nautical miles back to base
- Fly to conversion speed and convert to hover configuration in 1g flight
- HOGE for 1 min
- Land with 10% mission fuel reserve
- Payload is 2000 lb plus 1000 lb external payload
- Weight incorporated into the empty weight of the aircraft:
  - Fixed Equipment . . . . . 2000 lb
  - Mission Equipment . . . . . 2900 lb
  - Crew . . . . . 470 lb
- Other requirements:
  - Sustained g loading . . . . . -0.5, 3.5 (Helicopter)
  - . . . . . -1.5, 5.0 (Fixed Wing)
  - Ferry Mission . . . . . 1260 nmi unrefueled
  - Disk Loading . . . . . Not more than 20 psf
  - Vertical Climb Rate . . . . . 800 fpm

Table 1-1

Graphic Mission Profile Schematic

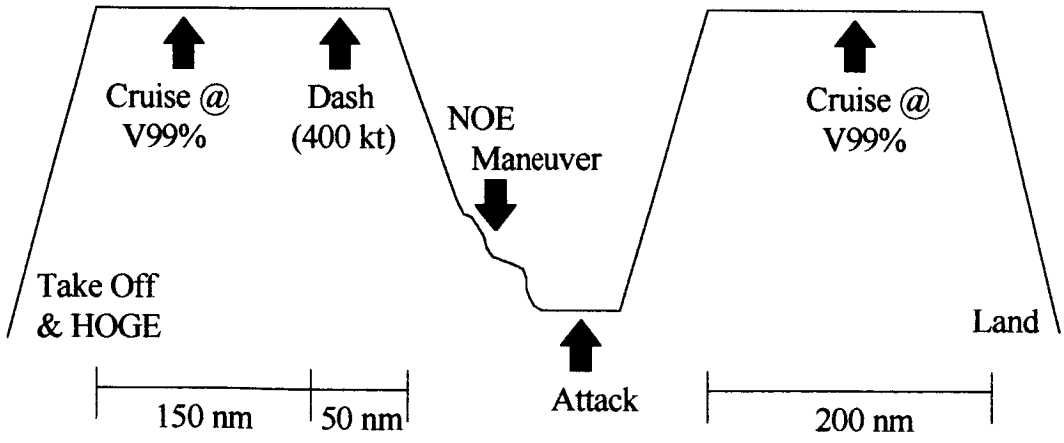

Figure 1-1

2. INITIAL CONFIGURATION SELECTION

When sifting through the many ideas that resulted from brainstorming sessions, the main criterion for choosing the 'best' design was the design that would result in both the best helicopter *and* the best airplane. Because the mission requires the aircraft to fly in rotary-wing mode with the capability to fly like an airplane (as opposed to an airplane that has the capability to fly like a helicopter), more importance was given to the helicopter aspects of each possible design than was given to the airplane aspects. A selection matrix was created to find the best design. Several different types of rotorcraft were considered. Typical mission parameters were chosen and given a weight depending on their importance to the mission. Each rotorcraft was scored in each parameter category. The score was then multiplied by the weight. The total score for each vehicle type was then the summation of all the weighted scores for each parameter. The highest overall score was the best design concept. The selection matrix is shown in Table 2-1. The result is a design that not only demonstrates superior characteristics in the helicopter mode, but it also exhibits many distinguishing attributes in the airplane mode.

The design that was finally chosen is basically a winged, attack helicopter. When in the helicopter mode, the aircraft will fly much like a general attack helicopter with two primary exceptions. The first exception is the addition of wings. Second, our aircraft design will have two thrust sources; one source is the main rotor while the second source is the two turbofan engines.

The addition of wings has many advantages. First, the wings will make the attack helicopter more maneuverable than a similar attack helicopter without the wings.

Moreover, the addition of wings will help in the production of lift, thereby delaying some of the high-speed rotor complications. With large tip speeds, retreating-blade stall and advancing-blade compressibility effects may occur. With the addition of a wing, however, the rotor is not required to produce as much lift. Other advantages that arise from the addition of wings include extra fuel space, external storage space and, possibly, landing gear housing.

However, the addition of wings also has some disadvantages. The main disadvantage of a winged helicopter is the downwash from the rotor on the wings. A second disadvantage of the added wings is the increased weight that accompanies them. Another possible disadvantage occurs if the wings produce too much lift, thereby excessively off-loading the rotor. This will result in vibration problems in the rotor blades. However, the many advantages of a compound helicopter far outweigh the disadvantages.

The method in which this aircraft is propelled is somewhat unique. In the helicopter mode, the main purpose of the engines is to drive the main rotor and tail fan. However, if this does not require the maximum power of the engines, the resulting available power can be used as thrust. In the airplane mode, the engines provide thrust just like those of a normal airplane, with the exception of a little power set aside to power the rotor for minimum drag. The main advantage of this is the increased performance of the aircraft in the helicopter mode. The engines not only allow the helicopter to fly faster, but it also delays some of the high-speed rotor complications as less rotor thrust is required. Therefore, this reduction in tip speed delays the high-speed rotor

complications. Some disadvantages include increased weight and drag due to the larger engines. Again, though, the advantages of this propulsive method far outweigh the disadvantages.

Selection Matrix

	Weight	Tilt Fan	Tilt Rotor	Vairiable Diameter Rotor	Stop Rotor	Tilt Wing	Fan in Wing	Folding Tilt
Conversion Time	6	4	3	5	1	3	5	2
	Wt. Avg	24	18	30	6	18	30	12
Gross Weight	7	3	1	3	3	2	3	1
	Wt. Avg	21	7	21	21	14	21	7
Combat	10							
Weapons		2	3	5	5	1	2	4
Speed		2	3	5	4	1	5	3
Manuverability		2	2	4	3	1	3	2
Survivability		1	2	4	1	2	4	2
Pilot Visibility		2	3	4	4	3	2	3
	Avg	2	2.75	4.5	4	1.5	3	3
	Wt. Avg	20	27.5	45	40	15	30	30
Stability	6	2	4	3	2	4	2	3
	Wt. Avg	12	24	18	12	24	12	18
Propulsion Efficiency	4	1	4	4	3	2	1	3
	Wt. Avg	4	16	16	12	8	4	12
Aerodynamics Efficiency	6							
Aircraft		1	2	4	4	2	4	3
Helicopter		4	4	4	3	2	1	4
	Avg	2.5	3	4	3.5	2	2.5	3.5
	Wt. Avg	15	18	24	21	12	15	21
Complexity	6	5	4	2	3	4	3	3
	Wt. Avg	30	24	12	18	24	18	18
General	3							
Looks		3	5	4	4	1	2	4
Technology		4	3	3	3	3	3	2
	Avg	3.5	4	3.5	3.5	2	2.5	3
	Wt. Avg	10.5	12	10.5	10.5	6	7.5	9
Totals		**136.50**	**146.50**	**176.50**	**140.50**	**121.00**	**137.50**	**127.00**
% Totals		**77.34%**	**83.00%**	**100.00%**	**79.60%**	**68.56%**	**77.90%**	**71.95%**

Table 2-1

3. SIZING METHODOLOGY

3.1 Plan

The sizing method begins with the selection of an overall configuration. This layout is based upon the needs of the mission profile along with aesthetic and performance characteristics determined by personal taste and design parameters for aircraft with similar missions. With the overall configuration in place, the sizing process begins. Because many of the parameters that are needed to reach a design point are only determined after the design point has been reached, this process is iterative and converges upon a final design point. Aircraft geometry, performance parameters, engine characteristics and weight and propulsion analysis all combine to establish a "design point" for the vehicle. By varying initial design variables, different design points can the reached; these different design points are compared on carpet plots. The carpet plots with known constraints lead to the final design selection. The following sections explain the sizing process in greater detail.

3.2 Code Development

The sizing code was developed using FORTRAN due to the iterative process. A flow chart of the algorithm is shown in Figure 3-1. The equations used in the code are from several sources. The Raymer (1992) text is the main source, and other equations come from VASCOMP, Prouty (1986) and Stepniewski (1984) as well as derived results. The following design variables control the program: initial gross weight guess (GWG), disc loading (GWG/A_d), rotor tip speed (V_T), conversion speed (V_{con}), maximum lift coefficient for the wing ($C_{L_{max}}$), aspect ratio (AR), design average rotor lift coefficient (C_L) and maximum load factor (N_U). These initial conditions were needed to start the sizing process.

Sizing Algorhythm

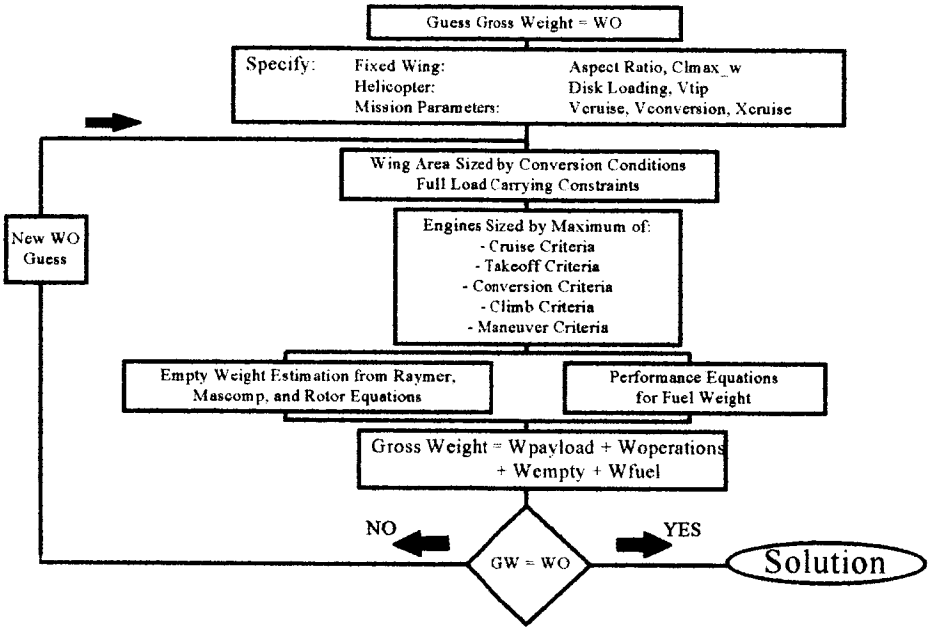

Figure 3-1

The wing is sized by cruise with zero fuselage angle of attack and no flap deflection. The wing area (S_W) is the reference area (S_{REF}) that is used many times throughout the code. After the wing area is found, the rest of the aircraft geometry is calculated, much of it based partly on the S_{REF}. The rotor radius can be found from the disc loading, and the wing loading results are calculated from S_W and GWG. The C_L gives C_T/σ which in turn is used to calculate the blade area (A_b) and chord length (C_R). V_T gives rotor RPMs (W_R) which is used in determining engine sizing. All of the initial design variables contribute to developing geometric and performance parameters needed for sizing the aircraft.

With the geometry calculation completed, the code next scales the engine. Three flight modes are considered to find which was the most critical: Vertical Climb, Dash and Maneuver. The mode that requires the most power will size the engine. The equations used for this process are derived using the provided baseline engine

engine deck provides thrust at different throttle settings as a function of Mach number and turbine inlet temperature. These values were then related to fuel flow rates. With the sizing of the engine, a scaling factor is determined. This factor scales the engine weight and dimensions as well as the fuel flow rates to the appropriate values needed to provided the critical power requirements.

Once the engine has been sized the structural weight equations determine the weight of the various aircraft components that contribute to the empty weight. The equations are statistical, based upon a database from similar aircraft. Since the considered configuration does not cleanly fall into one type of aircraft category, the equations are altered to reflect the differences between this design configuration with the aircraft type that the equation is based upon.

The next task in the sizing process is to determine the fuel consumed. This process is an involved process which requires calculating the parasite drag for each aircraft component for each mission segment, the induced drag for the entire aircraft and the rotor drag. When the drag is found, the power needed to perform that segment is then calculated. That required power is used as an input for a propulsion routine which returns a fuel flow rate. The fuel weight could then be determined from the fuel flow rate and the time required to fly that segment, which is found from the mission profile. After each segment, the fuel required to fly it is subtracted from the total weight so as to provide realistic modeling of the mission.

The last part of the sizing is the summing of the fuel weight, the empty weight and the fixed equipment and useful load weights, of which the last two were provided by the mission profile. This calculated weight is then compared to the original weight guess. If they are equal, a design point has been reached. If they are not equal, the calculated weight replaces the original weight guess weight and the process starts over.

3.3 Carpet Plots

The carpet plot is based on values provided by the code and is analyzed and plotted using a spreadsheet. The plot is of gross weight versus disc loading with lines of constant wing loading at a constant aspect ratio and tip speed. The disc loading is varied from 10 lb/ft^2 to 40 lb/ft^2, and the wing loading is varied from 60 lb/ft^2 to 140 lb/ft^2. The disc loading is varied through these values because, at lower and higher values, the weight increases and the code becomes unstable. The carpet plot used to find the final design point is shown in Figure 3-2 The main constraints are also displayed on these figures.

The disc loading (W_D/A_d) cannot exceed 20 lb/ft^2 as stated in the mission profile; this is to allow crewmen to work on the vehicle while it is on the ground. If the disc loading were greater, too much down loading would be created for crews to work. The rotor tip speed (V_T) could not exceed 750 fps; this is due to the fact that too much noise is created from shock waves on the rotor tips at higher tip speeds.

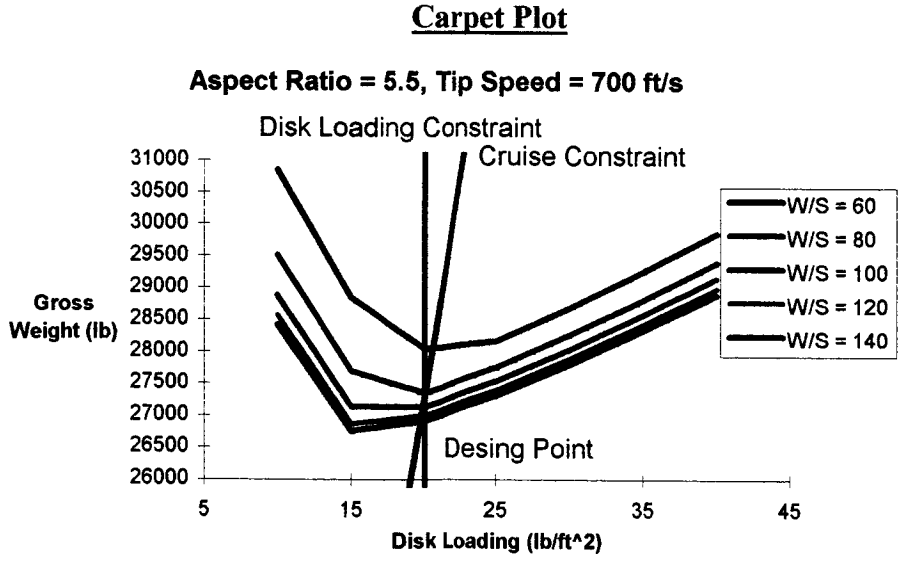

Figure 3-2

3.4 Conclusion

The sizing code demonstrates the effects that varying the design parameters have on the weight of the aircraft. By increasing aspect ratio (AR) and tip speed (V_T), the weight of the aircraft can be lowered. However, the weight can only be lowered to a certain point by this procedure; this is because there are constraints on the upper bounds of these variables due to physical considerations and mission profile requirements. Using the design code and the carpet plots with constraints, a final design point was selected; the rotor tip speed is 700 ft/s, and the downloading is the maximum 20 psf, as stated in the mission profile. The aspect ratio is 5.5; however, this value was chosen in the circulation control analysis. The values of these parameters result in a gross weight of 27,350 lbs.

4. DRAG BREAKDOWN

The parasite drag of the *Sun Devil* is determined using a component method. Wetted area (S_{WET}), skin friction coefficient (C_f), form factor (FF) and equivalent flat plate area (EFPA) are calculated for each component. Fifteen percent is added to the equivalent flat plat area to account for leakage and interference between components. The breakdown for cruise is found in Table 4-1. Included are the parameters stated above as well as the total parasite drag coefficient, the induced drag coefficient, the total drag coefficient, the rotor drag in cruise and the total drag encounter for those segments. The total flat plate area is 11.953 ft^2 for cruise, and the drag coefficient is 0.0221.

Drag Breakdown in Cruise

	S_{WET}	C_f	FF	EFPA
Wing	658.57	0.00198	1.318	2.626
Fuselage	1176.58	0.00186	1.140	2.499
Horiz. Tail	175.91	0.00247	1.493	0.641
Vert. Tail	26.53	0.00281	1.572	0.149
Canopy	18.75	0.00237	1.948	0.871
Nacelle	196.29	0.00250	1.525	0.972
Hub	45.78	0.00237	1.456	1.721
Rotor				0.915

Total 10.394

+ 15% for leakage and protuberances: 1.559

Total Flat Plate Area: 11.953

Induced drag coefficient 0.0024

Parasite drag coefficient 0.0160

Total drag coefficient 0.0221

Rotor Drag in Cruise (lb) 143.4

Total Drag in Cruise (lb) . . . . . 3956.4\

Table 4-1

5. PERFORMANCE

The following sections describe the performance characteristics of both the fixed-wing aircraft mode and the helicopter mode. As can be seen from the following data, the *Sun Devil* has exceptional fixed wing and helicopter performance.

5.1 Fixed-Wing Mode

One of the primary mission requirements is that the *Sun Devil* must be capable of 400 knots at IRP during the dash segment of the mission. The *Sun Devil* exceeds this requirement with a maximum velocity of 470.5 knots at IRP. The other major requirement for the *Sun Devil* involves the range. The *Sun Devil* attains a range of 1006.1 nautical miles (1863.30 km) using only its maximum internal fuel. In ferry configuration with internal stores replaced by 500 lbs of fuel and two 500-lb tanks suspended from the wing hardpoints, the *Sun Devil* can fly approximately 1489.95 nmi (2759.38 km) un-refueled. Table 5-1 provides a list of all of the fixed wing performance parameters.

5.2 Helicopter Performance

The helicopter performance is crucial to the *Sun Devil*'s mission because the attack phase will be performed in helicopter mode. The mission requires a vertical rate of climb (VROC) no less than 800 fpm. In designing the *Sun Devil*, it was found that this requirement sized the engine. Therefore, the *Sun Devil*'s VROC is 800 fpm (13.3 fps). Due to the winged configuration of the aircraft, download on the wing is a major concern since downwash directly impacts on the wing. Comparing typical downloading values for tilt rotors, the download on the wing for the *Sun Devil* in hover is estimated at 12% of the gross weight, which results in a load of 3282 lb. To decrease the download on the wings, the flaps may be rotated 180 degrees so that the flap area is effectively taken out of the rotor wash. However, the use of the circulation control during helicopter mode should further reduce the download on the wings; future research such as wind tunnel

tests is needed to show how much of a reduction a blown flap may have in the download on a wing.

Performance Data for the AV-95 Sun Devil *fixed-wing mode @ 4000 ft, 95 º F*	
Emax	10.58
Oswald Efficiency Factor (e)	0.801
Wing Loading (psf)	74.77
V_{stall} (kt)	77.45
V_{TO} (kt)	94.80
d_{TO} (ft)	1017.92
$V_{99\%}$ (kt)	228.41
V_{max} level flight (kt)	470.50
V_{dive} (kt)	588:13
Service Ceiling (ft)	37823.62
Best Range @ $V_{99\%}$ (nmi)	1006.05
Ferry Range @ $V_{99\%}$ (nmi)*	1489.95
Steepest Climb (deg; $\alpha_{fuselage}$)	13.55
Steepest Climb Velocity (kt)	195.13
Fastest Climb (deg)	8.87
Maximum Rate of Climb (fpm)	4773.92
Max Bank Angle (deg)	78.46
Maximum Turn Rate (deg/s)	15.84
χ_{TT} (deg/s) @ 5g	51.18
r_{TT} (ft) @ 5g	988.61

* Ferry Range fuel augmented by an internal 500 lb tank and two external 500 lb tanks suspended from hardpoints.

Performance Data for the AV-95 Sun Devil *helicopter mode @ 4000 ft, 95o F*	
Vertical Rate of Climb (fps)	200
Wing download (% GW)	12
Wing download (lb)	3282

Table 5-1 Performance Data for AV-95 Sun Devil

The V-n diagram, located in Figure 5-1, is an efficient way to explain many of the impressive performance features of the AV-95. The *Sun Devil* has required load factors of 5 and -1.5. With a factor of safety of 1.5, the ultimate load factors become 7.5 and -2.25. Moreover, due to the circulation control system, the AV-95 is able to produce sufficient lift at very low velocities. Consequently, the *Sun Devil* has a stall velocity of only 77 knots. Finally, the maximum dive velocity of this aircraft was calculated to be 584 knots; however, this does not include compressibility effects. Moreover, Sikorsky had performed tests on the telescoping rotor system that reached speeds just over 400 knots. As a result, further tests are needed for a such a rotor system at velocities over 400 knots.

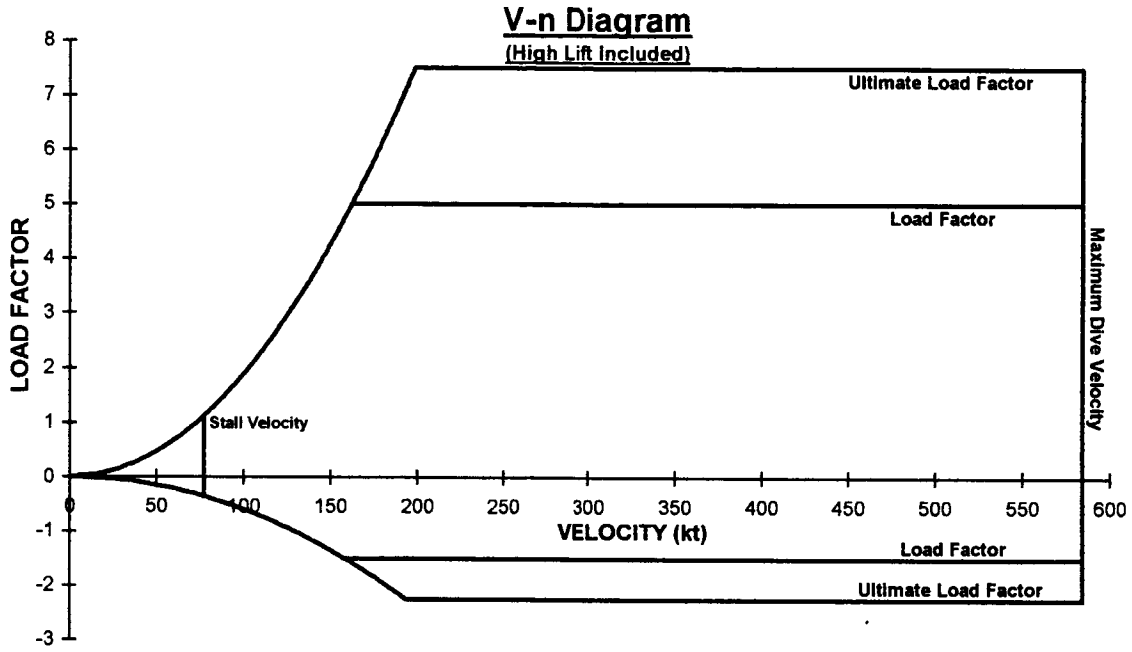
V-n Diagram
(High Lift Included)
Ultimate Load Factor
Load Factor
Maximum Dive Velocity
Stall Velocity
LOAD FACTOR
VELOCITY (kt)
Load Factor
Ultimate Load Factor
8
7
6
5
4
3
2
1
0
-1
-2
-3
0
50
100
150
200
250
300
350
400
450
500
550
600

Figure 5-1

6. PROPULSION

6.1 Engine Deck

The propulsion system for the AV-95 *Sun Devil* consists of two convertible turbofan engines. In cruise mode, these engines perform much like ordinary turbofan engines, but some power is needed to keep the rotors slightly powered. In helicopter mode, however, the power produced by the two engines are divided into several functions. Most of the power is used rotate the variable-diameter main rotor. Also, some power is required to power the ducted tail fan. The engine power can also be split for all functions, powering the main rotor shaft, the tail fan and providing jet thrust. This flexibility becomes important when flying at very low speeds in helicopter mode.

6.2 Engine Sizing

The convertible engines used for this rotorcraft design are sized using a provided engine deck. Along with other parameters, this engine deck gives values of the turbine inlet temperature at Maximum Continuous Thrust (MCT) and at Intermediate Power Rating (IRP). However, this engine deck is not equipped with a Contingency setting.

The first step to size the engine is to determine which segment of the mission will require the most power, or thrust; this is the segment that sizes the engine. Among the many required segments of the AV-95, one of the following three segments scales the engine:

1. Vertical climb at 800 feet per minute at MCT
2. Dash at 400 knots at IRP
3. 5 g maneuver at 1.3 times the stall speed at MCT

Using the drag subroutine and aircraft performance equations, the thrust required at each of these three segments is calculated. To find a scaling factor, the thrust from the

engine deck at the corresponding Mach number is needed. Therefore, a linear fit for Mach number versus the thrust at either Maximum Continuous Thrust or Intermediate Power Rating is created. The Mach number for each segment is set as the input, and the engine deck thrust is the output. Therefore, three scaling factors are calculated by dividing each engine deck thrust into the corresponding thrust required. Of these three scaling factors, the largest scales the engine; consequently, the corresponding segment requires the most thrust. Once the engine thrust has been scaled, physical dimensions of the engine are then scaled using scaling curves provided with the engine deck; these parameters include the diameter of the air intake and the overall length and the weight of the engine.

At this point, the mass flow rate of the fuel needs to be calculated at any given thrust required, or throttle setting. Therefore, linear regressions are made for the given values of the original engine deck. The first set of linear curves is created so that when the required thrust is set as the input, the output would yield the turbine inlet temperature. Numerous linear curves are created for Mach numbers ranging from 0.0 to 0.8 with a Mach number interval of 0.1. Then, a second set of linear regressions is made. The input to this set is the turbine inlet temperature that was just obtained from the first set of linear regressions. The output for the second set of linear curves is the fuel mass flow rate. Similarly, numerous linear regressions are made for the previously mentioned range of Mach numbers.

To find the mass flow rate of the fuel at any given throttle setting, the thrust at this throttle setting is first scaled back up to the engine deck using the same scaling factor. This thrust value is then used for the input into the first set of linear regressions, and a turbine inlet temperature is calculated. This turbine inlet temperature value is then used for the input into the second set of linear regressions to find the corresponding fuel mass flow rate. However, this fuel mass flow rate corresponds to the scale of the engine deck.

To obtain the mass flow rate of the fuel corresponding to the scaled engine, this fuel mass flow rate is scaled back down by the same scaling factor.

6.3 Specific Range and $V_{99\%}$

According to the mission profile, the rotorcraft must fly at $V_{99\%}$ at two different instances. $V_{99\%}$ is defined as the speed at 99 percent of the best, or maximum, specific range. The best range speed corresponds to the speed at which the specific range is maximum. It is important to note, however, that $V_{99\%}$ in not 99 percent of the best range speed. The specific range is found by dividing the velocity by the corresponding fuel mass flow rate.

A complex iteration process was developed as a subroutine in the design code to find this speed. The first step was to pick a velocity that is below the best range velocity. At this velocity, the drag was found using aerodynamic equations. Because the aircraft is cruising at $V_{99\%}$ in both instances, the drag must be equal to the thrust. Knowing the thrust, the fuel mass flow rate was found using the same process as previously described. Then, the specific range at this velocity was calculated by dividing the fuel mass flow rate into the velocity. Then, the velocity was incremented by a small amount, and the specific range at this velocity was found in the same manner. This iteration was performed until the specific range reached a maximum.

The maximum specific range is now known, so 99 percent of this value was found. The above iteration used to find maximum specific range was then repeated. However, the best range velocity plus an even smaller increment was then chosen as the starting point; by adding small increments to the maximum specific range velocity, the greater of the two possible $V_{99\%}$ was found. This process was performed until the specific range was equal, or nearly equal, to the known value of 99 percent of the

maximum specific range. The velocity which yields 99 percent of the maximum specific range is $V_{99\%}$.

7. STRUCTURES

7.1 Overview

The AV-95 *Sun Devil's* overall structure is that of a conventional fixed wing aircraft, with the exception of the variable diameter rotor system. Currently, structural analysis has been directed towards the aircraft's wing, landing gear system and rotor shaft(s). These structural components are designed to endure the loading generated by both the helicopter and airplane flight modes.

The wing is mid-mounted to provide easy access to the hardpoints and fuel tanks, and reinforced at the root to provide platforms for ground crew when servicing the engines. Its placement also allows for the use of the internal weapons bay. The carry-though structure is the typical box type, with the wing box continuing through the fuselage. This keeps the fuselage from being subjected to the bending loads of the wing, helping to minimize fuselage weight. The carry-through structure also helps support the transmission weight by providing attachment points for transmission supports.

7.2 Flight Loads

The first step in the design of the structural components involved determining the load distribution acting on the wings. Each side of the span will experience half of the total loading. The structural loading is a result of the lift generated by the wings, the weight of the structure, the weight of the fuel and the placement of external stores on the wing hard points.

In the ground attack mission profile, there are several loading conditions that could dictate the structural requirements of the AV-95. After examining the mission, the +5.0g maneuver requirement was found to be the highest loading that the AV-95 must endure. For reasons of safety, a 1.5 factor of safety was employed resulting in a maximum loading of +7.5g. It is for this loading that the wing was sized.

The lift for the span was determined using Schrenk's approximation for lift distribution on tapered planforms. This rule states:

> ...the distribution of the lift associated with the chord distribution without twist, is nearly proportional at every point to the ordinate that lies halfway between the elliptical and actual chord distributions for the same total area and span (Keuthe and Chow, p164-65).

The following two equations describe the lift on the span

$$L'_a = \frac{1}{2}\left[c + c_{sE}\sqrt{1-\left(\frac{y}{b/2}\right)^2}\right]\frac{L}{S}$$

$$c'_{l_a} = \frac{1}{2}\left[1+\frac{4}{\pi}\frac{\bar{c}}{c}\sqrt{1-\left(\frac{y}{b/2}\right)^2}\right]$$

where c is the *actual* chord and c_{sE} is the chord at the plane of symmetry for the elliptical planform of the same area and span. The overall effect of the tapered planform is to increase the load in the outboard portion above that which would occur if the additional lift were proportional to the chord. This method remains conservative for taper ratios close to 1/2, but becomes unconservative with taper ratios below 1/2. The taper ratio chosen for the AV-95 is 0.4. This is a typical value for fighter-attack aircraft, and is

consistent with this approximation. Figure 7-1 illustrates this loading on the aircraft wing-

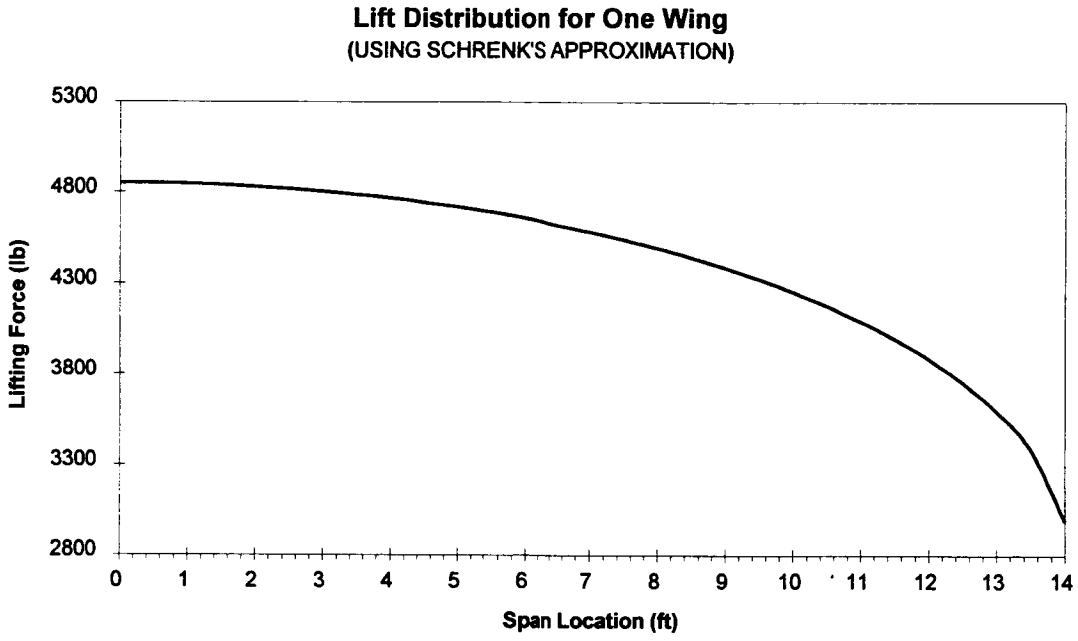

Figure 7-1 Spanwise Lift Distribution

The next two load categories, structural and fuel weight, were determined by first calculating area and volume functions for the wing section- These equations are based on the root and tip chord of the wing, integrated across the span- Then, the weight of the fuel and the structure were modeled according to this function- Figures 7-2 and 7-3 show the load curves for these components of the loading.

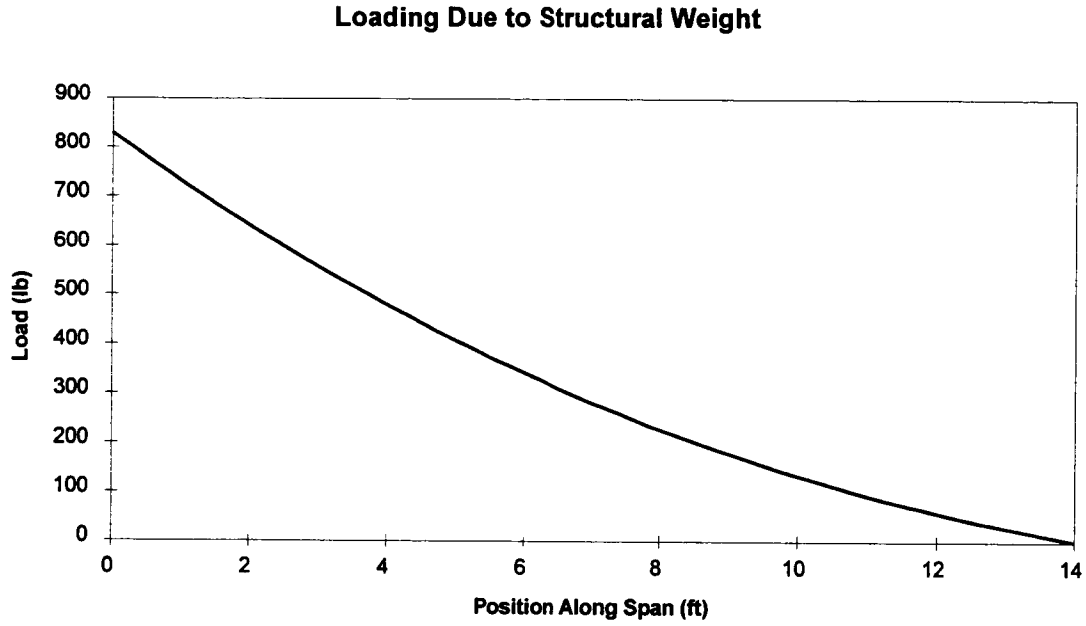

Figure 7-2 Spanwise Loading due to Structural Weight

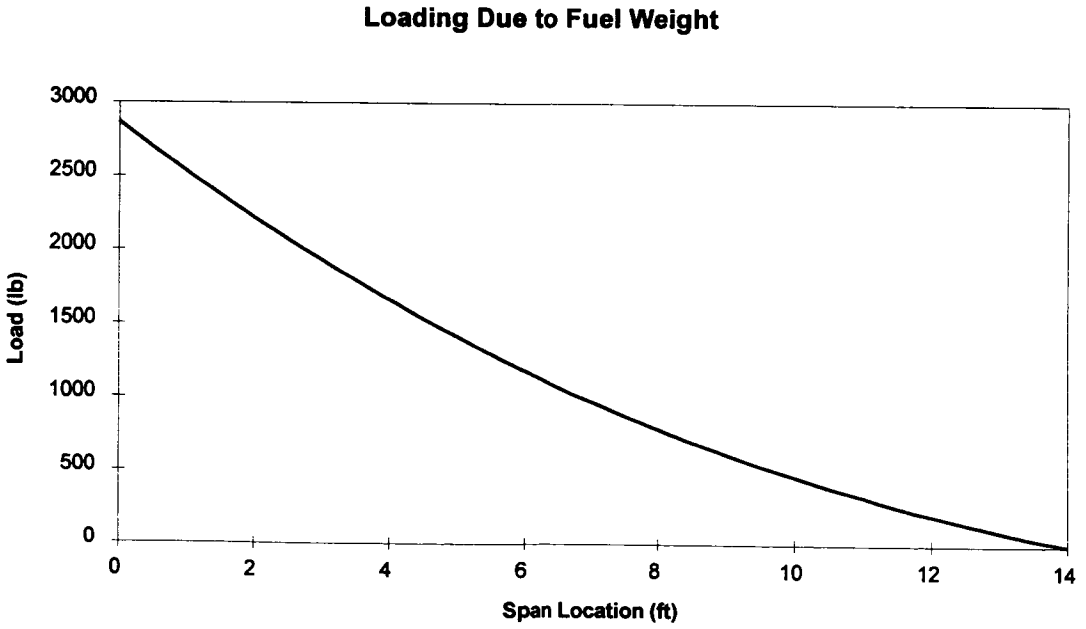

Figure 7-3 Spanwise Loading due to Fuel Weight

The loads due to the placement of external stores and the attachment of the landing gear to the wing were considered point loads and were included in the bending moment equation as such. After determining all of the load categories, the bending moment equation was determined for the loading on the wing. The resulting moment on the wing is depicted in Figure 7-4.

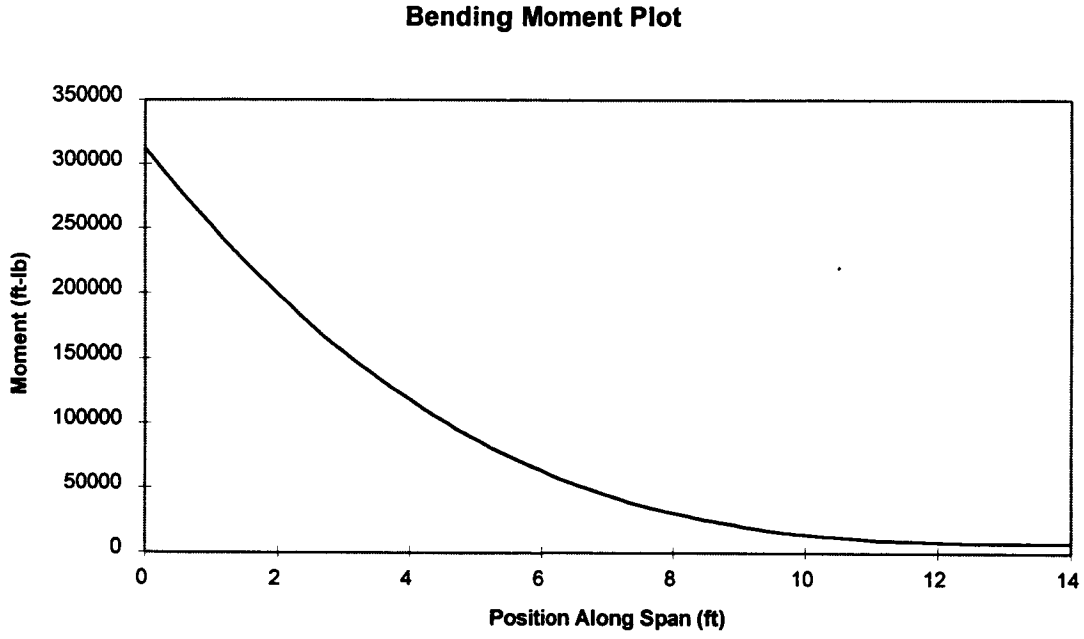

Figure 7-4 Bending Moment on Main Wing

7.3 Wing Box Layout

Once the loading on the main wing had been determined, the configuration for the spar caps and stiffeners was selected. The layout chosen places L-shaped spar caps at the 10%, 30%, 50% and 70% locations with two Z-section stiffeners evenly spaced on each panel between the spars as shown in Figure 7-5.

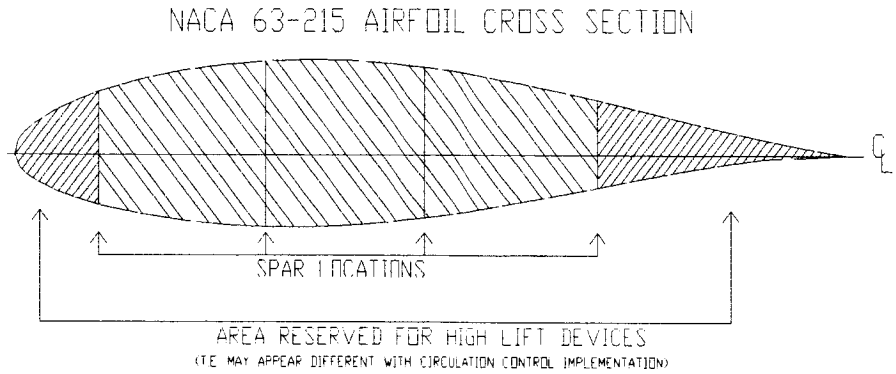

Figure 7-5 Wing Cross Sectional Layout

The wing box, or the area from 10% chord to 70% chord, was considered to be the load carrying portion of the wing and was the center of the analysis. Figure 7-6 depicts the cross sectional layout of the wing box.

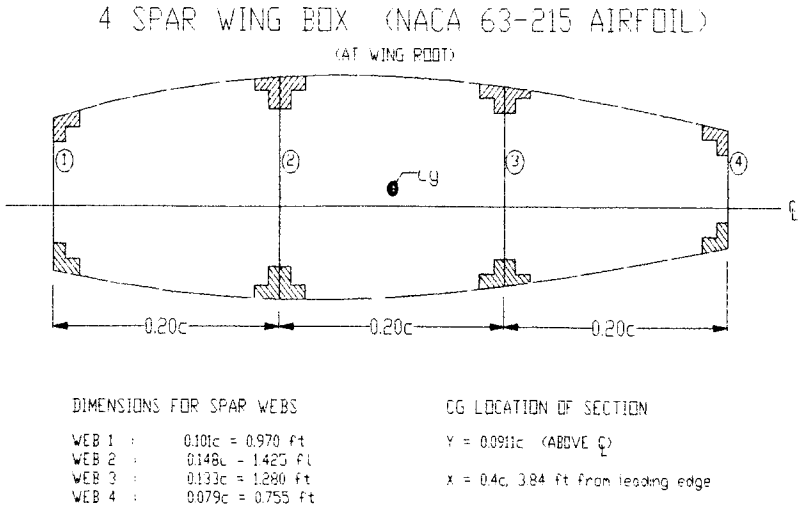

Figure 7-6 Wing Box Layout

Once the dimensions of the wing box and the locations of the structural members had been determined, a workbook was created using Microsoft Excel and the analytical techniques set forth in Bruhn's Analysis and Design of Flight Vehicle Structures to model the structural components and determine the characteristics of each member. The formulas for the constants which appear in the spreadsheet are as follows:

$$K1 = \frac{Ixz}{\left(IxIz - Ixz^2\right)}$$

$$K2 = \frac{Iz}{(IxIz - Ixz^2)}$$

$$K3 = \frac{Ix}{(IxIz - Ixz^2)}$$

It was then possible to calculate bending stresses using the following equation:

$$\sigma_b = -(K_3 M_Z - K_1 M_X)x - (K_2 M_X - K_1 M_Z)z$$

$$\sigma_b = \frac{P}{A}$$

Upon obtaining values for the bending stress in each member, it was necessary to check for buckling of the skin panels. With a rib spacing of 18 in., the following formula was used.

$$\sigma_{cr} = \frac{\pi^2 E k_c}{12(1-\nu^2)} \frac{t^2}{a^2}$$

where a = rib spacing
t = skin thickness
E = Young's Modulus
ν = Poisson's Ratio
k_c = 4.0 (simply supported edges)

The values for the thickness were then adjusted in the spreadsheet to make sure that the bending stress in the panels did not exceed the critical buckling stress.

The next phase of the wing analysis involved analyzing the crippling stress of the stiffeners and sparcaps. To carry out this analysis, Gerard's method was used

spar caps: $$\sigma_{cs} = 0.56\sigma_{cy}\left[\frac{gt^2}{A}\sqrt{\frac{E_c}{\sigma_{cy}}}\right]^{0.85}$$

stiffeners: $$\sigma_{cs} = 3.2\,\sigma_{cy}\left[\frac{t^2}{A}\left(\frac{E_c}{\sigma_{cy}}\right)^{1/3}\right]^{0.75}$$

These values were then checked to make sure the method was valid

spar caps: $\sigma_{cs} < 0.7\sigma_{cy} \Rightarrow \sigma_{cy} = 23.9ksi$
stiffeners: $\sigma_{cs} < 0.9\sigma_{cy} \Rightarrow \sigma_{cy} = 23.9ksi$

This analysis was carried out for every 5 percent of the wing span from root to tip; this determined the taper of the spar cap areas, stiffener areas and skin thicknesses taper.

The final dimensions for the wing are presented in Table 7-1 and the skin thickness taper in Figure 7-7.

Final Wing Design Data

SPAR CAP AREA:	1.75 $in.^2$	**SPAR CAP LOCATIONS:**	0.10c,0.30c,0.50c,0.70c
(ROOT)			
(TIP)	1.00 $in.^2$	**STIFFFENER LOCATIONS:**	0.167c,0.233c
STIFFENER AREA:	0.60 $in.^2$		0.367c,0.433c
(ROOT)			
(TIP)	0.25 $in.^2$		0.567c,0.667c
RIB SPACING:	18.0 in.		
WEB THICKNESS:	0.25 in.		
WING AREA:	372 $ft.^2$		
WING SPAN:	45.0 ft.		
(LIFT BEARING)	14.0 ft.		
WEIGHT OF WING STRUCTURE:	1001.55 LB		

Table 7-1

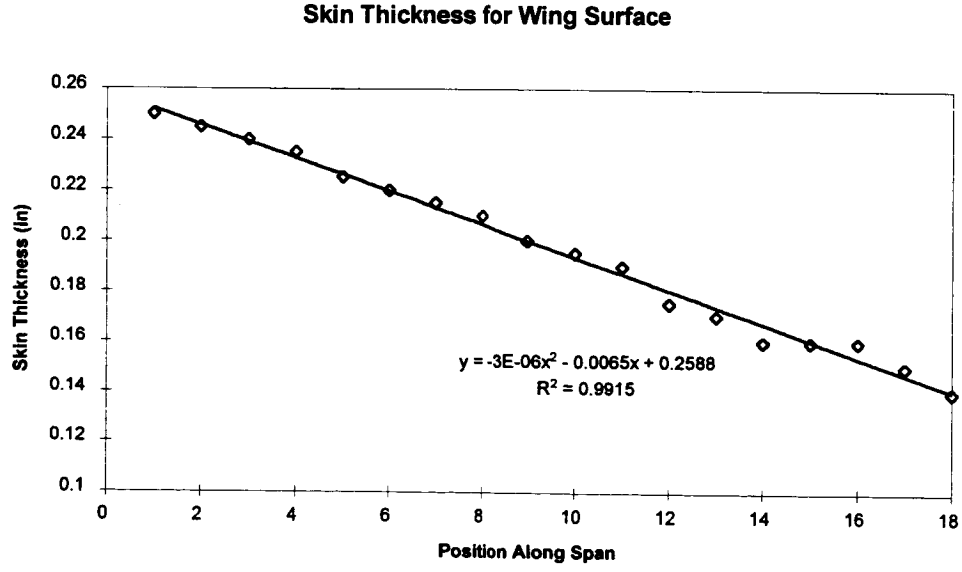

Figure 7-7
(equation is based upon a second order curve fit)

7.4 Material Selection

In order to minimize structural weight, graphite-epoxy composites are the primary material used in the construction of the wing. The only components that utilize other materials are those associated with the circulation control system. This is necessitated by the higher temperatures that exist due to the jet blowing over the coanda surface and the flap. Table 7-2 and Table 7-3 list the various material properties used in analysis and the components for which they are used.

Material Properties

MATERIAL	FIBER VOLUME (%)	PLY ORIENTATION (deg)	DENSITY (lb/in^3)	TEMP LIMIT (F)	F_{tu} (10^3 psi)	F_{cu} (10^3 psi)	E_c (10^6 psi)
Titanium Ti-4Al-6V	n/a	n/a	0.160	750	160	154	16.0
High Strength Graphite/Epoxy	60	±45	0.058	350	23.2	23.9	2.34

Table 7-2

Material Uses

MATERIAL	USE
Titanium	Circulation Control components, Coanda surface, flap retraction mechanism
Graphite/Epoxy Composite	Wing structure (spars, stiffeners, skins), control surfaces

Table 7-3

7.5 Fuselage Construction

The fuselage of the AV-95 is a traditional semi-monocoque structure constructed entirely from carbon-fiber composites. The skin of the AV-95 is composed of carbon-fiber composite sheets as are the numerous fuselage rings (frames), longerons (fuselage stringers) and bulkheads. The ability to control the orientation of the carbon fibers allows each piece of the fuselage to be tailored to its specific function. They are also easily molded and formed to conform to the many curved areas of the aircraft. The use of composites results in a substantial weight savings throughout the entire structure.

Currently, the structural layout of the fuselage has not been modeled. As stated previously, the main wing of the AV-95 is the part of the structure that has been most closely analyzed. However, it is assumed that the airframe for the AV-95 will be similar to other attack rotorcraft currently in production, such as the AH-64 *Apache*. There are obvious differences in the flight conditions and loading requirements for these two rotorcraft, but it is anticipated that the layout will remain similar. Future development in the strucutral layout will draw upon current aircraft such as the *Apache*.

7.6 Main Rotor Blade Design

The main rotor blade is one of the more intricate components of the AV-95's structure. This is due to the need for the blade to extend and retract in various parts of the flight program to allow for helicopter flight and maneuvering and high speed fixed-wing flight. The design of the blade mirrors that of the TRAC rotor system developed by Sikorsky Helicopter Company (Fradenburgh et al., pg 6-7). The blade itself is composed

of two segements: an outer portion which is responsible for most of the lift of the rotor blade, and an inner portion over which the outer blade slides. The inner segment was assumed to act as a torque. The arrangement of the rotor blade is shown in Figure 7-8.

Rotor Blade Schematic Arrangement

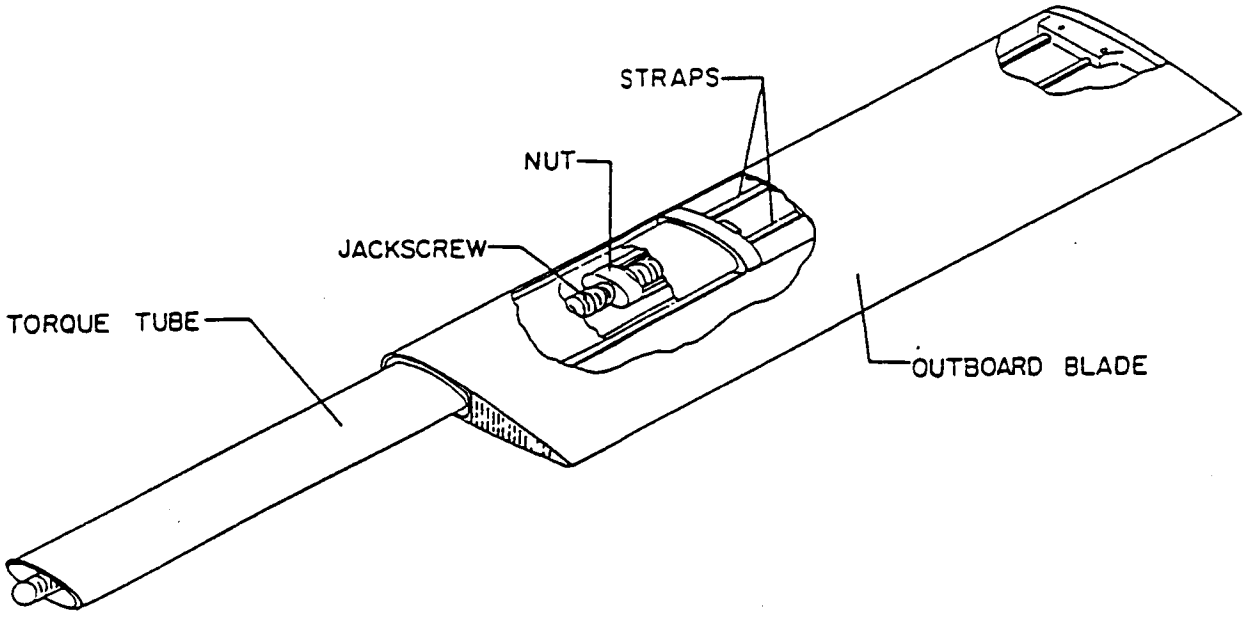

Figure 7-8
Sikorsky TRAC Rotor System (Fradenburgh et al., p54)

Further discussion of the components of the blade can be found in **Section 9.0 Variable Diameter Rotor System**.

At this time, the blade design is considered to be as shown. This is the design of the TRAC Rotor tested by Sikorsky Helicopter and is validated by their wind tunnel test data. Additional analysis of the blade has not yet been conducted but should be accomplished in the detailed portion of the design process.

7.7 Landing Gear Design

The landing gear arrangement chosen for the AV-95 is that of a tail-dragger, using an oleopneumnatic shock-strut for energy absorption. The two main wheels are housed in the wings and the aft wheel in the bottom part of the vertical stabilizer.

The first step in designing the landing gear was to determine the maximum amount of energy that the shock must absorb and the stroke required from the oleo to absorb it. For military requirements, the shock must be able to absorb the energy contained in a 24 ft/s impact without deforming the fuselage. This is determined through the following equations:

$$K.E.=\frac{1}{2}\frac{W_{landing}}{g}V^2=(\eta LS)_{shock}+(\eta_T LS_T)_{tire}$$

$$S=\frac{V^2 W_{landing}}{2g\eta_{shock}L}-\frac{\eta_{tire}}{\eta_{shock}}S_T$$

Landing Gear Data

VARIABLE	VALUE	DESCRIPTION
η_{shock}	0.825	shock absorbing efficiency
η_{tire}	0.47	tire shock absorbing efficiency
S_T	3.4 in	tire stroke*
D_T	39.8 in	tire diameter*
RR_T	16.5 in	tire rolling radius*
*tire data taken from Raymer (1992) for a Type VII tire, size 40 x 14		

Table 7-4

Once the stroke had been determined, the diameter and length of the oleo strut could be estimated. The total length of the oleo including the stroke distance is typically 2.5 times the stroke. Oleo diameter is determined by the load carried by the oleo. The oleo carries its load by the internal pressure of compressed air, applied across a piston. Typically, an oleo has an internal pressure of 1800 psi. Internal diameter is determined from the relationship which states that force equals pressure times area. The external diameter is typically 30 percent greater than the piston diameter, so the external oleo diameter can be approximated by the following equation.

$$D_{oleo} = 1.3\sqrt{\frac{4L_{elec}}{P\pi}} \cong 0.4\sqrt{L_{oleo}}$$

This results in the following dimensions for the oleo strut:

Total Stroke:	23.65 in
Oleo Length:	9.13 in
Oleo Diameter:	2.590 in

The material of choice for the landing gear structure is standard Aircraft Steel with the properties presented in Table 7.5.

Landing Gear Material Properties

Composition	Density (lb/in^3)	Ftu 10^3 psi	Fcy 10^3 psi	Fsu 10^3 psi	E 10^6 psi	Temp Limit (F)
5 Cr-Mo-V	0.281	260	240	155	30	1000

Table 7-5

It is expected that these properties will be sufficient to handle the loads on the landing gear structure. From a historical perspective, this is a typical material for landing gear systems. Some weight savings may be attained by using a Titanium alloy for portions of the landing gear, but at this time the structure is assumed to be entirely constructed from this steel.

8.0 CRASHWORTHINESS

The AV-95 is designed for crew survival in the event of a crash. The following characteristics are necessary in order to provide adequate protection for the crew:

- Cabin structure that retains a protective shell around the crew, keeping engines, transmission, landing gear, and rotor from becoming hazards
- Limiting the loads experienced by the crew during impact
- An interior that will not contribute to injury
- Adequate escape capability
- Prevention of postcrash fire
- Design of forward structure to minimize plowing

The fuselage, landing gear, and crew seats are designed to work as a system to dissipate the energy of impact around the occupants. The forward fuselage bulkhead is sloped to prevent plowing and push the cabin over instead of into the ground. The landing gear is now placed in the wing structure, outboard of the main fuel cells. This should minimize the possibility of puncturing the fuel tanks in the event of a hard crash landing.

The crew seats are designed to absorb some of the energy of impact as well. The seat is attached to its frame by means of carrier bearings (for adjustment purposes only) and its vertical travel is damped by a shock absorber system attached to the frame. This distributes the shock to the frame instead of the seat, minimizing the force on the occupant.

All of these characteristics are dependent upon placement of individual components inside the fuselage such that they will not cause injury. To accomplish this, major components are located below and/or beside the pilots in order to prevent them being crushed during impact.

9.0 VARIABLE DIAMETER ROTOR SYSTEM

The following figures depict the major components of the variable diameter rotor system as developed by the Sikorsky Helicopter Company (Fradenburgh et al.).

- Figure 9-1 Rotor Head Schematic Arrangement
- Figure 9-2 Rotor Blade Schematic Arrangement
- Figure 9-3 Preliminary Design Rotor Head and Retraction Mechanism
- Figure 9-4 Rotor Head Components

Detailed analysis of the components of the rotor retraction mechanism were not possible due the complexity of the system coupled with the time constraints. Validation of the concept is provided by wind tunnel testing performed on a scale model of this system by Sikorsky Helicopter. Loads experienced by the test model were not available, so these had to be approximated.

Rotor Head Schematic Arrangement

Sikorsky TRAC Rotor System (Fradenburgh et al., p55)

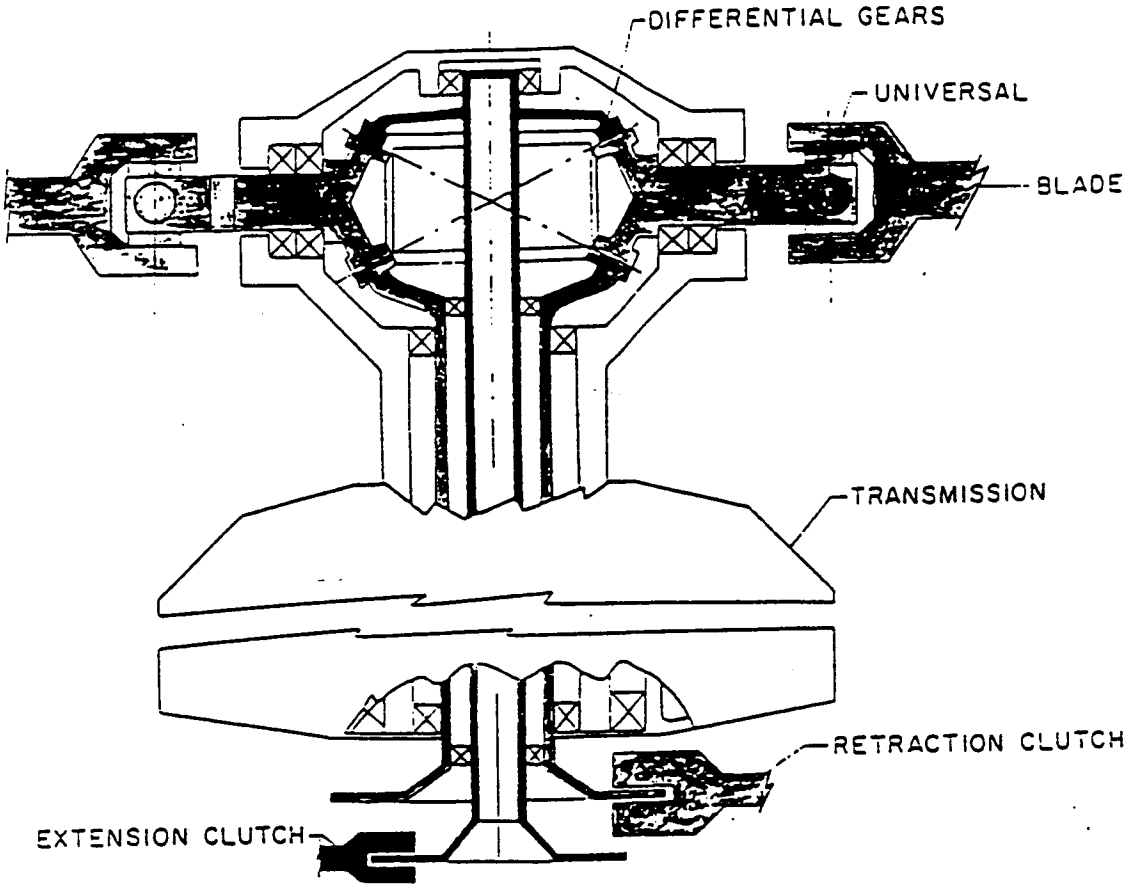

Figure 9-1

Rotor Blade Schematic Arrangement

Sikorsky TRAC Rotor System (Fradenburgh et al., p54)

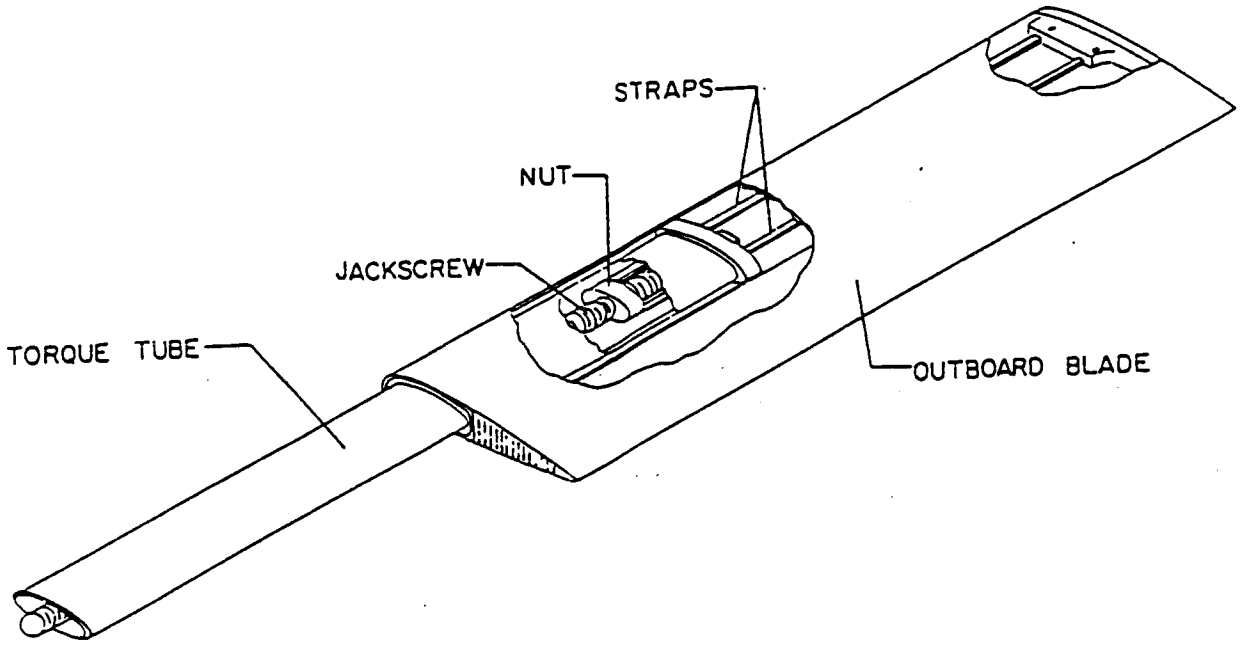

Figure 9-2

Preliminary Design Rotor Head and Retraction Mechanism

Sikorsky TRAC Rotor System (Fradenburgh et al., p175)

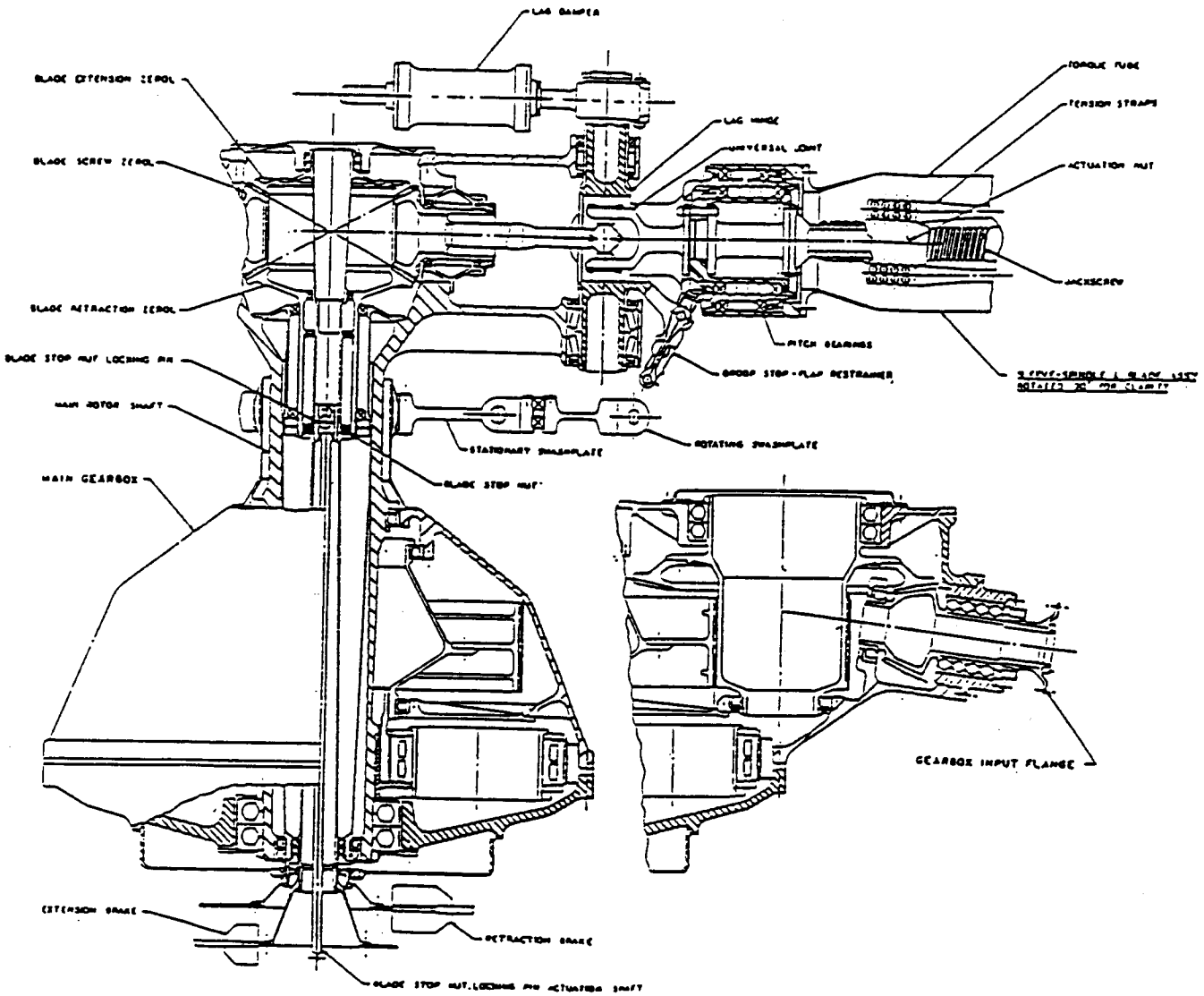

Figure 9-3

Rotor Head Components

Sikorsky TRAC Rotor System (Fradenburgh et al., p67)

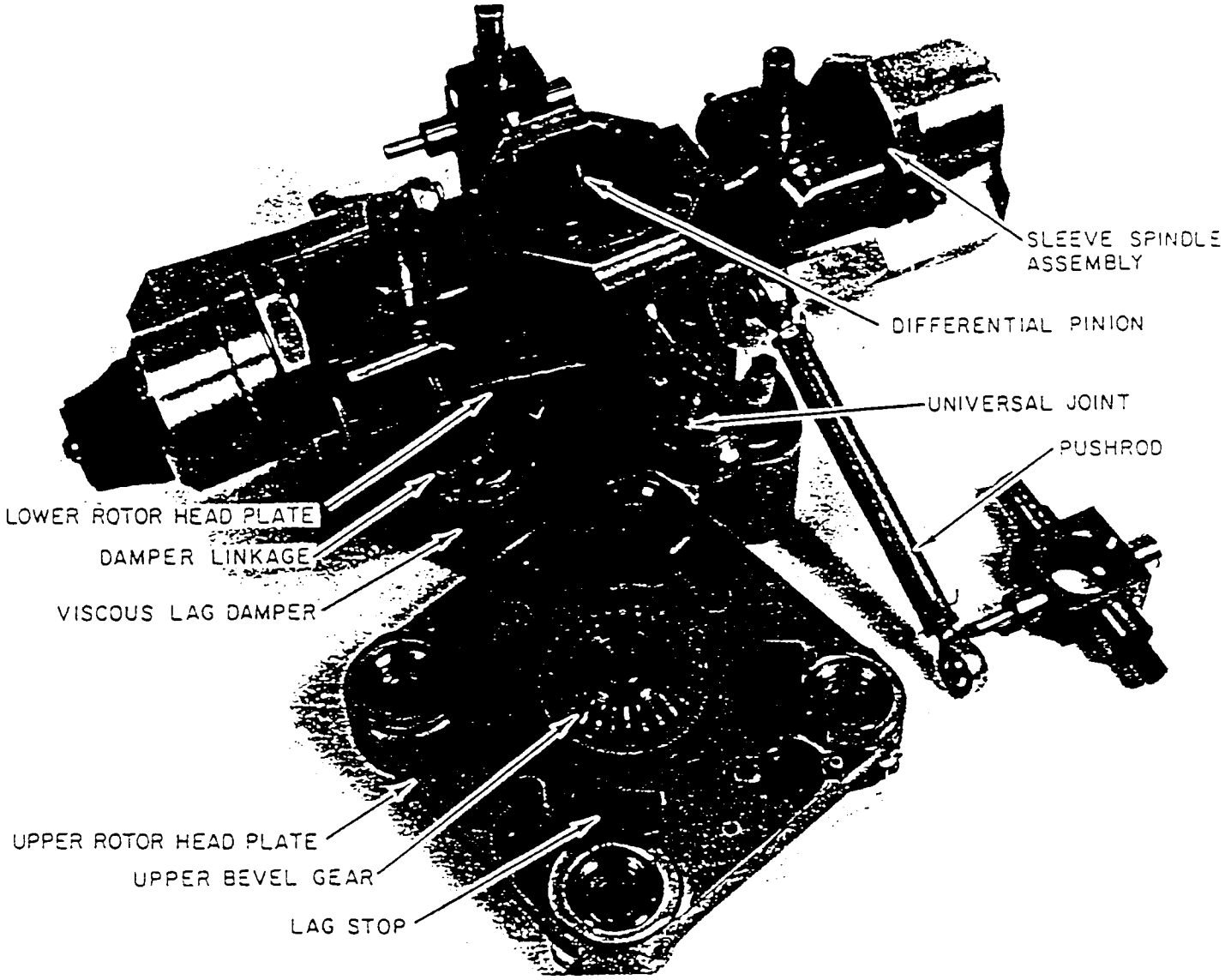

Figure 9-4

9.1 Description of Retraction/Extension Process

As shown in Figures 9-1 through 9-4, the transmission in the TRAC Rotor System employs two concentric rotor shafts connected to an upper and lower plate. On this plate are bevel gears which connect to the differential pinon gears at the end of the blades. To extend the blade, the inner shaft is braked causing it to rotate at a reduced angular velocity. This causes the rotation of the bevel gear attached to the upper plate of the hub, and subsequent rotation of the pinion gear. This pinion gear is attached to the jackscrew inside the rotor blade. Since the nut on the jackscrew inside the blade is fixed to the outer portion of the blade, this rotation of the screw causes extension of the blade. In a similar manner, braking the outer shaft causes blade retraction. The outer shaft is connected to the lower plate of the hub, so braking causes rotation of the pinion in the opposite direction and the blade retracts. It is envisioned that this process will be controlled by an automatic flight control system that will have full control over the movement of the blade so that over extension or retraction does not occur.

10. SUBSYSTEMS

10.1 Hydraulic System

The hydraulic systems in the AV-95 are responsible for flight control, landing gear actuation and flap control. Each of the systems operates independently of the other in case one system is damaged or inoperable. Pilot inputs are sent to the various control points on the aircraft by means of cables strung from the control column(s). Redundancy is built into each system, in case of damage during combat.

10.2 Electrical System

The electrical system is responsible for the power necessary to run all of the aircraft's avionics, fire control, hydraulic, environmental and countermeasures. Electrical power is produced by a generator attached to the main transmission and directed to each of the other subsystems.

10.3 Threat Avoidance

Due to the AV-95's high-risk mission, survivability is of paramount importance. The largest threat to the aircraft comes from radar guided and infra-red seeking surface to air missiles (SAMs). The design of the AV-95 does not lend itself readily to the new "stealth" technology employed on the latest generation of attack aircraft. Rather, missile avoidance is attained through the use of electronic countermeasures and jamming devices meant to scramble the signal received by enemy radar and/or the tracking missile. Radar

Warning Receivers are placed in fore and aft locations on the aircraft to detect and alert the pilot to the presence of enemy radar. Infra-red seeking missiles can be initially defeated through the use of infra-red jammers located on the boom between the engines.

In the event of a lock-on, there is a chaff/flare dispenser located in the aft section of the boom. These decoys are automatically released by the aircraft's threat assessment system.

Ground fire is another major threat to the AV-95. Since it is not possible to scramble or alter the course of incoming fire, the structure must be able to withstand some damage from ground fire. The rotor is designed with this in mind, as is the multi-spar wing. The cockpit will employ a titanium armor 'bathtub', similar to the one used in the A-10 Thunderbolt II, to protect the crew from projectiles, and the fuel tanks are self-sealing in order to reduce the possibility of fire or total fuel loss.

11. STABILITY

11.1 Overview

The AV-95 *Sun Devil* is a unique aircraft. It falls outside of the mainstream classifications for most aircraft, and thus is not always within the realm of standard analysis methods. Yet it is for this very reason that a VTOL rotorcraft design was chosen. The unusual challenge of performing a stability analysis on the AV-95 lies in the fact that it operates in both a fixed-wing mode as well as in a rotary-wing mode. At times, the *Sun Devil* acts more like one mode than the other, but the two modes are never completely separated. Any standard method for determining stability for a helicopter or an airplane needed to be altered to reflect the differences. The overall task of determining trim requirements was divided into two parts. The first was determining trim in fixed-wing mode, while the second was determining trim in rotary-wing mode. In the following pages the methods and results for each are presented.

11.2 Control

The control method for the AV-95 *Sun Devil* is a combination between helicopter cyclic and anti-torque control and fixed-wing control surfaces including ailerons, elevators and the rudder. However, the dominant control method will be determined by the current flight mode of the *Sun Devil*, as shown in Table 11-1.

Contols Matrix

	Cyclic *(& Elevators)*	Elevators *(& Cyclic)*
	Cyclic *(& Ailerons)*	Ailerons *(& Cyclic)*
	Anti - Torque *(& Rudder)*	Rudder *(& Anti - Torque)*

Table 11-1

While in helicopter mode, the cyclic controls the majority of the roll and pitch while the yaw is performed via the ducted tail fan. Elevators, ailerons and the rudder can also provide some control, however. In fixed-wing mode, the bulk of the control is provided by the conventional fixed-wing control surfaces. Again, cyclic control may be used to aid in control during fixed-wing flight. It should be noted, however, that the dominant control mehtod is indirectly dependent by the flight mode; a more precise description is that the dominant control method is dependent on the flight velocity, and the flight mode is dependent on the flight velocity. At low speeds, which usually corresponds to the helicopter flight mode, fixed-wing control surfaces are not efficient. And at higher velocities, or fixed-wing mode, rotor cyclic control will produce excessive drag. Also, for dash velocities and higher, compressibility effects and retreading blade stall may occur if cyclic control is initiated; this will not only provide very inefficient control, it will also greatly increase drag.

11.3 Trim Analysis of Fixed-Wing Mode

Research showed that there was no one set way of performing a stability analysis. The chosen method was a guess and verify approach based on statistical data. Ground attack aircraft, both fixed-wing and rotary-wing, with similar mission profiles were researched. Typical values for tail volume coefficient and tail-to-control surface area ratios were obtained. From the chosen values, the areas of the horizontal tail and elevator were determined. Then it was necessary to calculate whether the aircraft could be trimmed with these areas. The following equation was used to determine the pitching moment coefficient as a function of lift coefficient and elevator deflection. The equation is an approximation. Elevator contribution to total aircraft lift has been ignored.

$$C_{mo} = -\left[\frac{C_{m\delta e} * \delta e * C_{L\alpha} - C_{m\alpha} * C_{Ltrim}}{C_{L\alpha}}\right]$$

The moment coefficient was then plotted against the lift coefficient for elevator deflections ranging from -10° to 10°. This graph is shown in Figure 11-1 As the figure illustrates, the aircraft can be trimmed at lift coefficients between 0.2 and 1.15 for these elevator deflections. This indicated that the chosen areas for the horizontal tail would trim the aircraft at the velocities encountered in fixed-wing mode.

Moment Coefficient vs. Lift Coefficient

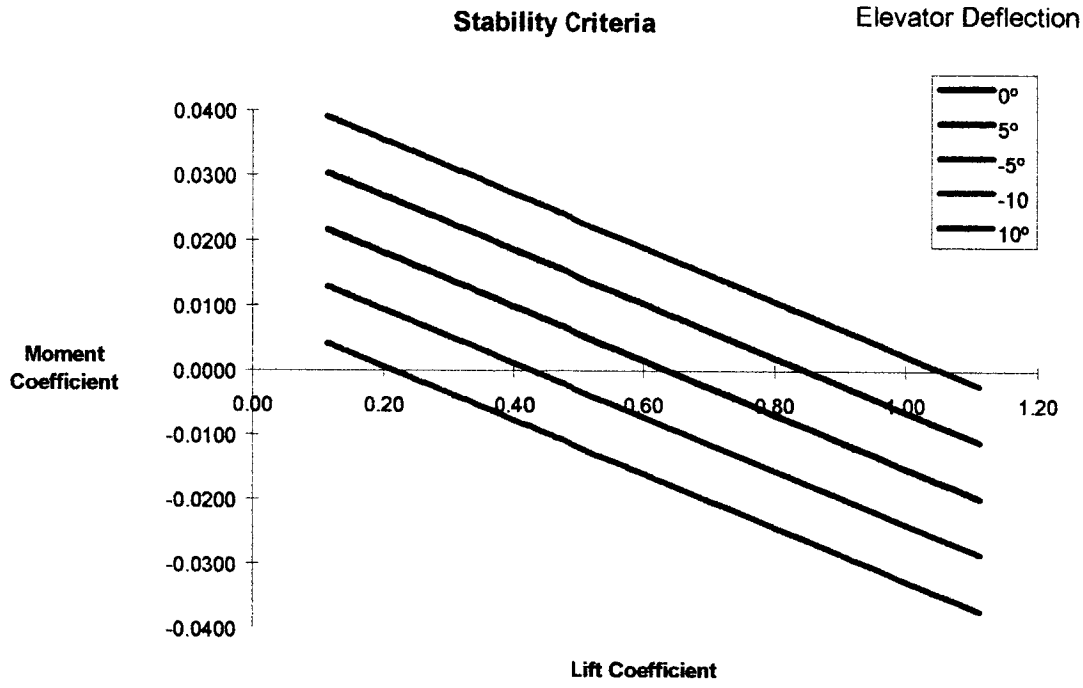

Figure 11-1

No lateral stability analysis was performed to determine the effectiveness of the vertical tail. These values are based upon calculations from the sizing code. Table 11-2 displays the tail and control surface properties.

Tail & Control Surface Properties

Horizontal Tail		Vertical Tail	
Horizontal Tail Area	**74.63** ft^2	Vertical Tail Area	**36.21** ft^2
H. Tail Span	**20.26** ft	V. Tail Span	**14.11** ft
H. Tail Root Chord	**4.91** ft	V. Tail Root Chord	**3.42** ft
H. Tail Tip Chord	**2.46** ft	V. Tail Tip Chord	**1.71** ft
Elevator Area	**15.67** ft^2	Rudder Area	**7.24** ft^2
Elevator Span	**9.28** ft	Rudder Span	**6.31** ft
Elevator R. Chord	**2.25** ft	Rudder R. Chord	**1.53** ft
Elevator T. Chord	**1.13** ft	Rudder T. Chord	**0.76** ft

Table 11-2

Next, the horizontal tail incidence angle was determined. The horizontal tail incidence angle trims the aircraft with zero elevator angle at a selected flight condition. Zero elevator deflection is the minimum drag configuration, and thus minimum fuel consumption configuration. The selected flight condition was cruise. Since the aircraft spends most of its fuel and flight time in cruise, this segment was the critical flight condition. However, before the incidence angle could be determined, a detailed look at the center of gravity position had to be performed. Finding the c.g. location is fundamental in trim analysis. By knowing the c.g. location, the distance to all forces acting on the aircraft could be determined. This is essential because the development of trim solutions at all flight conditions is based upon summing the moments to zero; this is the definition of trim. The c.g. location was found the following way. First, the weight of the major components of the aircraft was determined along with each corresponding distance from the nose. By summing the moment due to all of these components and dividing the total by the overall weight of the aircraft, the location of the center of gravity was found. The component weight breakdown and location is found in Table 11-3. With the c.g. location known, the moments of the wing and horizontal tail could be determined. With these values, it was found that a horizontal tail incidence angle of 1.3° would trim the aircraft with zero elevator deflection in cruise. The incidence angle is positive due to the fact that the lift of the wing is forward of the center of gravity. The horizontal tail is a variable incidence tail. The angle can be adjusted between flights. This was designed to allow for different mission profiles and in general make the aircraft more versatile.

There are several items that should be noted to complete the overview of the horizontal tail design.

- The reference area used to determine tail area was the wing area of 372 ft^2.
- The horizontal tail is geometrically similar to the wing.
- The elevator has a constant chord-ratio with the horizontal tail.
- Wing incidence angle is set at 3 degrees.

Weight Breakdown & Center of Gravity Location

Group	Group Weight(lb)	%Empty Weight	X-Direction Station(in)
Wing	1,001.55	4.6%	234.68
Rotor	814.24	3.7%	233.50
Tail Rotor	119.60	0.5%	608.02
Hub	964.76	4.4%	233.50
Circulation Control	1,100.00	5.0%	238.34
Vertical Tail	179.90	0.8%	604.20
Horizontal Tail	326.37	1.5%	597.84
Fuselage	3,997.63	18.3%	303.12
Landing Gear	1,093.98	5.0%	227.18
Engines	2,836.23	13.0%	229.14
Engine Mounts	29.65	0.1%	229.14
Engine Section	44.84	0.2%	229.14
Drive System	2,719.22	12.5%	214.97
Flight Controls	696.15	3.2%	137.48
Fixed Equipment	2000.00	9.2%	99.85
Avionics	541.10	2.5%	125.22
Mission Equipments	2900.00	13.3%	230.23
Crew	470.00	2.2%	145.22
Empty Weight	21835.22		
Fuel	2515.34		234.68
External Weapons	1000.00		230.23
Internal Weapons	2000.00		230.23
Total Take-off Weight	27350.56		
Xcg Position			**233.31**

Table 11-3

11.4 Trim Analysis of Rotary-Wing Mode

The trim analysis for rotary-wing mode was done using a pre-existing computer code. The code was based upon determining the rotor thrust required to balance the major horizontal and vertical forces. The process was iterative due to the transcendental nature of the problem. The major variables that the code iterated upon were horizontal rotor drag (H-force), collective, coning, tip-path-plane angle and induced velocity. The code had to be altered to include engine thrust. This was necessary because, without engine thrust, all forward thrust must be provided by the rotor. Due to the weight of the aircraft and forward speeds reached in helicopter mode, this was not feasible because the large collective needed would stall the rotor. It was known that the engine thrust would be needed to trim the aircraft, but the amount of the engine thrust was not known. An analysis of the horsepower required to operate in helicopter mode provided an envelope of engine thrust available at all flight speeds. It was then determined that there would always be enough engine thrust to overcome the drag. This was due to the fact that the engine was sized by the vertical climb requirement. It was decided that the engine would be throttled to equal the drag. This meant that the rotor and wing would provide the lift to keep the aircraft in flight, and the engine would provide thrust for forward velocity. Figure 11-2 displays available and throttled engine thrust plotted against forward velocity.

Available Engine Thrust & Throttled Engine Thrust vs. Forward Airspeed

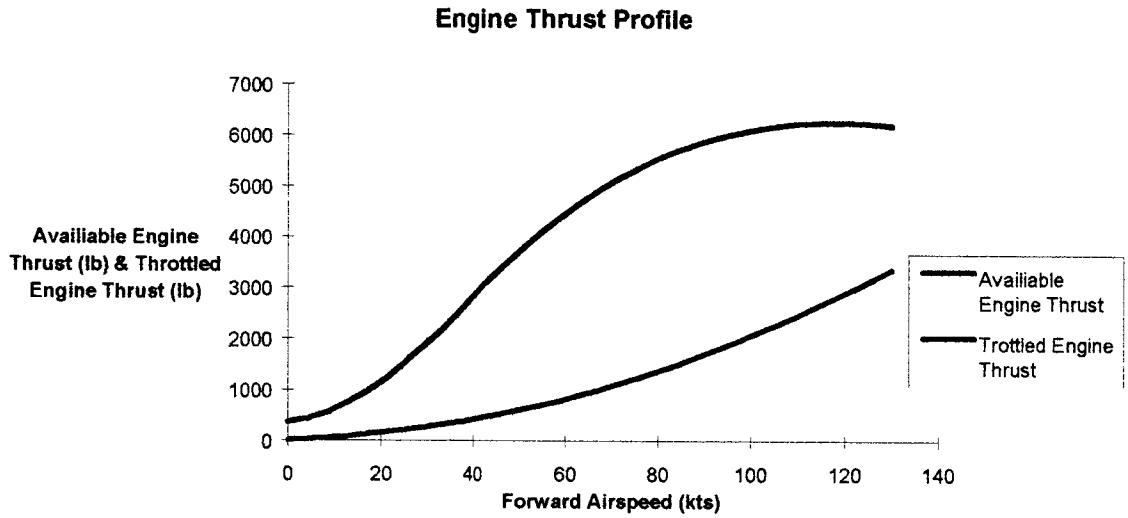

Figure 11-2

One of the results of this decision was that the tip path plane angle would always be zero. Although the aircraft has the capability of providing less throttle so that the forward thrust is then shared by the engine and the rotor, this was not the regime analyzed. All the results present are based upon the engine providing all forward thrust. The velocity range under consideration is from hover to the conversion speed of 130 knots. It is in this range that the vehicle will be in rotary-wing mode and the discussed analysis was performed. Figure 11-3 displays a plot of the collective as a function of airspeed.

Collective vs. Forward Airspeed

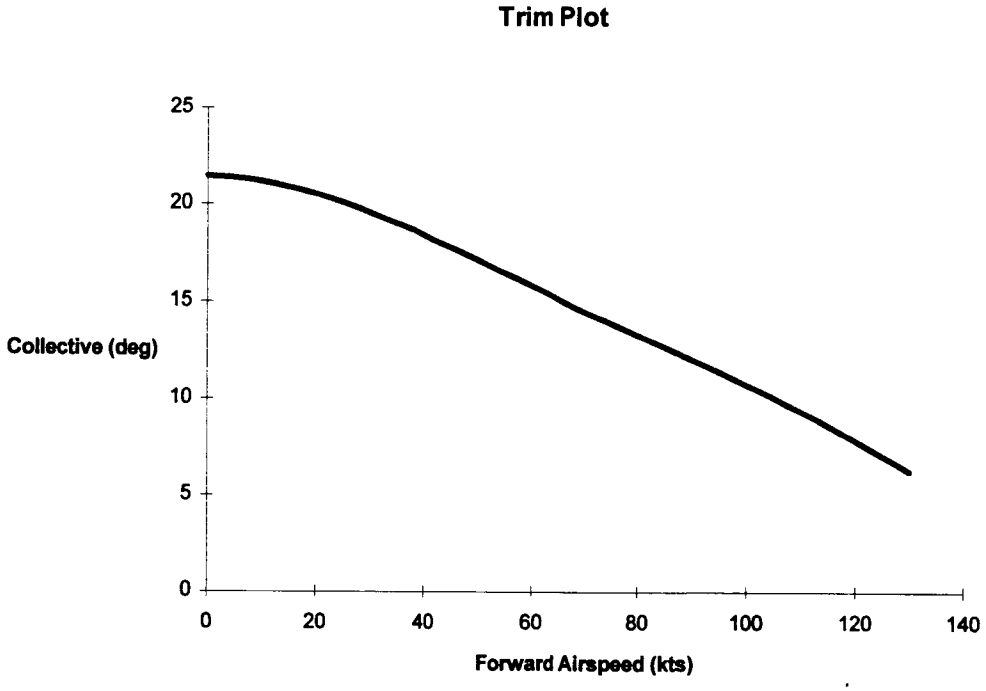

Figure 11-3

12. AERODYNAMICS

An aerodynamic analysis is an essential part of this design process. This analysis is not only used to obtain the drag breakdown, it is also crucial in determining the airfoil sections used for the fixed wing and the rotor blades of the *Sun Devil.*

12.1 Fixed Wing

The selection of the wing airfoil section is based on several items. One of the most important characteristics needed of a potential airfoil is a high maximum lift coefficient at a relatively low angle of attack. When converting either from a helicopter to an airplane or from an airplane to a helicopter, the aircraft will be at a relatively low airplane velocity. Even with the utilization of the circulation control device, the wing should produce a significant portion of the lift required during conversion. The ability to convert at an angle of attack significantly increases the flexibility of the *Sun Devil* because this greatly increases the conversion envelope. Therefore, an airfoil section with high lift characteristics at relatively low angles of attack is desired. Also, in the event of an engine failure, the aircraft may require a relatively high angle of attack during conversion. Choosing an airfoil with soft stall characteristics is also important due to the possibility of high angle of attack conversions.

Another property required of the wing section is beneficial drag profiles over a wide range of angles of attack. Another important aspect of a potential wing section is a large capacity to store fuel inside the wing.

After carefully considering all of the above requirements, a NACA 63_2-215 was chosen. This airfoil has the best combination of all of the previously mentioned requirements. Its high lift-curve slope is important because it allows relatively high lift values at low angles of attack. Because this airfoil section is 15 percent thick, it provides a good compromise between high storage capacity and low drag formation.

12.2 Rotor Blade

The selection of the rotor blade also takes into account several important parameters. Because of the aerodynamic requirements of a rotor blade, an airfoil section with a low pitching moment is very important. Taking into account the tip speeds associated with this aircraft, the critical Mach number must be delayed as much as possible. When stall does occur, it is preferable to have trailing edge stall as opposed to thin airfoil stall or leading edge stall. Trailing edge stall is preferable because, unlike the other two stall methods, trailing edge stall corresponds to both gradual lift and moment stall. Moreover, trailing edge stall has an advantage over leading edge stall and thin airfoil stall because it has no hysteresis involved in its stall process. Other important rotor blade airfoil section requirements include high maximum lift coefficient, low drag, enough thickness for efficient structure, and good performance over a wide range of Mach numbers.

After researching different airfoils to obtain the best compromise of the above parameters, an Eppler 361 (or E 361) airfoil section is chosen. The leading edge and pressure recovery have been specifically designed to obtain a high maximum lift coefficient. Moreover, the pressure recovery on the upper and lower surfaces have been designed to yield a zero pitching moment at an angle of attack of zero.

To induce trailing edge stall, roughening the nose of the airfoil and having a relatively thick airfoil are suggested. Although this airfoil is only 12.12 percent thick, inducing trailing edge stall is still be possible. However, because of the thickness of this airfoil, the resulting drag is very advantageous.

13. ROTOR AERODYNAMICS

13.1 Introduction

The objective of this part of the AV-95 design process was the designing of the rotor system of the aircraft. To accomplish this goal, three variables had to be optimized. The number of rotor blades, the twist and taper of the blades had to be optimized to find the 'best' design. However, each one of theses variables is very dependent on the remaining two variables. Moreover, the solidity also has a significant effect on the design of these three variables. Consequently, this optimization entails a design problem within itself.

Before the optimization process began, there were several characteristics of each of these three variables that were known. This is especially true for the number of rotor blades; the AV-95 is limited to having two, three, or four rotor blades. The limit of four blades exists because of the limited hub space available due to the variable-diameter rotor system.

The general characteristics of the taper of the rotor blades were also familiar. It was assumed that a relatively low taper ratio would be used due to the effectiveness of the rotor blades towards the blade tips. Most of the rotor blade thrust is generated near the rotor tips; this is especially true for the *Sun Devil*. In this variable diameter design, the outboard portion of the blade is the Eppler 361 airfoil while the inboard portion is a NACA 0012 airfoil. The outer portion will produce a larger percentage of the total thrust than a conventional rotor blade due to this change of airfoil section and area (the E361 portion is larger than the NACA 0012 portion due to the variable diameter limitations that are placed on the inboard airfoil). Consequently, having too much taper of the E361 portion will sacrifice the primary thrust source of the rotor blades. However, taper also reduces the drag of the rotor blades. Therefore, some blade taper would most likely be desired.

Finally, the basic characteristics of the twist of the rotor blades was known before the design process began. It was assumed that the rotor blades would be twisted linearly. Moreover, the slope of the linear twist needed to be optimized.

13.2 Method

To optimize the number of rotor blades, along with the rotor twist and taper, a blade element code was used. A pre-existing code was used for the design of the hover variables (Crossley, 1992). However, this code was not completely suitable for the AV-95 design optimization process; therefore, some changes were made. For example, the code was changed so that multiple rotor blade airfoil sections could be used; this was required due to the variable-diameter rotor system of the AV-95. Another change was the addition of the increased drag due to the Mach number. Moreover, a drag polar curve fit replaced the original tabular system. Finally, the process by which the input values were included in the code was dramatically altered. The new version calls an input file that contains all the necessary variables for each airfoil section (number of elements desired, $\alpha_{\text{zero lift}}$, C_{L_α}, Cl_{max}, etc.), the three coefficients for the second-order polynomial curve fit of the drag polar, various rotor dimensions, and the fifth-order polynomial curve fit for the increased drag due to the Mach number. Before entering the values for each blade element into the input file, the normalized radius was found for each element. This was required because the code emphasizes more stations towards the blade tip.

The original copy of the drag polar can be found in Figure 13-1. Points were taken off of this curve and entered into a computer; next, a third-order polynomial curve fit was found for this plot. The coefficients were then added to the input file, and the necessary equations were included in the blade element code.

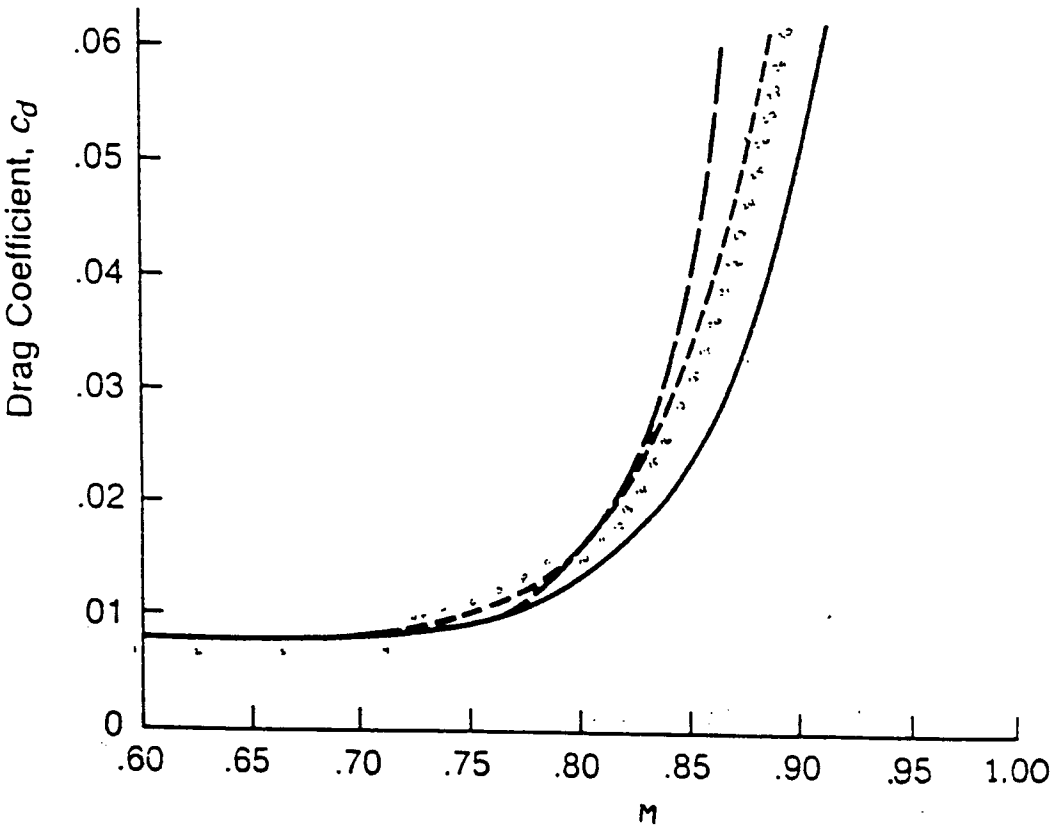

Figure 13-1

Figure 13-2 shows the original graph from which the critical Mach number was found for a given blade element lift coefficient. Because the inner portion of the rotor blade is a NACA 0012 airfoil section and the outer portion is an Eppler 361 (12.12 percent thickness), lift coefficients corresponding to a thickness of twelve percent were found along with the corresponding critical Mach numbers. These were then plotted and fitted with a linear regression; the original plot along with its curve fit can be located in Figure 13-3. After writing the necessary equations in the code, the critical Mach number is now known for a given lift coefficient of any airfoil.

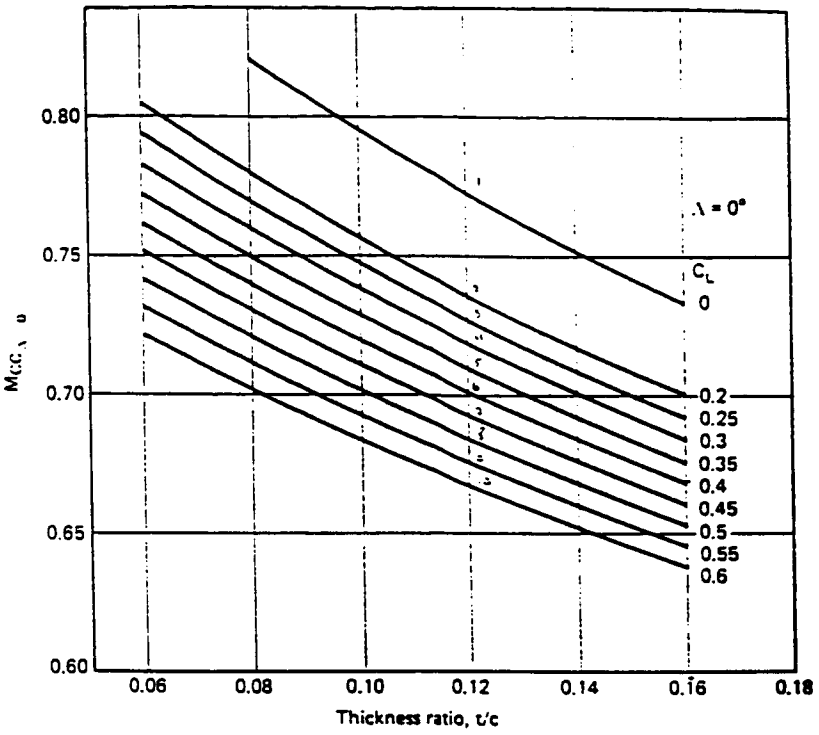

Figure 13-2

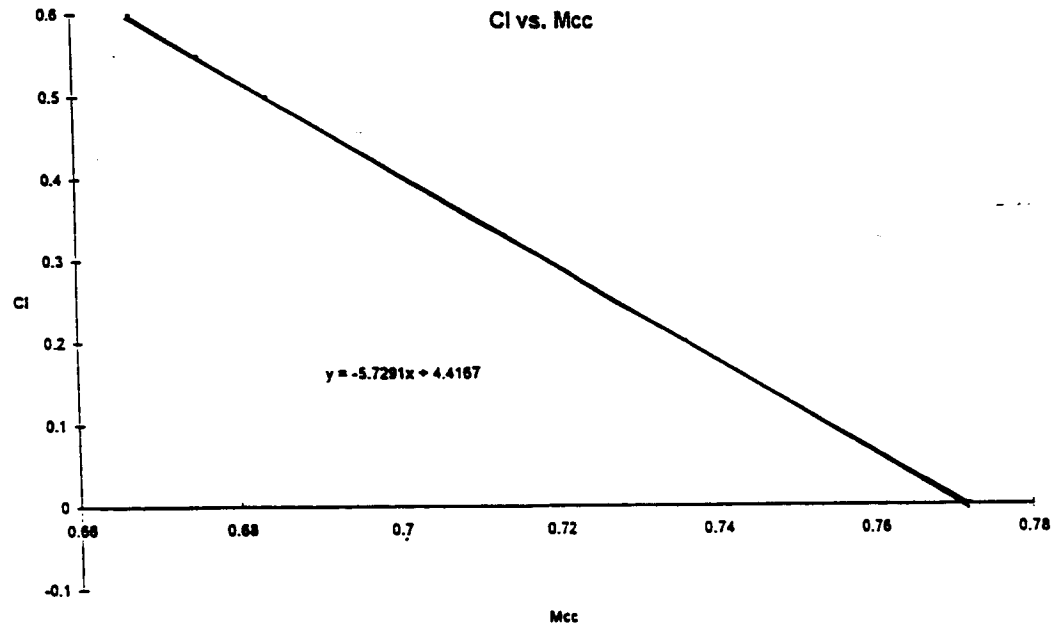

Figure 13-3

Figure 13-4 is the original curve from which the drag due to the Mach number was found. In this graph, M_{div} was found to be 0.7083. This value was then used to normalize the same graph.

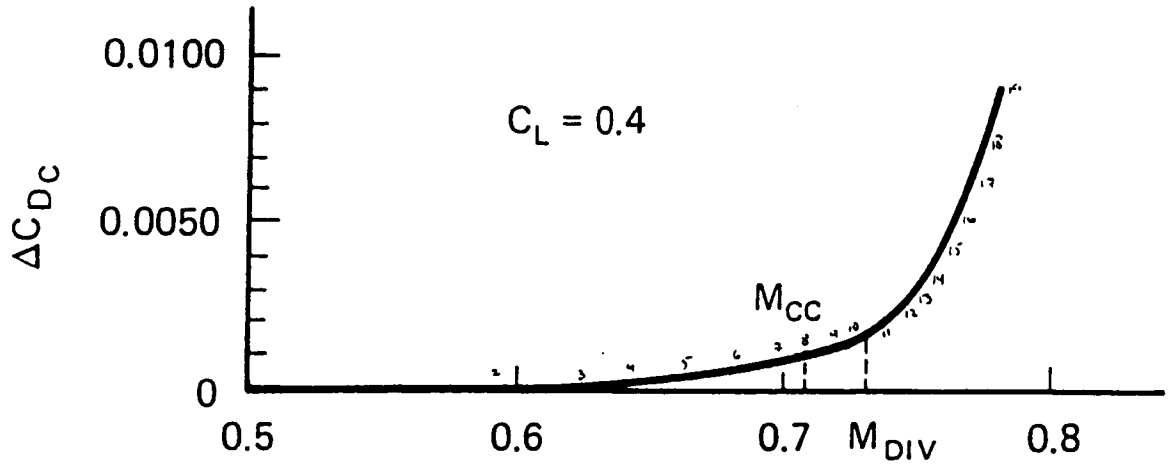

Figure 13-4

An illustration of this normalization, along with its fifth-order polynomial curve fit, is illustrated by Figure 13-5. This curve fit data was added to the input file from which it was called in DRAGCF, a subroutine written to find the added drag coefficient due to the Mach number.

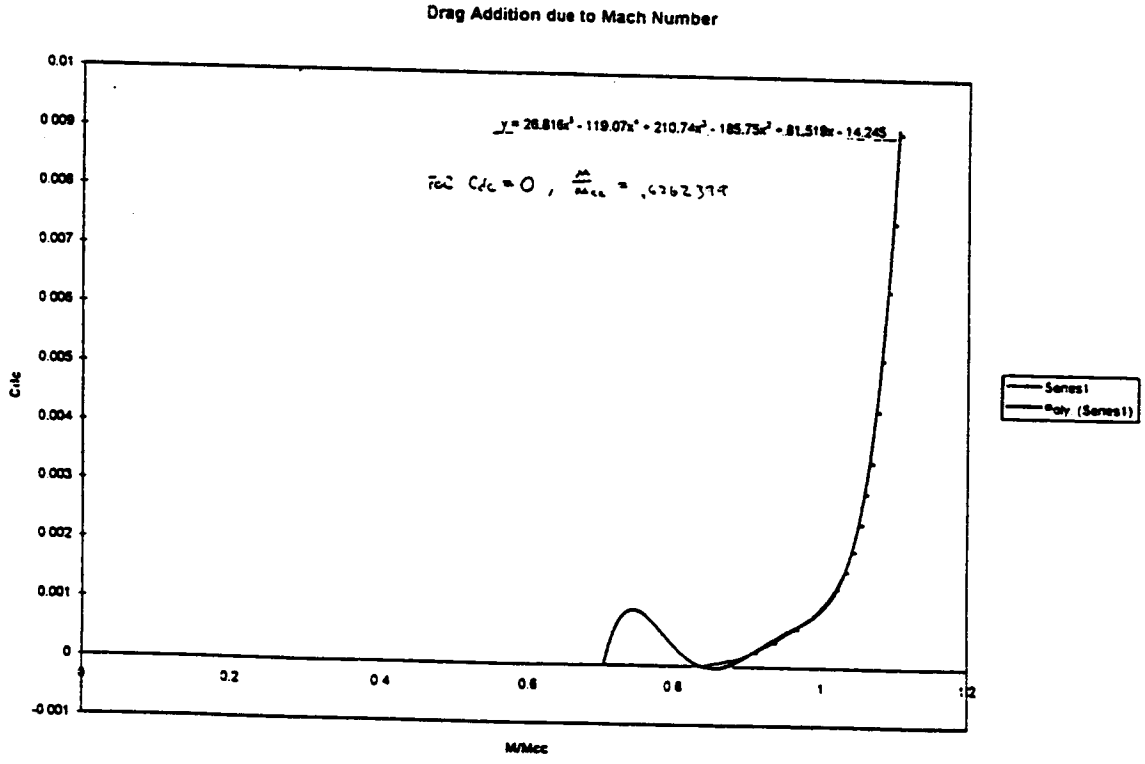

Figure 13-5

It was determined using TK-Solver that when the normalized Mach number, M_r, has a value of greater than 0.67624, an extra drag due to the Mach number would be required. Note that, in Figure 13-5, a sudden increase in the drag coefficient exists before the curve fit becomes accurate. This 'hump' in the curve fit lies before the M_r limit of 0.67624. Consequently, the 'hump' is not used. An *If* statement used in the code does not add the extra drag term to the total drag unless M_r is greater than the limit of 0.67624. The 'hump' in the curve fit lies at an M_r value below this limit. Consequently, the 'hump' in the curve fit is not used.

Finally, the code was altered so that it requested the three design variables from the user. These changes made the program more efficient for this particular optimization process.

Once the blade element code was debugged, a solidity was needed. Consequently, Figure 13-6 was generated in which the power required was plotted versus the solidity for a taper of 1.0, a twist of -9 degrees, and a blade number of four. An excessive solidity results in excessive weight; consequently, the solidity corresponding to the minimum power required may not be the optimum choice. In fact, a solidity of 0.15 was chosen as the best compromise between minimizing weight and power required. Once a solidity was determined, carpet plots were generated.

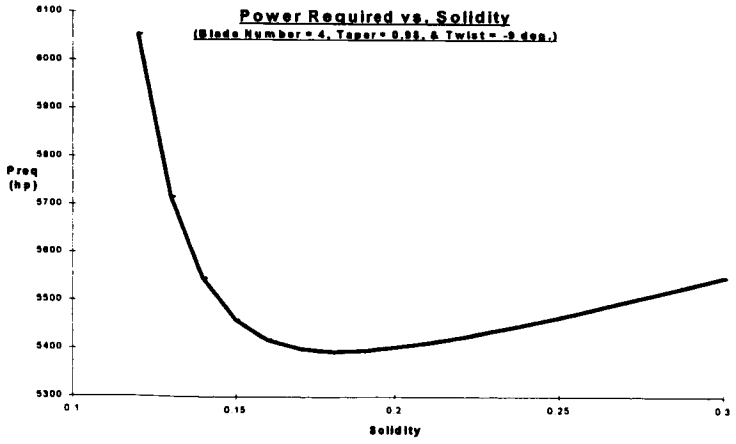

Figure 13-6

13.3 Results

Figures 13-7 through 13-12 contain all of the carpet plots of the AV-95 rotor system design for hover. Figures 13-7 and 13-8 contain the carpet plots in which the data was generated with a two-bladed rotor system. Similarly, Figures 13-9 and 13-10, along with Figures 13-11 and 13-12, show the carpet plots that were generated with a three- and four-bladed rotor system, respectively. All of these plots have either the figure of merit or the power required to hover plotted versus the blade twist for different values of taper. It should be noted that this taper refers to the outer airfoil section only. The inner section, the NACA 0012, has no taper and will have a chord just small enough to fit in the tip of the outer section, the E361, when the rotor is retracted.

There are two trends that are common to all six of these plots. First, as the taper increases (or, the ratio of C_{tip}/C_{root} decreases), the design becomes more desirable (that is, the figure of merit increases and the power required decreases). The second trend is, for a blade twist below -30 degrees, the design becomes more desirable as the twist increases. As the number of blades increases, the trend changes for a twist greater than -30 degrees. For instance, for a rotor system of two blades, the figure of merit increases, and the power required decreases up to -40 degrees. However, for the three- and four-bladed rotor designs, this is not the case. After -30 degrees, the figure of merit decreases, and the power required increases; however, this is more severe for the four-bladed rotor system than for the three-bladed rotor system. It should be pointed out that, according to these carpet plots, a twist of -30 degrees is the optimum design point. However, this is true only for hover; a lesser amount of twist is needed for forward flight.

Another general trend of these carpet plots is that, while the number of blades increases, the figure of merit increases and the power required decreases for a given taper and twist.

It should be noted that the spreadsheets containing the carpet plot data can be found in Appendix A.

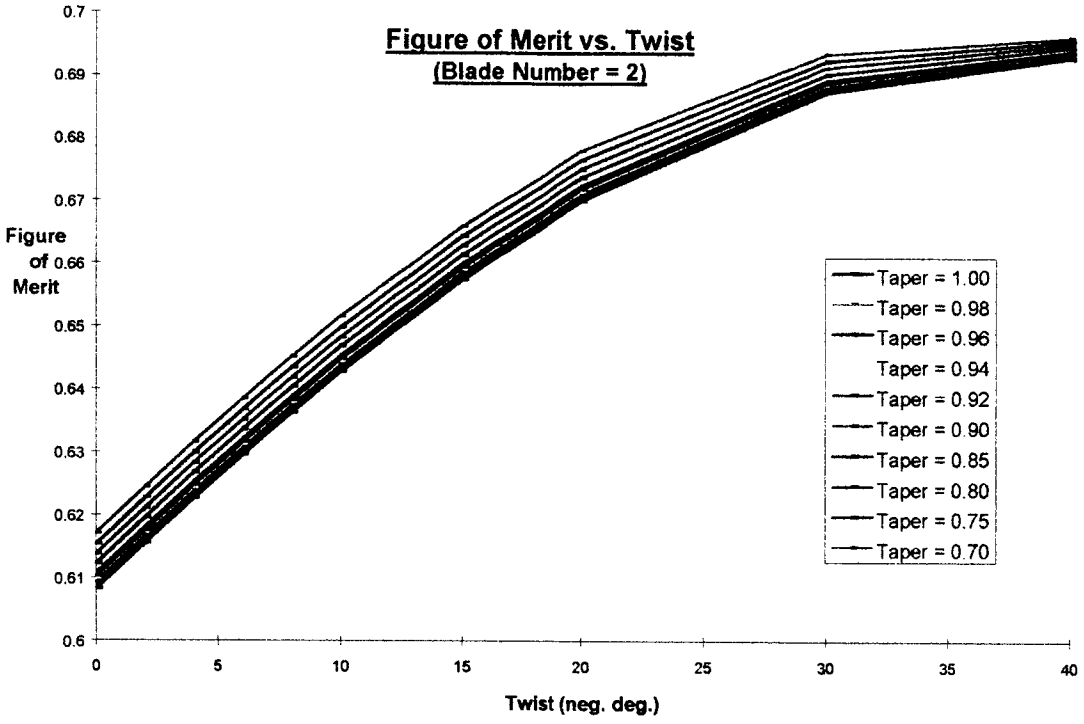

Figure 13-7

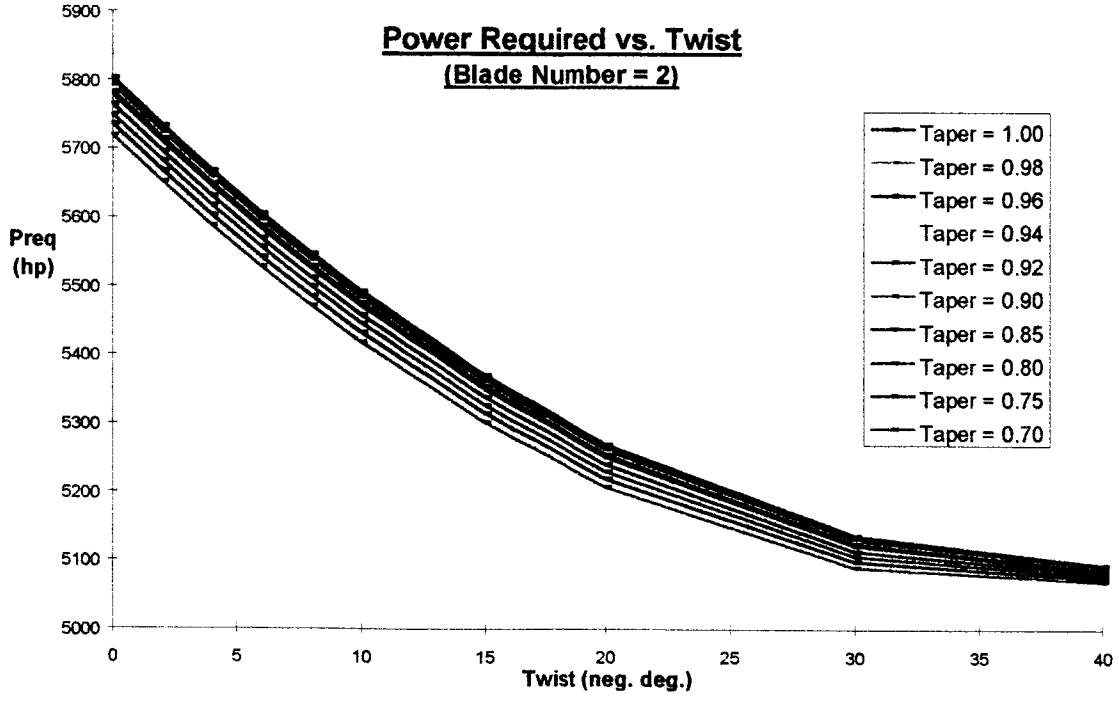

Figure 13-8

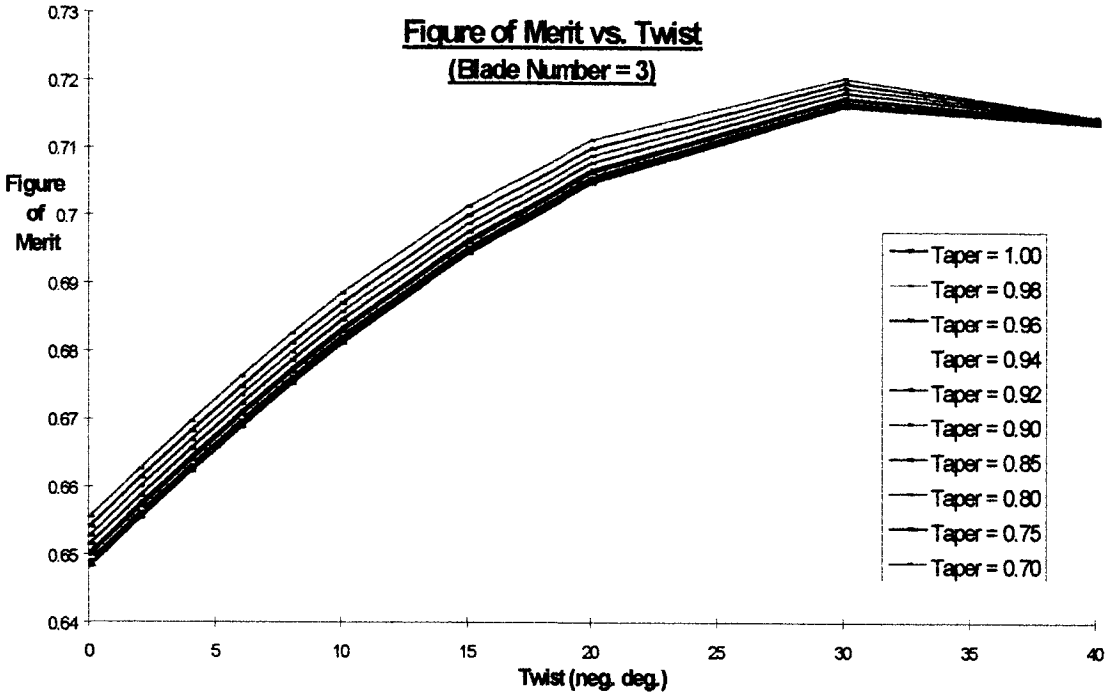

Figure 13-9

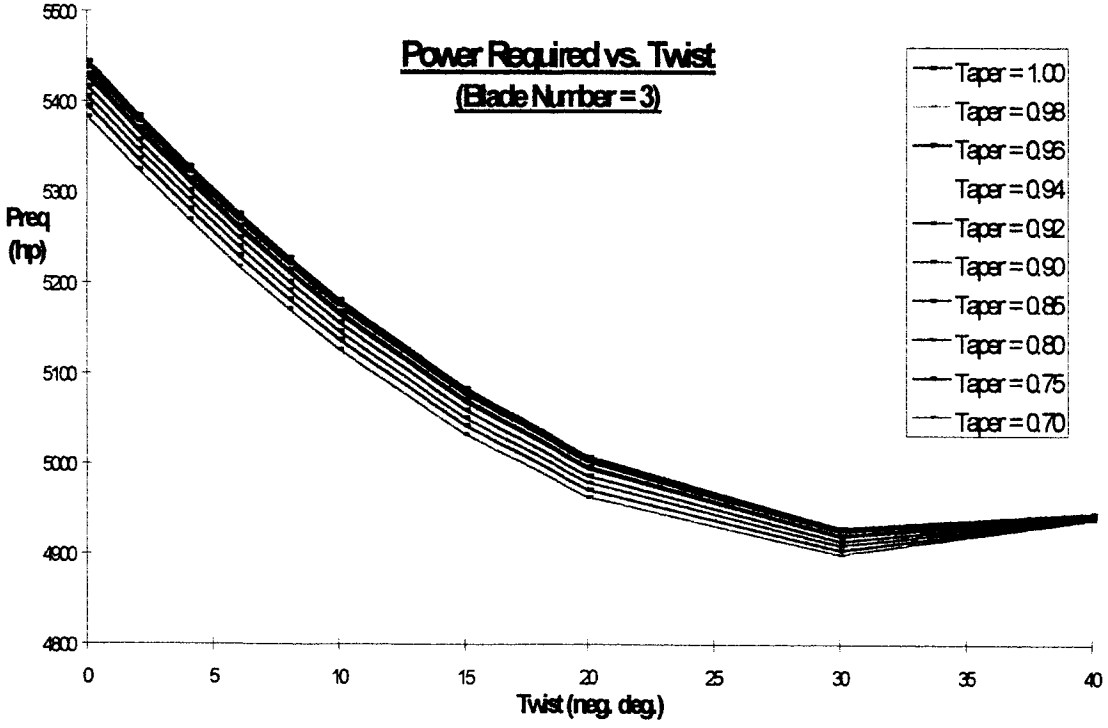

Figure 13-10

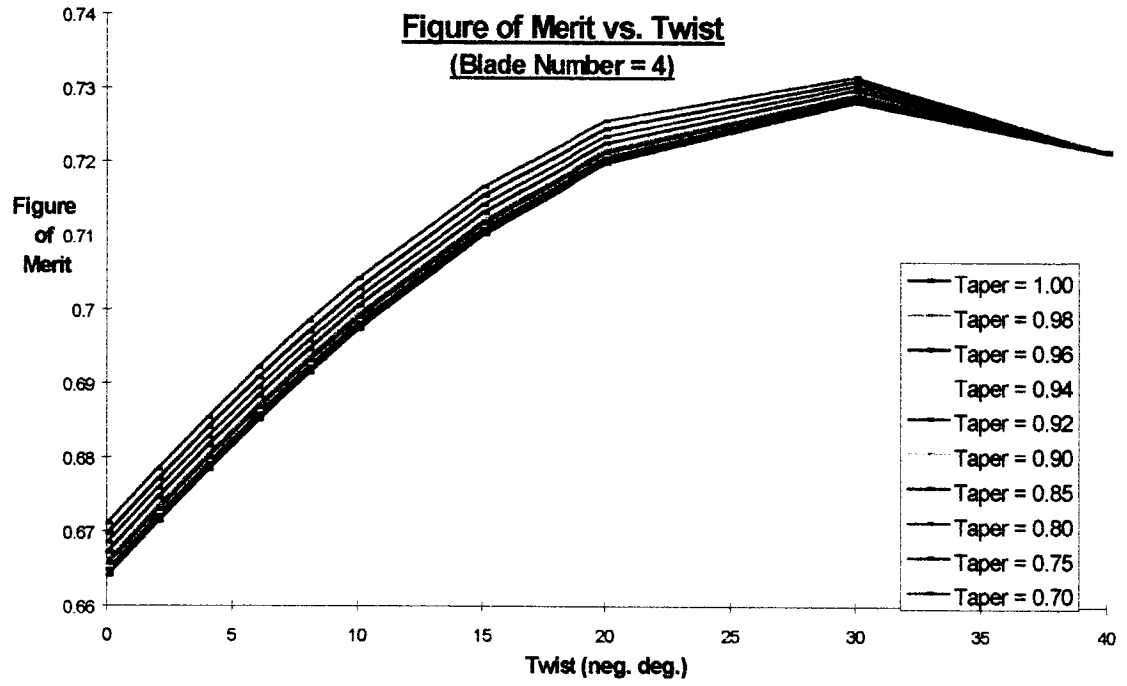

Figure 13-11

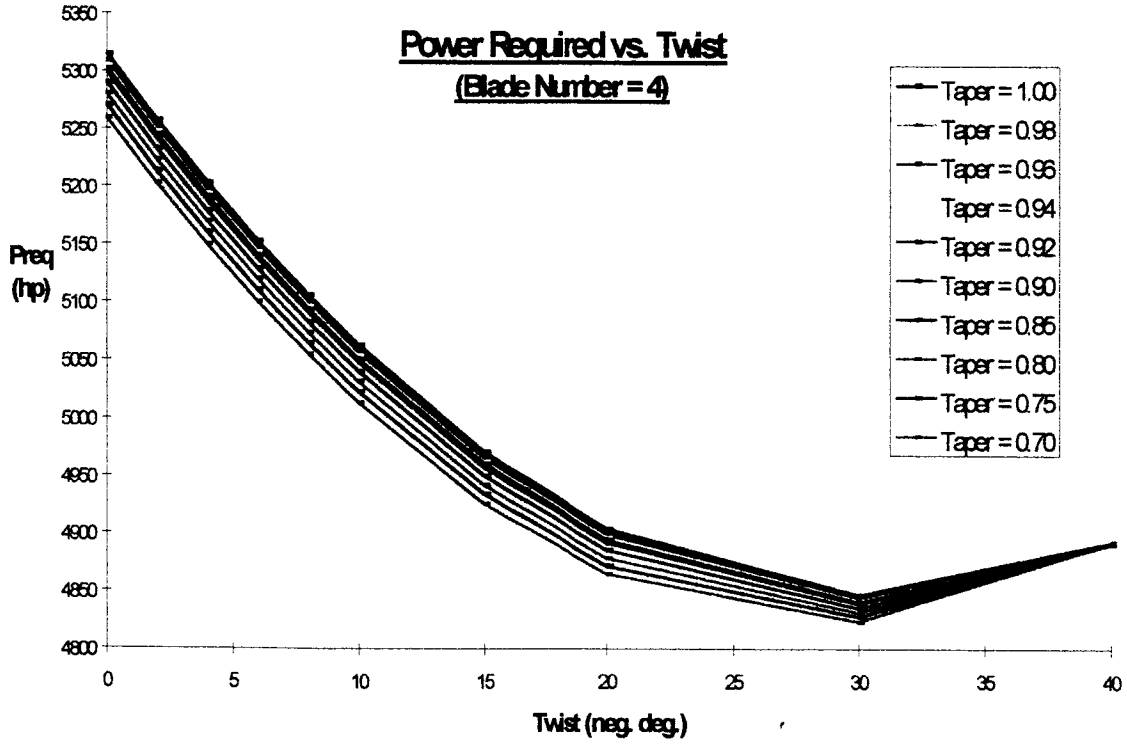

Figure 13-12

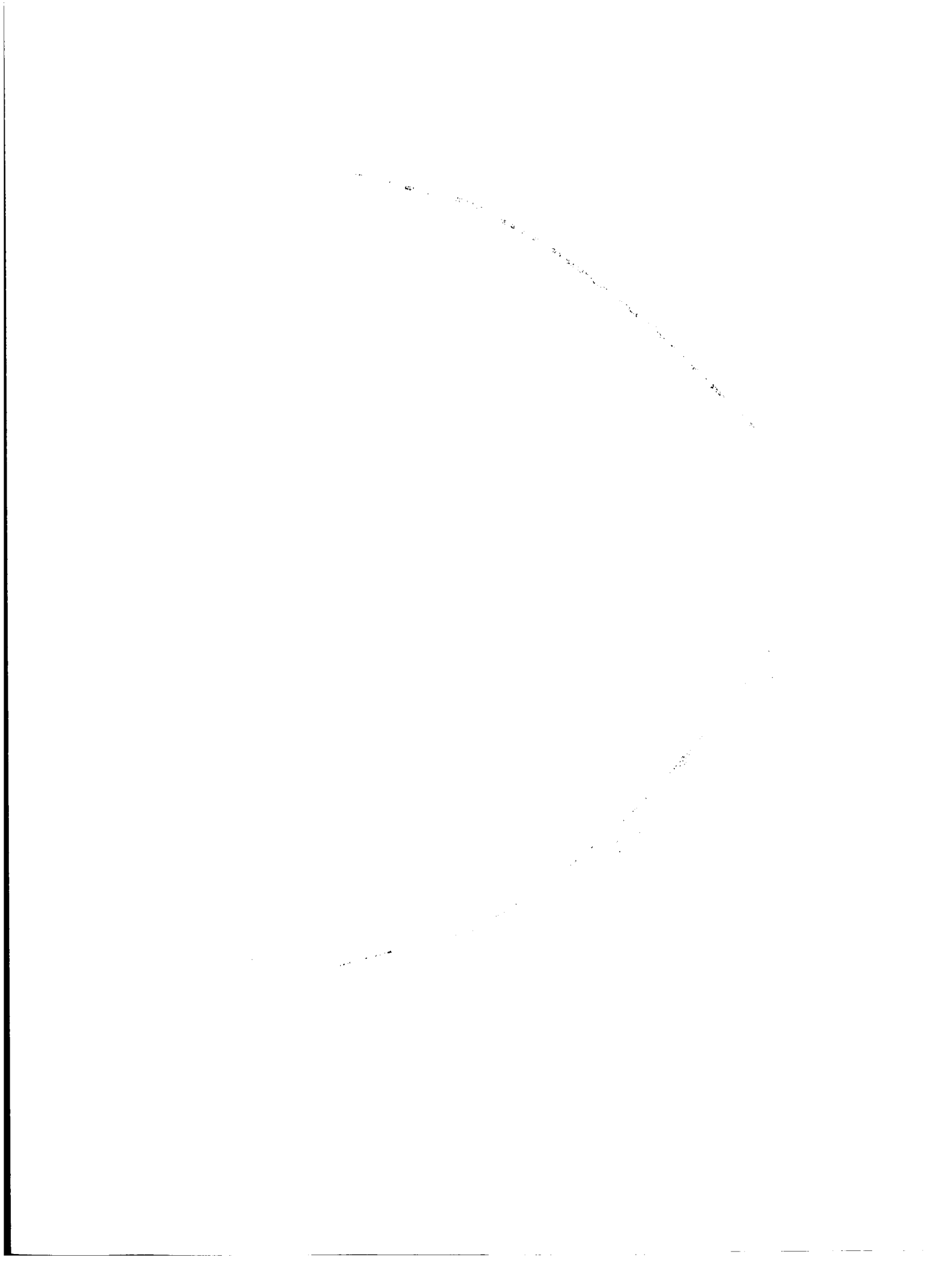

13.4 Conclusion

After reviewing the data generated from the blade element code, the AV-95 will have four rotor blades, each with -9 degrees twist and a taper ratio of 0.98 (again, this taper refers to only the outer portion of the blade). Although it will result in a heavier aircraft generating more drag, the advantages of having four rotor blades can not be compromised. This design results in a figure of merit of 0.6947 and a power required to hover of only 5079.66 horsepower. By choosing a design with four blades, the taper and twist choices do not have to be as dramatic as they would if three blades were chosen. A taper ratio of 0.98 was chosen for several reasons. Most importantly, there was relatively no advantage for having a for a four-bladed rotor system that incorporated a higher taper ratio. Finally, the twist was chosen to be -9 degrees because no significant advantage occurs for choosing a larger angle. However, choosing a smaller angle would again result in too much of a power requirement increase.

Because the solidity was chosen to be 0.15, the area of the blades is constant at 228.08 ft^2. Therefore, a two-bladed rotor design must have the same blade area as a four-bladed rotor design. Consequently, the blades of a two-bladed rotor must have twice the area than the blades of a four-bladed rotor design. Therefore, as the number of blades increases, the weight per blade decreases; as the weight of each blade decreases, the centrifugal force of each blade decreases. The force of each blade is very important in this design due to the variable diameter rotor; if the centrifugal force becomes excessively large, the retraction of the outer blade will result in much heavier parts required to handle this excessive load. Consequently, minimizing the centrifugal force, or the weight of each blade, is vital. This is one of the primary factors which drove the design to a four-bladed rotor.

For a solidity of 0.15, the root and tip chords were determined to be 33.41 and 32.74 inches, respectively. Finally, the constant chord of the inner portion of the rotor is

29.14 inches; this chord value allows the inner airfoil section to fit inside the outer section while also producing a significant amount of lift.

Once the design variables were determined, several other values were found. For instance, Figure 13-13 shows a plot of the rotor blade lift distribution. This graph clearly shows the different amount of lift generated by the inner and outer airfoil blade sections. As expected, the lift generated significantly increases from the NACA 0012 to the Eppler 361; this is due to the larger area and higher effective velocity of the Eppler blade section.

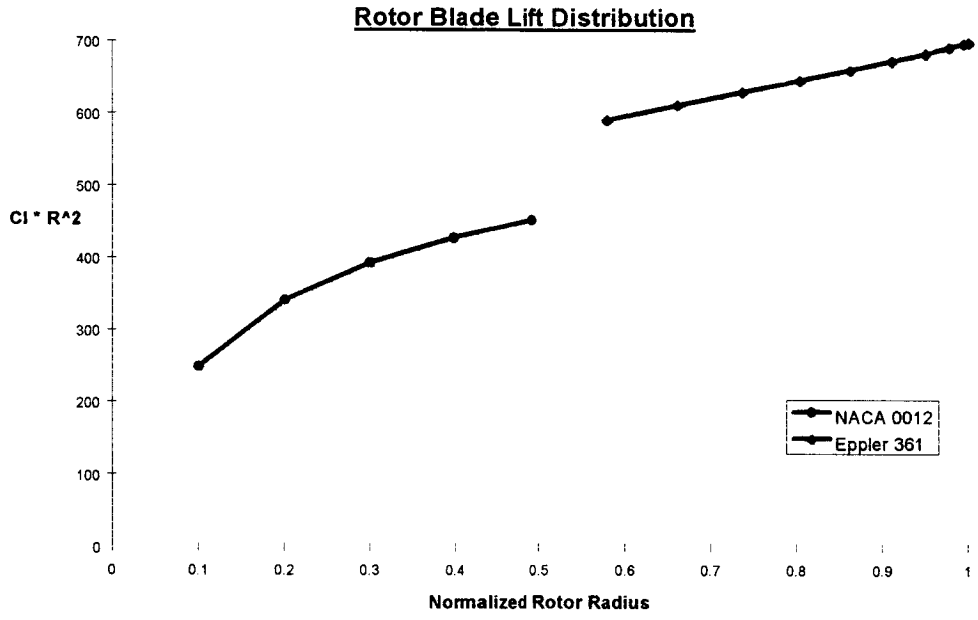

Figure 13-13

Another plot that was generated once the design variables were determined is Figure 13-14; this plot contains the rotor power required and throttled engine thrust plotted against the forward flight velocity. On this plot, the left vertical axis shows the rotor power required while the right vertical axis shows the throttled engine thrust; as discussed previously, the engine thrust is throttled to counter the total drag of the *Sun*

Devil. The horizontal axis contains the forward velocity in knots. Also on this graph is the total available engine horsepower; this is a constant value because this plot was generated at a constant altitude of 4000 feet and temperature of 95 ^{o}F. As expected, the required rotor power decreases as the forward flight velocity increases. This is expected because the rotor is off-loaded to compensate for the increasing lift generated by the wings. Similarly, the throttled engine thrust increases with an increasing forward velocity. This is also expected due to the increased drag that accompanies a larger forward velocity.

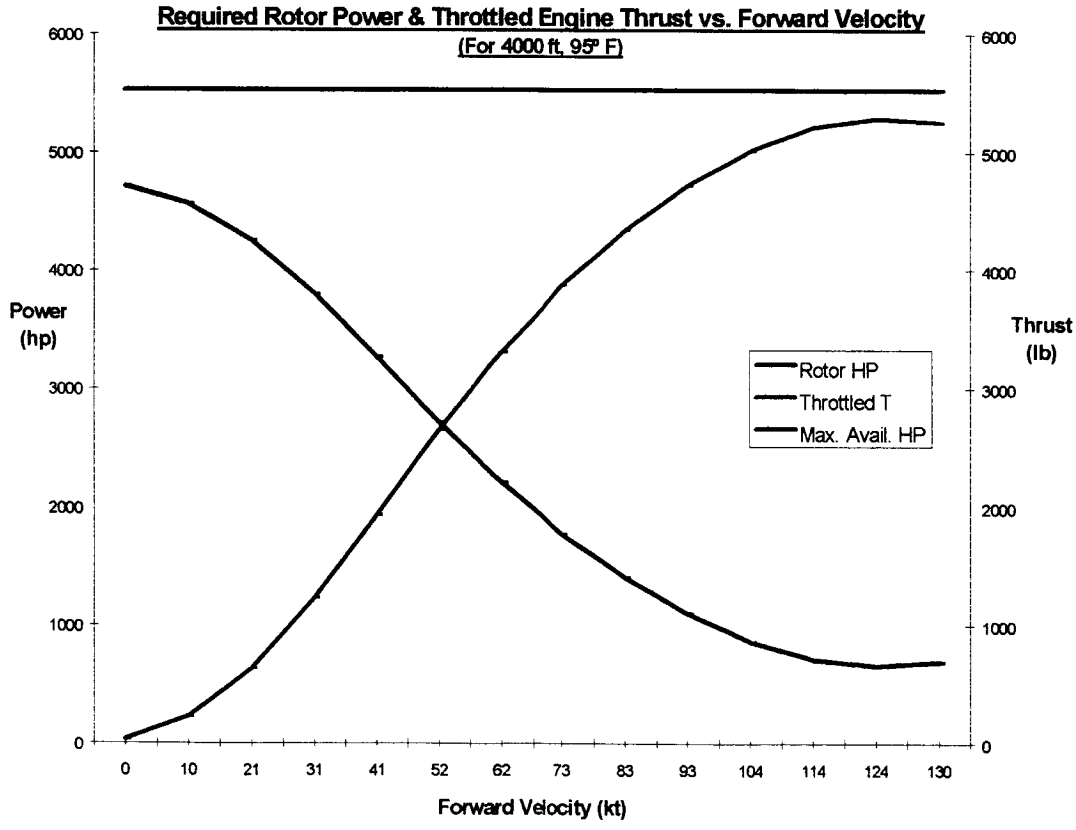

Figure 13-14

The rotor drag is shown in Figure 13-15. Here, the H-force, or the total rotor drag, is plotted against the forward velocity. As expected, the rotor drag increases as the forward airspeed increases. The unique appearance of this plot can be attributed in part to the continual off-loading of the rotor as the forward airspeed is increased. Finally, as seen in the drag breakdown, the rotor drag in cruise is 143 lbs.

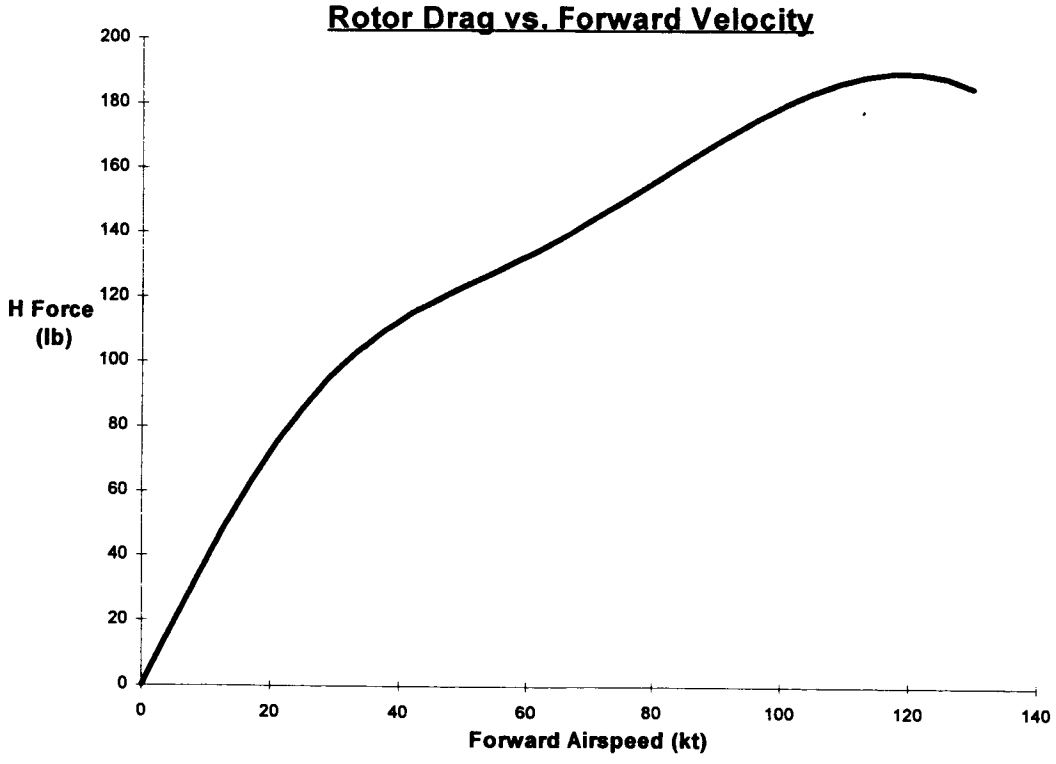

Figure 13-15

14. CIRCULATION CONTROL

14.1 Background

The main reason for utilizing a circulation control device for the AV-95 design is to reduce the angle of attack needed during conversion. Without any added high lift devices, the AV-95 needs to convert at a high angle of attack for the range of conversion velocities (~ 100 - 175 knots). However, a circulation control device, such as a blown flap, can provide the extra lift needed for a considerable range of angles of attack, including negative angles.

The possibility of using a circulation control device was researched; numerous papers were found dealing with many different techniques of using circulation control to provide higher lift coefficients. Of these many circulation control devices, the most applicable to the AV-95 design include blowing air bled off the engine over a Coanda trailing edge, blowing engine bleed air over a flap (blown flap), using the jet exhaust to provide the upper surface blowing, and combinations of the above techniques.

Blown Flap Cross Section

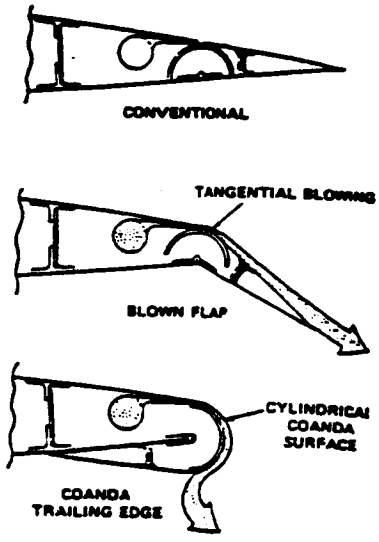

Figure 14-1

The circulation control design chosen for the AV-95 is a the combination of the Coanda trailing edge and the blown flap concept (see Figure 14-1). Under normal operating conditions (unblown), the flap operates as a conventional flap. When air is bled off the engine, the flap functions as a blown flap, which provides moderate to high lift coefficients at greatly reduced drag. Also, the blown undeflected flap may be operated during cruise to assist in high speed maneuverability (Englar, 1981). However, when the flap rotates 180 degrees, a Coanda trailing edge is revealed; the flap rotates flush with the underside of the wing. In this configuration, the wing performs as a blown wing with a Coanda trailing edge allowing the rear stagnation point to move further downstream, thus creating more lift. According to wind tunnel tests and results from full-scale tests performed on an A-6 demonstrator aircraft headed by Englar, the maximum lift coefficient increases by 96 percent compared to a conventional A-6.

Engine Bleed Schematic

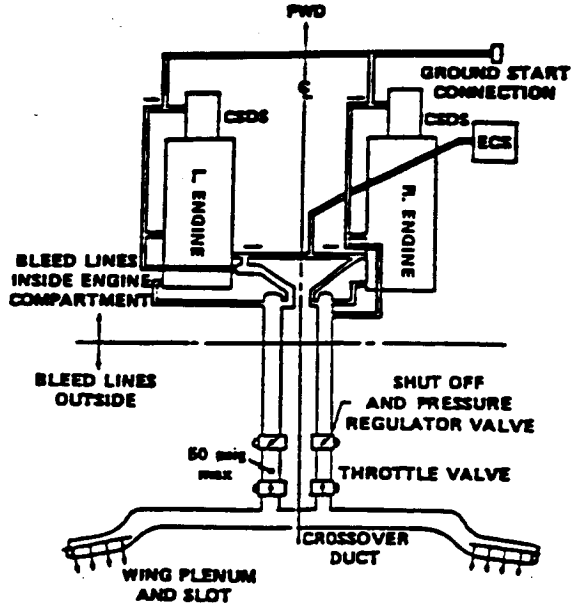

Figure 14-2

Included in one of the papers by Englar was a schematic of the circulation control device used on the A-6 (see Figure 14-2). Each engine provides air for both wings. However, in the case of an engine failure, the air bled of both engines is cross-fed to equalize the mass flow rate over each wing. Therefore, an engine loss would not result in one wing losing the lift generated by the failed engine while the second engine continuing to provide the supplemented lift over the other wing.

Another important requirement in the design of the circulation control is having the throttle setting and the blown lift independent of one other; a change in speed of the aircraft should not affect the lift developed by the circulation control. This separation is achieved by the addition of pressure regulators; these regulators limit the maximum pressure in the plenums and provide a one-way flow check valve in case an engine fails. Because the pressure at the bleed ports exceeds the plenum pressure at almost all power settings, the throttle setting and the blown lift are independent of each other as long as the plenum pressure is kept at the maximum.

14.2 Analysis

The circulation control system may be used during many segments of the mission; however, the circulation control system should not be required for speeds at or above cruise velocity because of the thrust lost when air is bled off the engines. Therefore, cruise at $V_{99\%}$ (228.4 knots) with a factor of safety of 1.2 is used to size the wing without the added lift from blowing. Also, flap deflection is not desired due to the high cruise speed. The smallest wing needed to provide level flight is 1183.26 ft^2 without an incidence angle.

$$S = \frac{W}{qC_L}$$

To lower this excessive wing area, the wing is given an incidence angle of three degrees which lowers the wing area to an acceptable 372.35 ft^2. This wing area provides the lower constraint of sizing the wing; however, if desired, a larger wing area may be chosen.

Another important parameter involving the wing area relates both the air mass flow rate and the air velocity through the slot versus the dynamic pressure and entire wing area during conversion; this term is called the momentum coefficient. Figure 14-3 shows the relationship between the wing area and the required momentum coefficient for a conversion velocity of 130 knots. For an arbitrary momentum coefficient, the change in the total lift coefficient due to the blowing can be calculated using experimental results obtained from Englar (see Appendix B). Adding this delta C_L to the lift coefficient of the wing at a chosen angle of attack, a wing area can be calculated. Varying the momentum coefficient and the angle of attack yields the carpet plot shown in Figure 14-3. Therefore, the required momentum coefficient for level-flight conversion at a desired angle of attack is easily obtainable using this carpet plot. Similar carpet plots with different conversion velocities can be found in Appendix C.

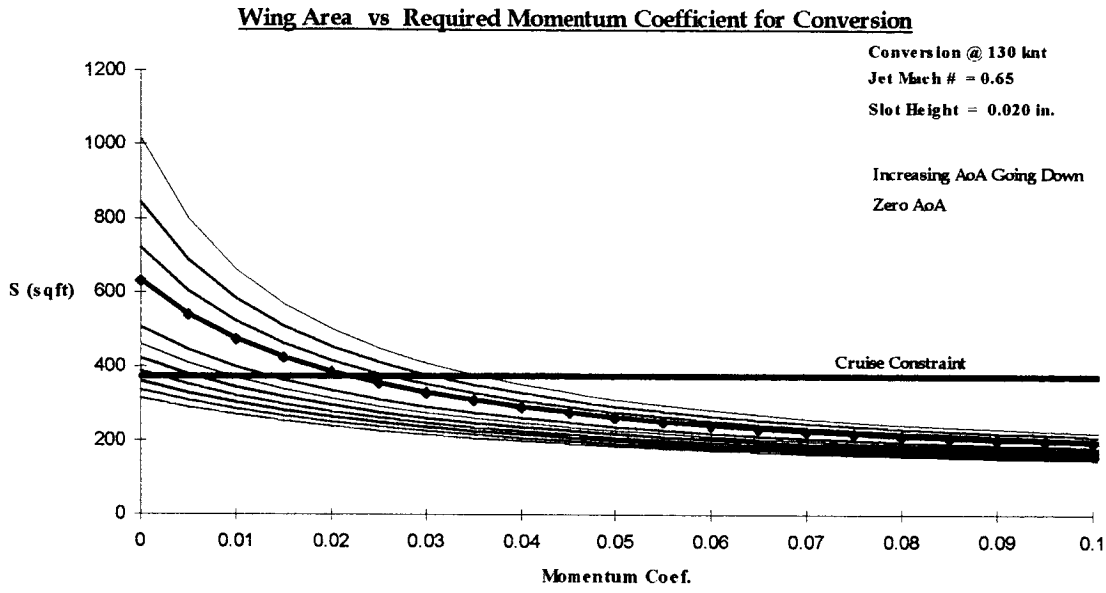

Figure 14-3

More importantly, however, is the 'best' combination of the momentum coefficient and the wing area; the wing area should be kept as small as possible to minimize the weight of the entire aircraft. Also important is the fuselage angle of attack during conversion. An ideal design would use the lowest wing area possible (sized by Cruise: 372.35 ft2) at a zero fuselage angle of attack. The momentum coefficient needed for this scenario corresponds to the intersection of the *Zero Angle of Attack* curve with the *Wing Sized by Cruise* constraint. For a constant wing area of 372.35 ft^2 and at zero angle of attack during conversion, Figure 14-4 shows the required momentum coefficient as a function of the conversion speed.

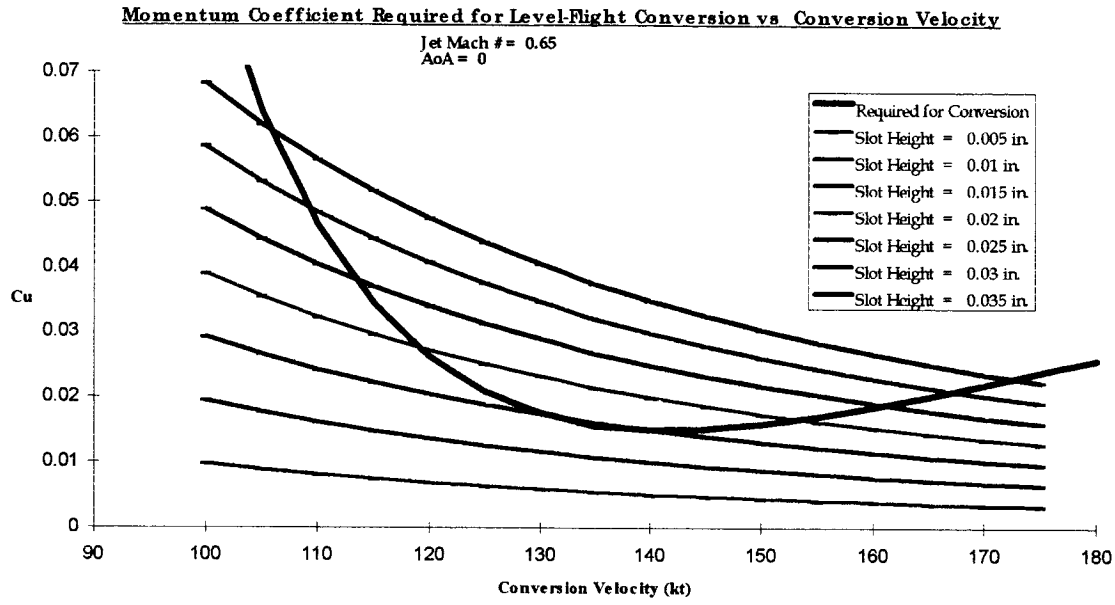

Figure 14-4

Figure 14-4 also shows the available momentum coefficient for a given slot Mach number for different slot heights versus the conversion speed. Using the following equations,

$$C_\mu = \left[\frac{m_{slot} V_{slot}}{q_{conv} S} \right]$$

$$V_{slot} = M_{slot} a_{slot}$$

where

$$\dot{m}_{slot} = \rho_{slot} a_{slot} A_{slot} M_{slot} \left[1 + \frac{\gamma - 1}{2} M_{slot}^{\,2} \right]^{\left[\frac{\gamma + 1}{2*(\gamma - 1)} \right]}$$

and

$$P_{plenum} = 4.4 P_\infty$$

$$\rho_{plenum} = \left[\frac{P_{plenum}}{R T_{plenum}} \right]$$

$$a_{slot} = \sqrt{\gamma R T_{plenum}}$$

$$A_{slot} = b_{slot} h_{slot}$$

$$b_{slot} = 0.80\left(\frac{b - width_{fuselage}}{2}\right)$$

a design point can be chosen by varying the slot Mach number. On one hand, a large slot Mach number is desired to obtain a large conversion envelope. However, a small slot Mach number is desired in the event that much more lift is required by choking the slot, such as an engine failure, increased payload capacity, etc. If the chosen design slot Mach number is too large, choking the slot may not provide the added lift required in an engine out scenario. A slot Mach number of 0.65 was chosen for the conversion design point because this value yields an excellent compromise. A slot Mach number of 0.65 creates a sizable conversion envelope (120-155 knots @ zero AoA; see Fig. 14-4), and choking the slot for an engine out scenario easily produces the required lift (see Fig. 14-6). Figure 14-4 shows the design point slot Mach number of 0.65 under normal operating conditions. With this Mach number, a slot height of 0.020 in. was chosen; this is very close to the slot height of the A-6 demonstrator aircraft (0.015 in.). As shown in the figure, conversion is possible for conversion speed ranging from about 120 knots to 155 knots at a zero fuselage angle of attack. Although the slot height is fixed, the conversion range can be significantly increased, or decreased, by changing the angle of attack and/or changing the slot Mach number.

Figure 14-5 shows the required lift coefficient versus the conversion speed at zero angle of attack for the slot height design point. For level-flight conversion, the sum of the lift coefficient generated from the circulation control (slot Mach number @ design point = 0.65) and the conventional lift coefficient generated from the wing must be equal to the required lift coefficient. Also, the lift coefficient produced by choked slots (slot Mach number = 1) is shown.

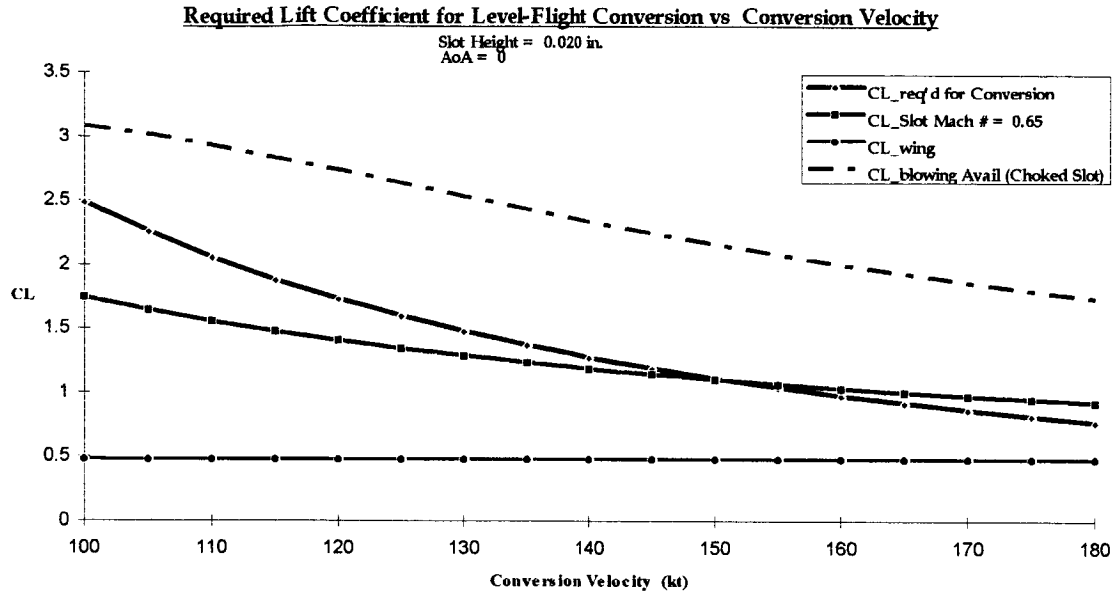

Figure 14-5

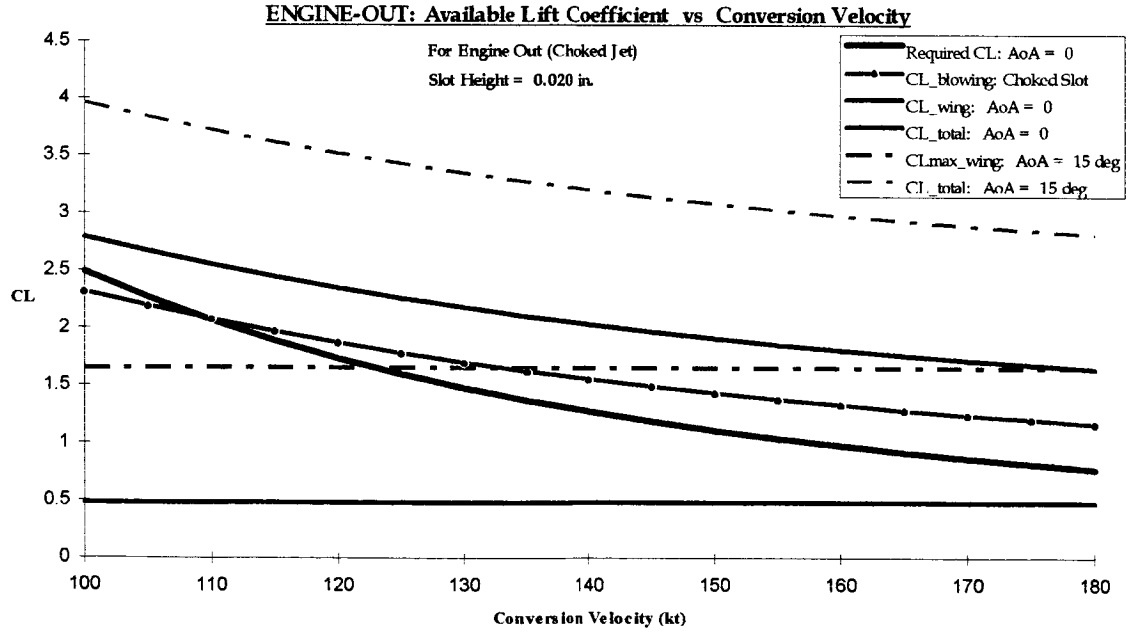

Figure 14-6

The circulation control system also provides enough lift in the event one engine fails. Figure 14-6 shows the available lift coefficients at zero-degree and 15-degree angles of attack for the one engine out scenario. Even at zero angle of attack, enough lift can be generated from just one engine to sustain level flight; for most velocities, the lift coefficient produced conventionally by the wings is not needed under one engine maximum blowing conditions. This situation is beneficial because, in the event that one engine fails, it would not be desirable to overwork the remaining engine by bleeding the mass flow required for choked slot conditions.

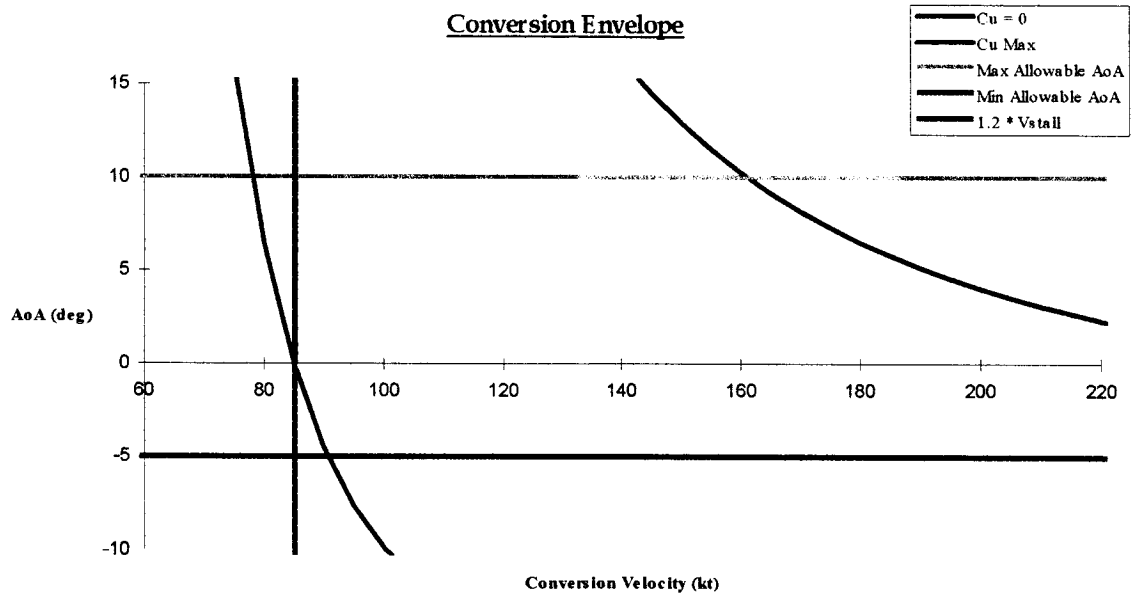

Figure 14-7

Figure 14-7 shows the conversion envelope for the AV-95. Because of helicopter difficulty flying at these angles, the upper and lower constraints are set at an angle of attack of 10 degrees and at -5 degrees, respectively. The left constraint is 1.2 times the stall speed, while the other constraints are set by maximum blowing and no blowing. A maximum helicopter velocity, or right constraint, could not be calculated because the AV-95 is not a conventional helicopter. Most helicopters are limited in maximum

velocities due to advancing blade compressibility effects and retreading blade stall. However, the *Sun Devil* does not face this problem because the rotor will not be required to produce any lift or thrust at high velocities. Also, the rotor diameter can be reduced at high velocities. Therefore, compressibility and blade stall are not of concern in limiting the AV-95 in high speed flight. Further tests are probably required to show at what maximum velocity the *Sun Devil* can fly in helicopter mode.

Figure 14-8 shows the percentage of the specific thrust lost when air is bled off the engine. For a slot Mach number of 0.65, the slot-to-fan mass flow ratio is 0.658 percent. When the slot is choked, this ratio increases to 1.371 percent. These values are not the bleed air percent because only a percentage is taken from the bleed air; this allows the plenum to be kept at the maximum pressure. However, a small bleed percentage (about 5%) is needed for these small slot mass flow rates while still keeping the plenum pressure up.

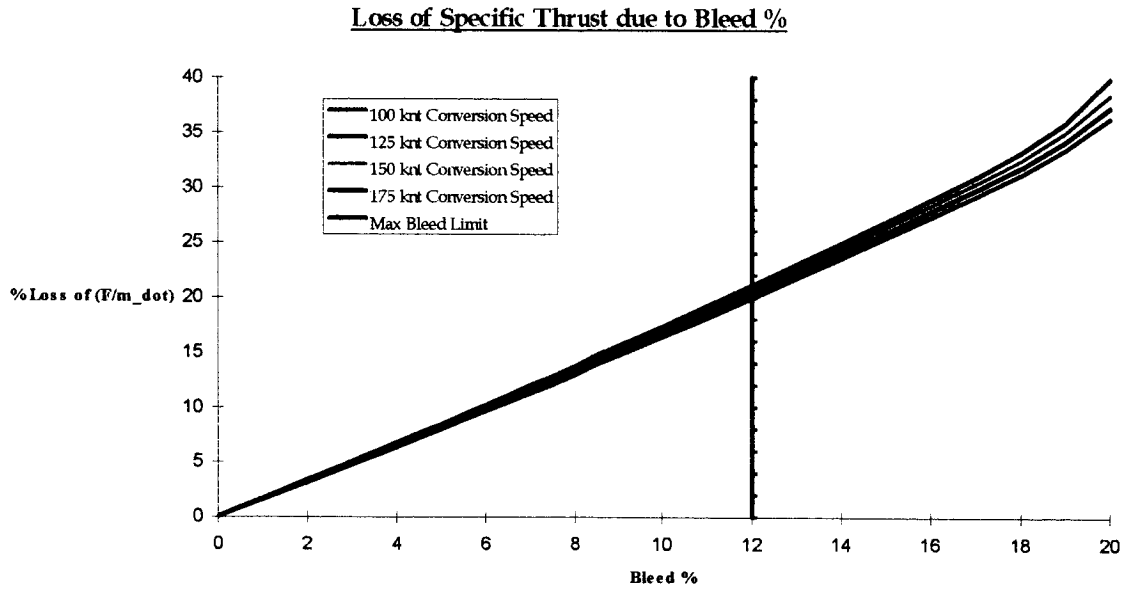

Figure 14-8

15. CONVERSION

Throughout the mission profile, there are a total of four aircraft conversions; two conversions occur from the helicopter mode to the airplane mode and two conversions from the airplane mode to the helicopter mode. Figure 15.1 shows the conversion process in detail.

Conversion Process

Velocity ➡

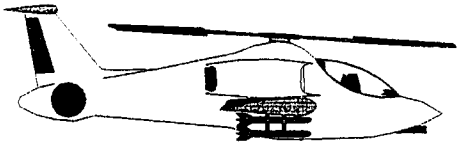

✈ High forward velocities (180 - 470 kt)

✈ Lift generated entirely from wings (circulation control may also be used)

✈ Mostly fixed-wing control surfaces used

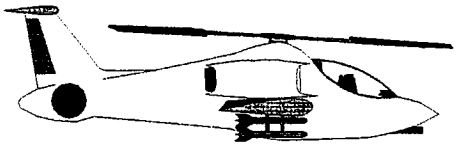

✈ Mid-range forward velocities (50 - 180 kt)

✈ Wing produces some lift, rotor off-loaded to compensate

✈ Cyclic, collective and fixed-wing control surfaces used either separately or simultaneously

✈ For conversion, rotor completely off-loaded and circulation control initiated to compensate

Rotor diameter reduced and oriented for zero lift (minimum drag)

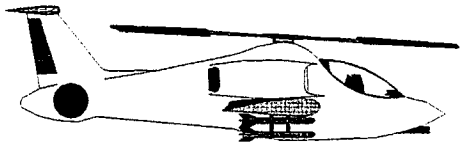

✈ Very low forward velocity (0 - 50 kt)

✈ Negligible wing lift (circulation control may be used)

✈ Mostly cyclic and collective controls used

Figure 15.1

15.1 Helicopter-to-Airplane Conversion

First, the helicopter-to-airplane conversion will be discussed for a level flight condition. The following is a list, in order, of the conversion procedure:

STEP 1:	accelerate to conversion velocity; as wing produces lift, required rotor lift decreases
STEP 2:	at conversion speed, engage circulation control device while simultaneously off-loading rotor
STEP 3:	minimize rotor diameter; orient rotor for minimum drag (zero lift)

STEP 1

The AV-95 *Sun Devil* is unique compared to other high-speed aircraft configurations in that conversion actually begins when forward flight is initiated from hover. The first step for helicopter-to-airplane conversion is to accelerate the helicopter from hover. A negative pitching angle is used to accelerate quickly from hover; however, utilizing both shaft power and jet thrust from the convertible engines will decrease or eliminate the need for downward pitching angles.

As the AV-95 increases speed, the wings produce more lift. Therefore, in level flight, the rotor lift must be decreased; the sum of the wing lift and the rotor lift must equal the weight of the aircraft; Figure 15-2 illistrates the lift-sharing between the wing and the rotor during helicopter flight. This plot displays the rotor thrust, the lift thrust and the sum of the two as a function of airspeed. The gross weight constraint is also displayed. As can be seen from the plot, the sum of the rotor thrust and wing lift is always either equal to or greater than the weight of the aircraft. As the airspeed increases,

the offloading effect that the wing has on the main rotor. This was expected and illustrates the AV-95's conversion process; the conversion process starts as soon as the aircraft enters forward flight and ends when the wing is carrying the full weight of the aircraft.

Rotor Thrust & Wing Lift vs. Forward Airspeed

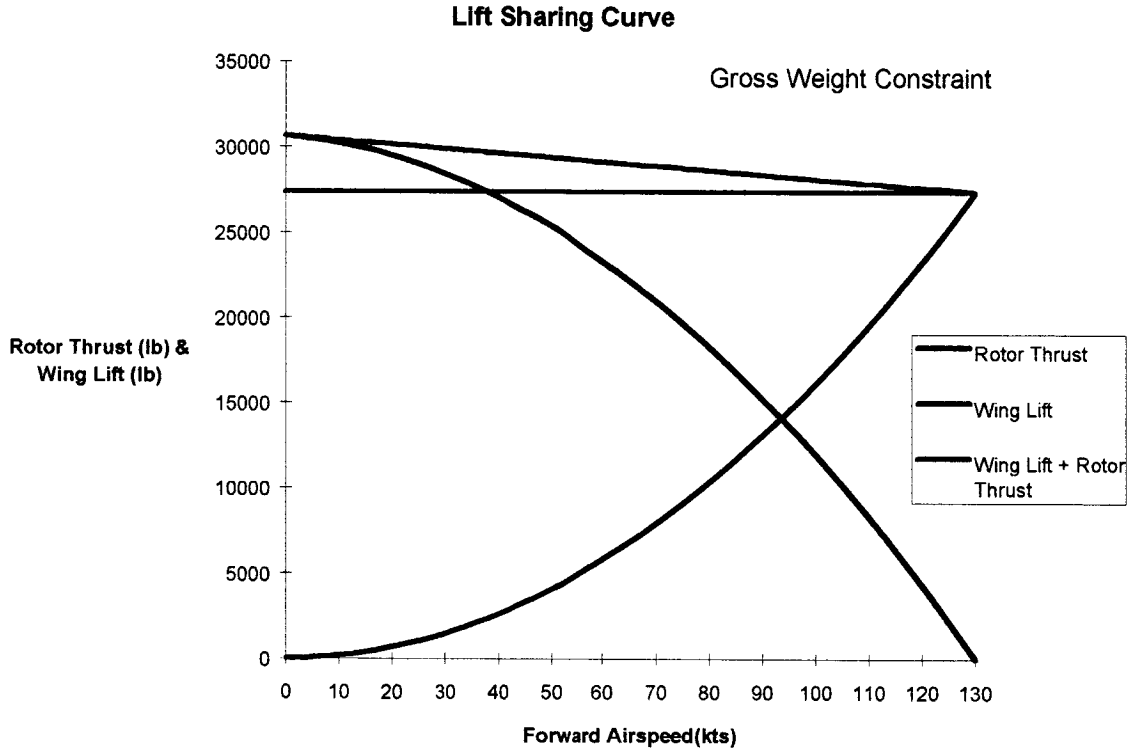

Figure 15-2

STEP 2

Once the *Sun Devil* has accelerated to the desired conversion velocity, the rotor is off-loaded while simultaneously engaging the blowing device. The AV-95 exhibits great flexibility in conversion; the *Sun Devil* can convert at any velocity from 120 to 155 knots safely. However, increasing the angle of attack or increasing the momentum coefficient of the circulation control device will make the AV-95 even more flexible during conversion.

STEP 3

The final step in converting from helicopter mode to airplane mode is orienting the rotor so that it creates a minimum drag; this orientation corresponds to zero rotor lift. Also required for minimum drag is a small amount of power from the convertible engines to keep the blades spinning. Also, the rotor diameter is reduced to its minimum diameter using the telescoping retraction system.

15.2 Airplane-to-Helicopter Conversion

The airplane-to-helicopter conversion is in many ways similar to the helicopter-to-airplane conversion discussed above. However, for this conversion, the order of the step is different.

STEP 1:	decelerate to conversion velocity speed; maximize rotor diameter
STEP 2:	disengage circulation control device while simultaneously increasing rotor lift
STEP 3:	as wing lift is decreased, required rotor lift increases;

STEP 1

The first step of the airplane-to-helicopter conversion is to decelerate to the conversion speed. At this velocity, the rotors are extended to the maximum diameter using the telescoping extension system.

STEP 2

In the second step, the rotors are oriented to produce lift while the circulation control system is deactivated.

STEP 3

As the AV-95, now in helicopter mode, decelerates from the conversion speed, the wing lift decreases. Therefore, the rotor lift needs to increase to maintain level flight.

16. FUTURE INVESTIGATIONS

The AV-95 Sun Devil will meet the future void of a high-speed attack rotorcraft. However, it should be noted that this design is only a conceptual one; there still are a few areas that need further investigation in the detailed design analysis to determine just how well the *Sun Devil* will meet its future demands. In particular, the following areas are in need of further analysis: sizing code, structures, cost analysis, and rotor blade aerodynamics in airplane forward flight.

In the sizing code, a search to find more accurate weight and drag predictions will be conducted. A more detailed structural analysis will include further crashworthiness and finite element analyses. Also, the maximum helicopter velocity is needed. Wind tunnel tests could prove to be useful in determining this limit.

The interaction of the circulation control device with the rotor wash is also in need of further study. A blown flap should decrease the downloading resulting from the induced velocity from the main rotor; however, the amount of reduction is not known until further wind tunnel tests or computational fluid dynamics models are developed to help study this interaction.

Finally, it is not yet known what the rotor drag penalty will be for velocities exceeding 400 knots. Wind tunnel testing had only been performed up to this velocity (Sikorsky, 1975). In the detailed design of this vehicle, wind tunnel testing should be performed to estimate this impact.

The AV-95 *Sun Devil* is the next generation of high-speed rotorcraft. Given the proper analysis and dedication to reach its optimal design, the *Sun Devil* will surely succeed on countless missions in hostile territories.

17. SUMMARY

The final design was chosen to be a compound rotorcraft because of its inherent advantages. These advantages include excellent airplane performance *and* impressive helicopter performance. Moreover, the survivability of the AV-95 *Sun Devil* is greatly improved over its competitors because of the independence of the propulsion systems.

Because the turbofans supply power to the rotor and provide jet thrust, the helicopter performance is significantly greater than VTOL competitors such as tilt rotors and tilt wings. Moreover, the addition of wings yields improved performance over attack helicopter competitors.

Finally, the *Sun Devil* has inherently better survivability characteristics than its competitors because of the independence of its propulsive systems. Because the turbofans can generate jet thrust, helicopter rotor lift/thrust, or any combination thereof, it is extremely versatile in what type of propulsion mode it can use. Therefore, if the rotors were heavily damaged during combat, the power supply from the turbofans to the rotors would be terminated so that the engines and wings would be the sole provider of thrust and lift, respectively. This would not only allow the *Sun Devil* and its crew to complete its mission, it would also provide them a means to return home. Unlike tilt rotors, tilt wings and other VTOL aircraft, the *Sun Devil* has the ability to take-off and land in fixed-wing mode as well. Being a military aircraft, this versatility is vital if the *Sun Devil* was damaged by the enemy and unable to fly in helicopter mode; this capablity also allows the *Sun Devil* to carry more payload because take-off power required is less for conventional fixed-wing and STOL aircraft.

REFERENCES

Abbot, Ira H. and Albert E. Von Deonhoff, *Theory of Wing Sections*, New York: Dover Publications, 1959.

Bertin, John J. and Michael L. Smith, *Aerodynamics for Engineers*, Englewood Cliffs, New Jersey: Prentice Hall, 1989.

Crossley, William, Original Hover Blade Element Code, 1992.

Englar, Robert J. et. al, *Design for the Circulation Control Wing STOL Demonstrator Aircraft*, Brumman Aerospace Corporation, Bethpae, N.Y., Jan. 1981

Englar, Robert J., *Circulation Control Technology for Powered-Lift STOL Aircraft*, Advanced Flight Department, Lockheed-Georgia Company, Vol 47, Lockheed Horizons

Englar, Robert J., *Circulation Control for High Lift and Drag Generation on STOL Aircraft*, Journal of Aircraft, Vol. 12, No. 5, May 1975.

Hale, Francis J., *Introduction to Aircraft Performance, Selection, and Design*, New York: John Wiley and Sons, 1984.

Fradenburgh, E. A., "*The Variable Diameter Rotor - A Key to High Performance Rotorcraft*" Vertiflight, March/April 1990.

Glinka, A., et al., *AV-13 Mohave, High-Speed Rotorcraft, Military Ground Attack*, Arizona State University, Tempe, AZ, 1993.

Lowndes, Jay C., *Studies Show Lift Coefficient Tripling*, Aviation Week and Space Technology, December 1, 1980.

Mayfield, Jerry, *Circulation Control Wing Demonstrator*, Aviation Week and Space Technology, March 19, 1979.

Nelson, Robert C., *Flight Stability and Automatic Control*, New York: McGraw-Hill,1989.

Nielson, Jack N. and Biggers, James C., *Recent Progress in Circulation Control Aeordynamics*, AIAA Jounal, 1987.

Peery, David J. and Azar, J. J., *Aircraft Structures*, New York: McGraw-Hill, 1982.

Prouty, Raymond W., *Helicopter Performance, Stability, and Control, Boston*: PWS Engineering, 1986.

Raymer, Daniel P., *Aircraft Design: A Conceptual Approach*, Washington D.C.: American Institute of Aeronautics and Astronautics, 1992.

Regulski, J., et al, *The AV-88 Knightmare: The Variable Diameter Tilt Rotor Alternative*, Arizona State University, Tempe, AZ, 1993.

Rutherford, J., et al., *Technology Needs for High-Speed Rotorcraft*, NASA Contractor Report 177578, April, 1991.

Saczalski, Kenneth, et al., *Aircraft Crashworthiness*, Charlottesville: University Press of Virginia, 1975.

Scott, M. W., *Technology Needs for High-Speed Rotorcraft*, NASA Contractor Report 177590, August, 1991.

Stepniewski, W. Z. and C. N. Keys, *Rotary-Wing Aerodynamics*, New York: Dover Publications, 1984.

APPENDIX A

Hover Carpet Plot Spreadsheet

Blade Number = 2

Twist Neg. Deg.	Fig. of Merit Taper = 1.00	Fig. of Merit Taper = 0.98	Fig. of Merit Taper = 0.96	Fig. of Merit Taper = 0.94	Fig. of Merit Taper = 0.92	Fig. of Merit Taper = 0.90	Fig. of Merit Taper = 0.85	Fig. of Merit Taper = 0.80	Fig. of Merit Taper = 0.75	Fig. of Merit Taper = 0.70
0	0.60823	0.60872	0.60923	0.60975	0.61028	0.61082	0.61224	0.61374	0.61535	0.61706
2	0.61554	0.61604	0.61654	0.61706	0.6176	0.61814	0.61956	0.62107	0.62268	0.62439
4	0.62266	0.62315	0.62367	0.62419	0.62472	0.62527	0.62669	0.6282	0.6298	0.63152
6	0.62956	0.63006	0.63057	0.63109	0.63163	0.63217	0.63359	0.6351	0.6367	0.6384
8	0.63622	0.63672	0.63723	0.63775	0.63829	0.63883	0.64025	0.64175	0.64334	0.64503
10	0.64262	0.64312	0.64363	0.64415	0.64468	0.64522	0.64663	0.64811	0.64969	0.65137
15	0.65732	0.65781	0.6583	0.65881	0.65932	0.65985	0.66121	0.66265	0.66416	0.66577
20	0.66987	0.67033	0.6708	0.67128	0.67176	0.67226	0.67354	0.67489	0.6763	0.67779
30	0.68724	0.6876	0.68798	0.68836	0.68874	0.68913	0.69013	0.69116	0.69223	0.69333
40	0.69285	0.69307	0.69329	0.6935	0.69372	0.69394	0.69449	0.69503	0.69557	0.6961

Twist Neg. Deg.	Power Req. Taper = 1.00	Power Req. Taper = 0.98	Power Req. Taper = 0.96	Power Req. Taper = 0.94	Power Req. Taper = 0.92	Power Req. Taper = 0.90	Power Req. Taper = 0.85	Power Req. Taper = 0.80	Power Req. Taper = 0.75	Power Req. Taper = 0.70
0	5801.99	5797.27	5792.44	5787.53	5782.5	5777.36	5764.02	5749.88	5734.89	5718.94
2	5733.11	5728.47	5723.74	5718.91	5713.98	5708.94	5695.86	5682.03	5667.37	5651.78
4	5667.57	5663.01	5658.38	5653.65	5648.83	5643.89	5631.09	5617.56	5603.23	5588.03
6	5605.42	5600.97	5596.44	5591.8	5587.07	5582.25	5569.73	5556.52	5542.55	5527.76
8	5546.72	5542.36	5537.93	5533.4	5528.78	5524.07	5511.84	5498.96	5485.37	5470.97
10	5491.46	5487.21	5482.88	5478.46	5473.96	5469.37	5457.47	5444.94	5431.72	5417.76
15	5368.65	5364.7	5360.67	5356.56	5352.37	5348.1	5337.09	5325.52	5313.36	5300.57
20	5268.09	5264.48	5260.79	5257.04	5253.23	5249.36	5239.37	5228.92	5217.99	5206.53
30	5134.98	5132.23	5129.45	5126.63	5123.77	5120.89	5113.48	5105.84	5097.97	5089.83
40	5093.35	5091.75	5090.15	5088.55	5086.96	5085.36	5081.34	5077.37	5073.43	5069.59

Blade Number = 3

Twist Neg. Deg.	Fig. of Merit Taper = 1.00	Fig. of Merit Taper = 0.98	Fig. of Merit Taper = 0.96	Fig. of Merit Taper = 0.94	Fig. of Merit Taper = 0.92	Fig. of Merit Taper = 0.90	Fig. of Merit Taper = 0.85	Fig. of Merit Taper = 0.80	Fig. of Merit Taper = 0.75	Fig. of Merit Taper = 0.70
0	0.64822	0.64863	0.64904	0.64947	0.6499	0.65035	0.65151	0.65275	0.65408	0.65551
2	0.65534	0.65575	0.65617	0.6566	0.65704	0.65749	0.65866	0.65991	0.66124	0.66267
4	0.66222	0.66263	0.66305	0.66348	0.66392	0.66438	0.66555	0.66681	0.66814	0.66957
6	0.66882	0.66923	0.66965	0.67009	0.67053	0.67098	0.67216	0.67341	0.67475	0.67617
8	0.67511	0.67552	0.67595	0.67638	0.67682	0.67727	0.67845	0.67969	0.68102	0.68242
10	0.68106	0.68147	0.6819	0.68232	0.68276	0.68321	0.68438	0.68561	0.68692	0.68831
15	0.69427	0.69467	0.69507	0.69549	0.69591	0.69634	0.69746	0.69863	0.69987	0.70118
20	0.70474	0.70511	0.70549	0.70587	0.70626	0.70665	0.70768	0.70875	0.70986	0.71104
30	0.7161	0.71636	0.71662	0.71689	0.71716	0.71744	0.71813	0.71884	0.71957	0.7203
40	0.71358	0.71367	0.71377	0.71386	0.71394	0.71403	0.71423	0.7144	0.71455	0.71466

Twist Neg. Deg.	Power Req. Taper = 1.00	Power Req. Taper = 0.98	Power Req. Taper = 0.96	Power Req. Taper = 0.94	Power Req. Taper = 0.92	Power Req. Taper = 0.90	Power Req. Taper = 0.85	Power Req. Taper = 0.80	Power Req. Taper = 0.75	Power Req. Taper = 0.70
0	5444.02	5440.62	5437.15	5433.6	5429.95	5426.25	5416.55	5406.24	5395.27	5383.53
2	5384.87	5381.52	5378.09	5374.58	5370.98	5367.31	5357.75	5347.61	5336.82	5325.32
4	5328.97	5325.67	5322.28	5318.83	5315.29	5311.66	5302.26	5292.3	5281.71	5270.46
6	5276.4	5273.13	5269.81	5266.4	5262.93	5259.38	5250.14	5240.38	5230.03	5219.05
8	5227.22	5224.01	5220.75	5217.41	5214.01	5210.52	5201.5	5191.96	5181.88	5171.2
10	5181.53	5178.39	5175.2	5171.94	5168.61	5165.21	5156.41	5147.13	5137.33	5126.97
15	5082.96	5080.04	5077.07	5074.05	5070.97	5067.83	5059.71	5051.21	5042.27	5032.9
20	5007.45	5004.81	5002.14	4999.44	4996.67	4993.87	4986.66	4979.14	4971.29	4963.1
30	4928.03	4926.21	4924.4	4922.56	4920.69	4918.81	4914.06	4909.21	4904.27	4899.25
40	4945.42	4944.76	4944.12	4943.49	4942.88	4942.28	4940.9	4939.7	4938.72	4937.96

Blade Number = 4

Twist Neg. Deg.	Fig. of Merit Taper = 1.00	Fig. of Merit Taper = 0.98	Fig. of Merit Taper = 0.96	Fig. of Merit Taper = 0.94	Fig. of Merit Taper = 0.92	Fig. of Merit Taper = 0.90	Fig. of Merit Taper = 0.85	Fig. of Merit Taper = 0.80	Fig. of Merit Taper = 0.75	Fig. of Merit Taper = 0.70
0	0.66404	0.66443	0.66483	0.66523	0.66565	0.66608	0.66719	0.66839	0.66967	0.67104
2	0.67132	0.67171	0.67211	0.67252	0.67294	0.67337	0.6745	0.6757	0.67698	0.67835
4	0.67832	0.67871	0.67911	0.67953	0.67995	0.68038	0.68151	0.68271	0.68398	0.68535
6	0.685	0.68539	0.68579	0.6862	0.68663	0.68706	0.68818	0.68937	0.69064	0.692
8	0.69131	0.69171	0.69211	0.69252	0.69294	0.69337	0.69448	0.69566	0.69692	0.69825
10	0.69724	0.69763	0.69802	0.69843	0.69884	0.69927	0.70037	0.70153	0.70277	0.70408
15	0.71009	0.71047	0.71084	0.71123	0.71162	0.71202	0.71306	0.71415	0.7153	0.7165
20	0.71978	0.72012	0.72046	0.72081	0.72116	0.72153	0.72245	0.72342	0.72443	0.72548
30	0.72825	0.72847	0.72869	0.72891	0.72913	0.72935	0.72992	0.73048	0.73106	0.73163
40	0.72136	0.72139	0.72143	0.72146	0.72149	0.72151	0.72155	0.72155	0.72151	0.72142

Twist Neg. Deg.	Power Req. Taper = 1.00	Power Req. Taper = 0.98	Power Req. Taper = 0.96	Power Req. Taper = 0.94	Power Req. Taper = 0.92	Power Req. Taper = 0.90	Power Req. Taper = 0.85	Power Req. Taper = 0.80	Power Req. Taper = 0.75	Power Req. Taper = 0.70
0	5314.33	5311.24	5308.06	5304.81	5301.49	5298.1	5289.21	5279.77	5269.67	5258.89
2	5256.71	5253.65	5250.52	5247.32	5244.05	5240.69	5231.95	5222.66	5212.78	5202.23
4	5202.46	5199.46	5196.39	5193.22	5190.02	5186.72	5178.15	5169.06	5159.38	5149.1
6	5151.76	5148.8	5145.77	5142.69	5139.54	5136.32	5127.94	5119.06	5109.64	5099.64
8	5104.69	5101.79	5098.83	5095.8	5092.72	5089.59	5081.42	5072.78	5063.64	5053.97
10	5061.31	5058.49	5055.61	5052.67	5049.68	5046.62	5038.7	5030.32	5021.49	5012.17
15	4969.67	4967.09	4964.44	4961.75	4959.01	4956.23	4949.03	4941.47	4933.55	4925.23
20	4902.77	4900.49	4898.16	4895.8	4893.39	4890.94	4884.68	4878.14	4871.35	4864.28
30	4845.77	4844.32	4842.86	4841.41	4839.93	4838.45	4834.73	4830.96	4827.18	4823.4
40	4892.09	4891.83	4891.59	4891.38	4891.2	4891.05	4890.8	4890.79	4891.06	4891.67

APPENDIX B

Curve Fit for $(C_L)_{blown}$ and C_μ Relationship

(CL)blown vs Momentum Coefficient

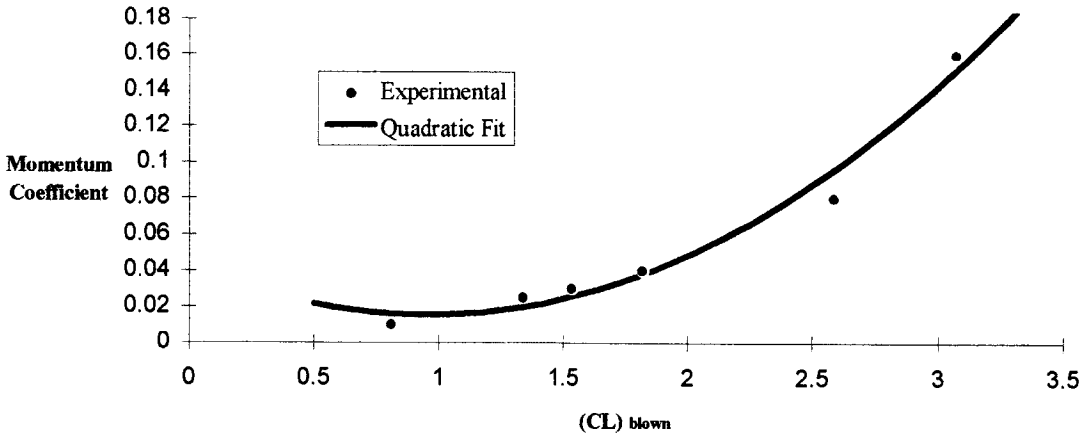

(CL)blown vs Momentum Coefficient

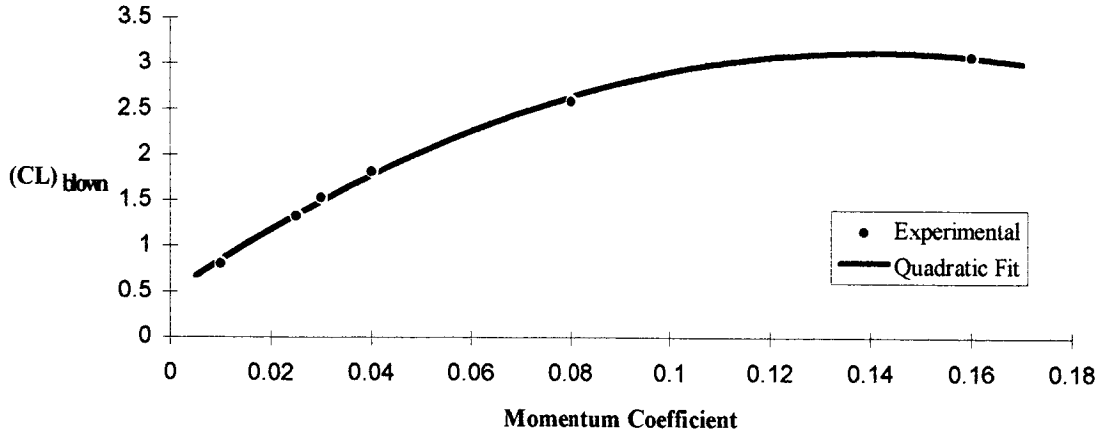

APPENDIX C

Wing Area vs $(C_\mu)_{req'd}$ for Level-Flight Conversion

Wing Area vs Required Momentum Coefficient for Level-Flight Conversion

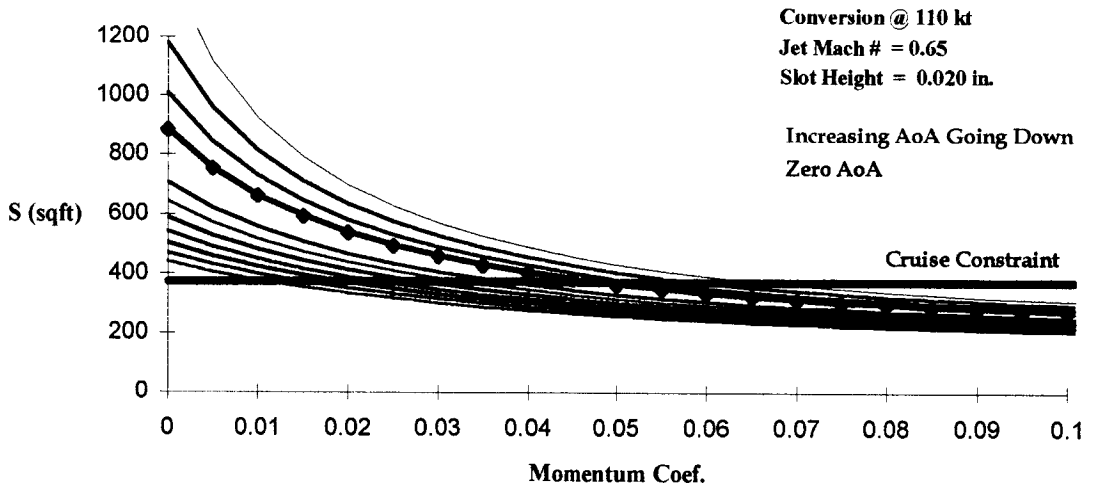

Wing Area vs Required Momentum Coefficient for Level-Flight Conversion

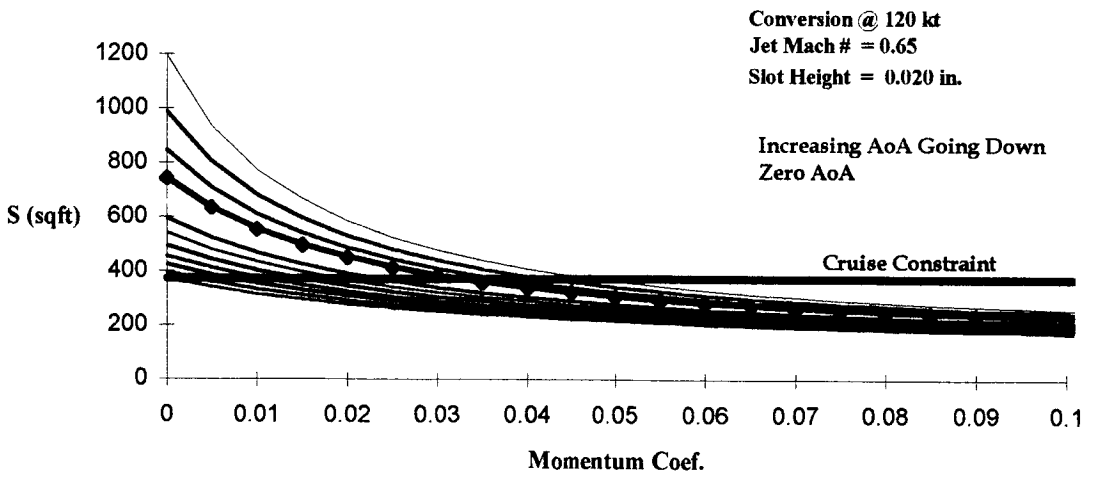

Wing Area vs Required Momentum Coefficient for Level-Flight Conversion

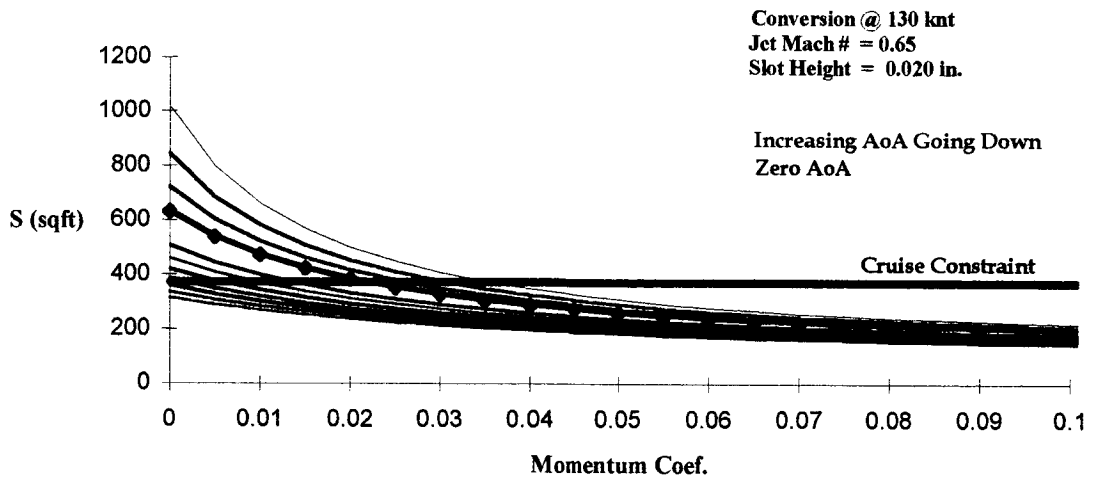

Wing Area vs Required Momentum Coefficient for Level-Flight Conversion

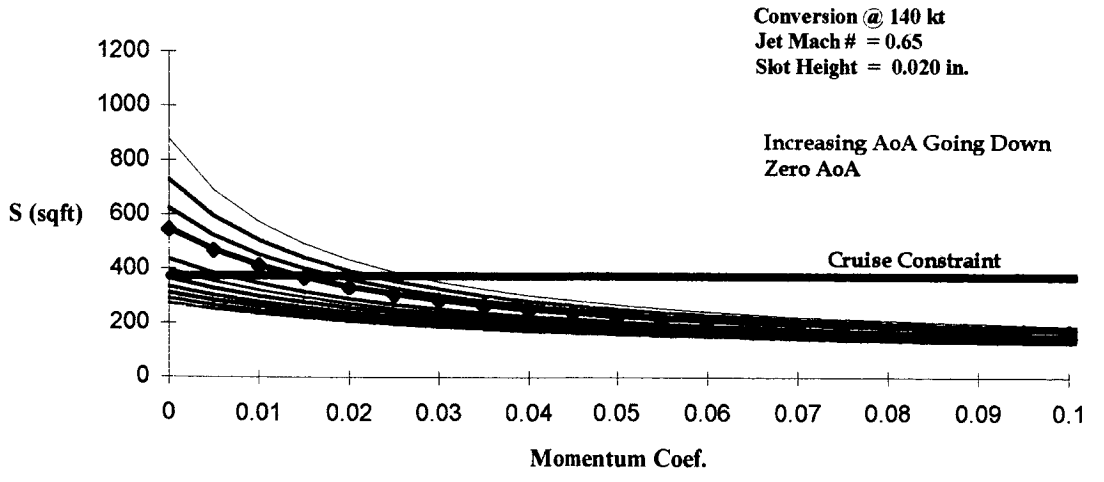

Wing Area vs Required Momentum Coefficient for Level-Flight Conversion

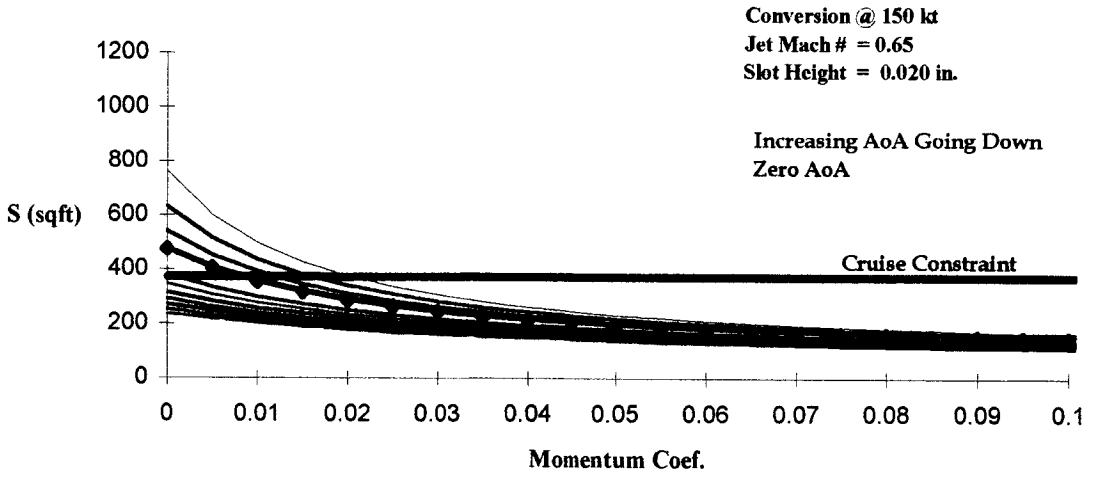

Wing Area vs Required Momentum Coefficient for Level-Flight Conversion